ULTIMATE LOADS AND MODES OF FAILURE

FOR

CIRCULAR-ARC BOW GIRDERS

by

I.J. JORDAAN

A thesis presented to the University of the Witwatersrand, Johannesburg in partial fulfilment of the requirements for the degree of Master of Science in Engineering

December, 1964.

DECLARATION:

I hereby declare that this Thesis is my own work and has not been submitted for a degree at any other University.

Nordaas

ACKNOWLEDGMENTS

The author wishes to express his gratitude for the financial assistance afforded him by bursaries from the South African Council for Scientific and Industrial Research and from the Hennen Jennings Fund.

In addition, the author is indebted to:

Professor A.J. Ockleston, who supervised the work, for the interest shown and the many helpful suggestions made during the course of the investigation,

Mr. A.B. van Gorp, of the Department of Statistics, for his advice on some of the statistical aspects of the work, and

The Staff of the Civil Engineering Workshop for their help in the preparation of the apparatus.

-- oOo --

SYNOPSIS

This work describes the behaviour at collapse of steel circular beams when loaded at right angles to the plane of the beam. Methods for the calculation of collapse loads for girders with one and two concentrated loads are given; the calculation has been carried out using, for the most part, an electronic computer. The effect of torsional movements of the supports is investigated. A kinematic approach to the calculation of collapse loads is given; the usual method is based on a static approach. Experiments have been carried out on eight miniature bow girders in which the analytical work was tested. Reasonable agreement between theory and experiment was obtained.

- oOo -

CONTENTS

		Page
1.	Introduction	1
2.	Basic Principles	4
	2.1 Background Plastic Theory and Yield Criterion	
	2.2 General Picture for Circular-Arc Bow Girders	
	2.3 Rules for the Formation of Plastic Hinges.	
3.	Single Concentrated Load	11
	3.1 Introduction	
	3.2 Fully Fixed Case	
	3.3 No Torsion at Supports	
	3.4 No Bending at Supports	
	3.5 Effect of Lack of Torsional Restraint	
4.	Two Concentrated Loads	25
	4.1 Introduction	
	4.2 Fully Fixed Case	
	4.3 Effect of Lack of Torsional Restraint	
	4.4 Several Concentrated Loads	
5.	A Kinematic Approach	35
	5.1 Introduction	
	5.2 Basic Principles	
	5.3 Examples of Application	
6.	Experimental Investigation	43
	6.1 Introduction	
	6.2 Preparation of Specimens and Description of Apparatus	
	6.3 Scope of Tests	
	6.4 Results of Tests and Comparison with Theory	
7.	Summary	63
8.	Appendix	66
9.	List of References	75

CHAPTER I

INTRODUCTION

The subject of this work is the behaviour at collapse of steel beams curved in a plane to a circular shape and loaded at right angles to the plane. The analysis of such beams is complicated by the presence of twisting moments in addition to the action of bending moment and shearing force which exists in a straight beam.

Comprehensive investigations[1, 2] covering both theoretical and experimental aspects of the problem have been made of the elastic behaviour of circular-arc bow girders.

The calculation of collapse loads has received the attention of several authors. Johansen[3] has described methods of calculating the collapse load for plane beams bent into shapes composed of successions of straight lengths, and also uniformly curved beams and circular rings. Various support conditions were considered: the fully fixed support, the support with no torsional restraint, and the support with no bending restraint. Johansen has considered only single concentrated loads, and for the circular-arc girder has for the most part given solutions for the load at the central point of the girder. Boulton and Boonsukha[4] have extended Johansen's work for the fully fixed case to a graphical solution for a point load at any position on the girder arc and have also given a solution for a uniformly distributed load over the whole girder. Both theoretical treatments have used an approximate lower bound yield criterion for combined bending and torsion proposed by Hill and Siebel[5].

Tests have been conducted by Johansen[3] and by Boulton and Boonsukha[4]; the former were not to complete failure, but did provide some information on the formation of the plastic hinges. The tests by Boulton and Boonsukha were to collapse and yielded results in reasonable agreement with the theory.

The present work includes both analytical and experimental aspects of the problem. The scope of the work is as follows:

(i) the extension of the existing graphical methods for a girder with a single load to complete solutions for the fully fixed case and the case with no torsion at the supports using the digital computer where direct computation was not possible. The results of these investigations form the basis of a discussion of the effect of support movements, particularly rotations of the supports in a torsional direction.

(ii) the calculation of the collapse load for girders with two point loads and with fully fixed support conditions. Some comments on the effect of incomplete fixity and on the calculation of collapse loads for girders carrying several concentrated loads have been included. The digital computer was used for most of the solutions.

(iii) the calculation of collapse loads using a kinematic approach: the existing methods use a static approach. In this section a method for calculating the collapse loads applying the virtual work equation is described.

(iv) an experimental investigation in which eight miniature bow girders of different cross sections were tested to failure. Sufficient readings were taken so that the behaviour of individual hinges could be investigated. The collapse loads were compared with values predicted from control tests in pure bending and pure torsion. The behaviour of the hinges was also compared with the theoretical behaviour, based on the results of the control tests.

The bulk of the theoretical aspects of the present work is based on the geometric approach developed by Johansen and by Boulton and Boonsukha.

After completion of the present work but before submission of the thesis, Imegwu[6] described a general method for calculating collapse loads for plane curved girders. Imegwu also used the digital computer for his solutions.

Imegwu states that Johansen's method and extensions are not readily adapted to automatic computation; in the present work, however, automatic computation is used without difficulty. Imegwu also states that these methods are not easily used for more complicated loading cases. In the present work it is shown that most loading cases can be calculated using extensions of Johansen's method, although the method due to Imegwu does in some cases yield a quicker solution. Imegwu's work is discussed further where it is pertinent, and is compared to the solutions in the present work where applicable.

One advantage of the methods used in the present work is that, particularly for the kinematic approach described, a clear visualization of the collapse mechanism is necessary. This visualization of the collapse mechanism is sometimes very important, as a false mode of failure may be obtained which superficially appears to satisfy the equilibrium, yield and mechanism conditions. Examples of this are given in Chapter 5.

Aspects which it is considered require further study are suggested in the final section of this work.

CHAPTER 2

BASIC PRINCIPLES

2.1 Yield Criterion

In most bow girders, bending moment and torsion are the most important structural actions: the effect of shear is usually negligible. Hence in the yield criterion the combination of bending moment and torsion which causes full plasticity of a cross-section is sought.

For cross-sections with two orthoganal axes of symmetry, an approximate lower bound yield criterion for a plastic hinge at a section subjected to a bending moment M and a torque T has been proposed by Hill and Siebel[5]:

$$\left(\frac{M}{M_p}\right)^2 + \left(\frac{T}{T_p}\right)^2 = 1 \quad \ldots\ldots\ldots\ldots\ldots\ldots\ldots \quad (2.1)$$

where M_p is full plastic moment in pure bending, and T_p is the full plastic moment in pure torsion.

This assumes that the effect of shearing force is negligible, and also that the material is rigid plastic.

Estimates of the error involved in equation (2.1) have been made analytically assuming the member to be fully plastic throughout its length which practically never occurs in a circular-arc bow girder. If the square root of the left hand side equation (2.1) exceeds unity by ε, then:

(i) Steele[7] has estimated $\varepsilon < 0.15$ for a square solid or hollow cross-section: if $M = 0$, ε is a maximum, and for $T = 0$, $\varepsilon = 0$.

(ii) Boulton and Boonsukha[4] have estimated ε for an I-section on the assumption that transverse shearing stress is horizontal in the flanges and vertical in the web. The value of ε obtained was $\varepsilon = .05$.

In the discussion[4] on the paper by Boulton and Boonsukha, Brown and Gent have pointed out that the yield criterion given by equation (2.1) is not necessarily a good one. The value of T_p obtained from the standard torsion test might be different from that in a torsion hinge in a bow girder, in which plasticity occurs at an isolated point. Brown and Gent further pointed out that the non-plastic parts of the structure would restrict, if not entirely prevent, plastic warping of the cross-section.

In the reply to the above discussion, Boulton and Boonsukha agreed that restraint on the warping of a pure torsion hinge would prevent the formation of a fully plastic hinge.

The results of some tests carried out at the University of Sheffield were then described by Boulton and Boonsukha which showed that equation (2.1) gave a true lower bound to experimental points for combined bending and torsion. It was also found that the restriction of warping could increase the value of the plastic moments in pure torsion substantially.

Imegwu[6] has described a method of estimating collapse loads using a more exact interaction equation.

Equation (2.1) has been adopted in the present work as the yield criterion. This is justified by:

(a) the favourable analytical work already described,
(b) the experimental work conducted at the University of Sheffield described above,
(c) the favourable results of tests on miniature bow girders by Boulton and Boonsukha, and
(d) the tests described in the present work, in which reasonable results were obtained. The plastic hinges in pure torsion in circular bow girders showed considerable spread and the mean value of torsion exceeded the value of pure torsion found in straight lengths of the same ross-section by only 7 per cent.

If T_p/M_p is written as α, equation (2.1) becomes:

$$\alpha^2 M^2 + T^2 = T_p^2 \quad \ldots\ldots\ldots\ldots \quad (2.2)$$

It has also been shown[3, 5] that if γ is the angle between the radius of the bow girder and the axis of rotation of a plastic hinge that:

$$\tan \gamma = T/\alpha^2 M \quad \ldots\ldots\ldots\ldots \quad (2.3)$$

2.2 The Circular-Arc Bow Girder

For the equilibrium of a body in space, in which an arbitrary set of co-ordinates are X-Y-Z, six equations are necessary:

$$\Sigma P_x = o,\ \Sigma P_y = o,\ \Sigma P_z = o,$$
$$\Sigma M_x = o,\ \Sigma M_y = o,\ \Sigma M_z = o,$$

where ΣP_x denotes the sum of all the components of force in the X-direction, and ΣM_x denotes the sum of all the components of moments about an axis parallel to the X-axis; the other terms have a similar meaning.

Considering a bow girder which lies in the X-Y plane. and which is loaded in the Z-direction, then the forces and moments in the X-Y plane may be assumed to be negligible compared with the forces and moments in the X-Z and Y-Z planes. Hence the three equations of the first order of magnitude are

$$\Sigma P_z = o,\ \Sigma M_x = o \text{ and } \Sigma M_y = o.$$

Therefore three essential reactions are needed for the equilibrium of a bow girder, and if it is fully fixed at the supports, the three additional reactions are redundant. If there is no torsion at the supports of the bow girder, there is one redundant reaction.

The number of plastic hinges found in a bow girder is not, in general, one more than the number of redundancies, as is the case for a plane frame loaded in its plane. The reason for this is that the number of hinges required to form a mechanism constituting complete collapse of a plane frame is one more than the number of redundancies, whereas in the case of the bow girder, the number of hinges required to cause a collapse mechanism is not dependant on the number of redundancies. A simple example of this is collapse about an axis joining the supports, requiring two hinges, one at each support. The number of hinges occurring during collapse of a bow girder is usually two, three or four.

Johansen has shown that in the case of four hinges, the static conditions are sufficient for solution; for three hinges the geometric condition that the axes of rotation of the hinges must intersect in a point is necessary, while if there are two hinges collapse must take place about a common axis joining the two hinges.

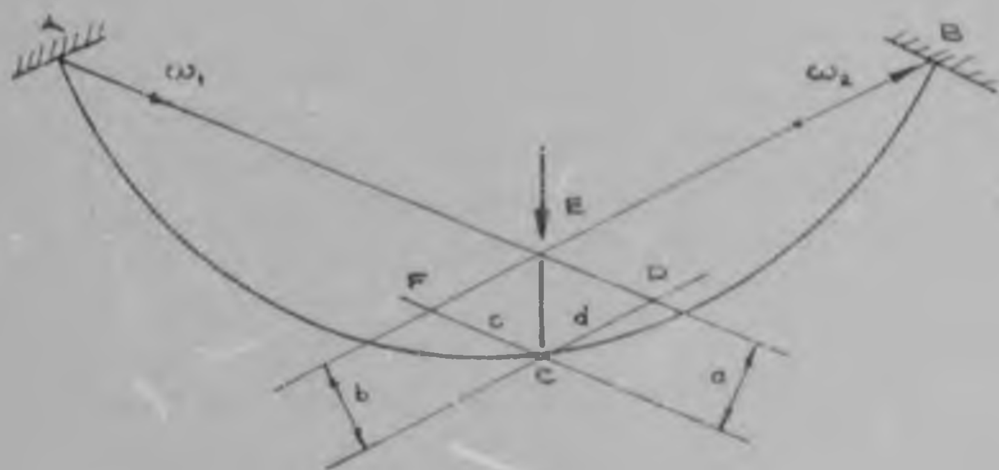

FIGURE 2.1

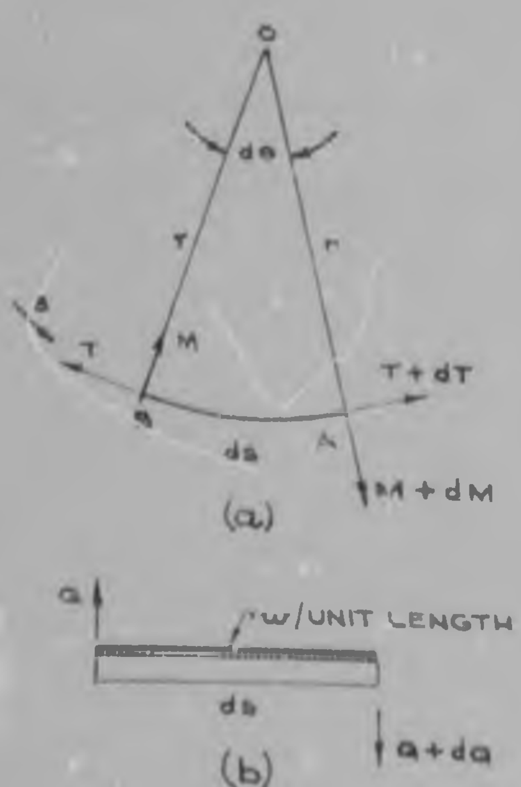

FIGURE 2.2

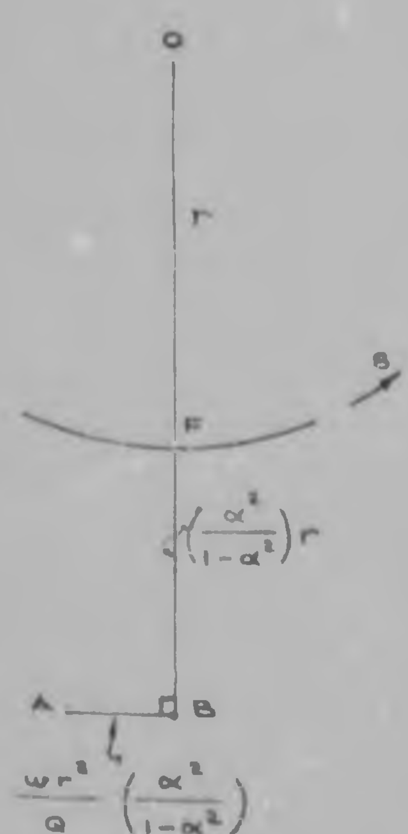

FIGURE 2.3

Johansen does not give a proof of the condition necessary for the formation of three hinges, that is, that the axes of rotation of hinges must intersect in a point. This is quite easily demonstrated: consider the curved beam shown in Fig. 2.1. Hinges during collapse are assumed to form at the supports A and B and at any other point C; the rotations at A and B are ω_1 and ω_2 in the directions shown (rotations viewed in the direction of the arrows are clockwise). The point C, as a result of these rotations, moves vertically downward a distance x, where

$$x = a\omega_1 = b\omega_2$$

and a and b are the perpendicular distances shown.

Hence:

$$\frac{\omega_1}{\omega_2} = \frac{b}{a} = \frac{c}{d},$$

where c and d the lengths of the sides of the parallelogram CDEF as shown.

Since the rotation at the hinge at C is the rotation of length C B relative to C A, it is equal to vectorial difference between ω_1 and ω_2, which are in the ratio of the sides c and d of parallelogram CDEF as demonstrated above. As a result of this, the axis of rotation at hinge C must fall along the diagonal EC of CDEF, and must therefore pass through the point E.

2.3 Rules for Formation of Hinges in a Circular-Arc Bow Girder

The distinction between free and fixed plastic hinges has been recognised by Johansen and by Boulton and Boonsukha; a fixed hinge is one which occurs at a support or at the point of application of a concentrated load, while a free hinge occurs at any other point of the girder where the load is either distributed or zero.

Johansen has developed certain rules for the determination of free hinges. Consider an element AB of a circular beam of radius r with the central angle dθ of the element ds as shown in Fig. 2.2(a).

The girder is loaded with a uniformly distributed load w per unit length as shown in Fig. 2.2(b). The bending moment, torque and shearing force acting at the end B are M, T and Q respectively.
For vertical equilibrium:

$$w + \frac{dQ}{ds} = 0 \quad \ldots\ldots\ldots\ldots\ldots\ldots\ldots\ldots \quad (2.4)$$

Taking moments about the tangent at A gives:

$$M d\theta + dT = 0,$$

or $$\frac{M}{r} + \frac{dT}{ds} = 0 \quad \ldots\ldots\ldots\ldots\ldots\ldots\ldots\ldots \quad (2.5)$$

Taking moments about radius OA gives:

$$dM = Q ds + T d\theta,$$

or $$\frac{dM}{ds} = Q + \frac{T}{r} \quad \ldots\ldots\ldots\ldots\ldots\ldots\ldots\ldots \quad (2.6)$$

In the above, quantities of second order of smallness and smaller have been neglected.

For the formation of a free hinge it follows from the yield criterion given by equation (2.2) that $\alpha^2 M^2 + T^2$ must be a maximum,

i.e. $$\frac{d}{ds}(\alpha^2 M^2 + T^2) = 0,$$

or $$2\alpha^2 M \frac{dM}{ds} + 2T\frac{dT}{ds} = 0,$$

where α is regarded as a constant.
Hence,

$$M\left(\alpha^2 \frac{dM}{ds} + \frac{T}{M}\frac{dT}{ds}\right) = 0.$$

Substituting for $\frac{dM}{ds}$ and $\frac{dT}{ds}$ from (2.5) and (2.6),

$$M\{\alpha^2 Q - \frac{T}{r}(1 - \alpha^2)\} = 0.$$

For this to be satisfied, either $M = 0$, or if $M \neq 0$,

$$\alpha^2 Q = \frac{T}{r}(1 - \alpha^2) \quad \ldots\ldots\ldots\ldots\ldots\ldots \quad (2.7)$$

These two conditions are the necessary but not sufficient conditions for the formation of a plastic hinge; a plastic hinge will exist if the yield criterion given by equation (2.2) is satisfied, in addition to the left hand side of (2.2) being a maximum.

For $\alpha^2 M^2 + T^2$ to be a maximum, the second derivative must be negative, or

$$\alpha^2\{M\frac{d^2M}{ds^2} + (\frac{dM}{ds})^2\} + T\frac{d^2T}{ds^2} + (\frac{dT}{ds})^2 < 0 \ \ldots \quad (2.8)$$

Case M = 0

Equation (2.5) shows that $\frac{dT}{ds} = 0$.

Inequality (2.8) reduces to:

$$\alpha^2 \left(\frac{dM}{ds}\right)^2 + T\,\frac{d^2T}{ds^2} < 0.$$

If (2.5) is differentiated, it is found that

$$\frac{d^2T}{ds^2} + \frac{1}{r}\,\frac{dM}{ds} = 0.$$

Using (2.6) and this expression, (2.8) becomes:

$$\left(Q + \frac{T}{r}\right)\left\{\alpha^2 Q - (1 - \alpha^2)\,\frac{T}{r}\right\} < 0.$$

Hence, for this to be true, either:

$$-\frac{T}{r}\left(\frac{\alpha^2 - 1}{\alpha^2}\right) > Q > -\frac{T}{r}, \quad \dots\dots\dots\dots\dots\dots \quad (2.9a)$$

or

$$-\frac{T}{r}\left(\frac{\alpha^2 - 1}{\alpha^2}\right) < Q < -\frac{T}{r} \quad \dots\dots\dots\dots\dots\dots \quad (2.9b)$$

Since $\alpha > 0$ always,

$$-\frac{T}{r} \leq -\frac{T}{r}\left(\frac{\alpha^2 - 1}{\alpha^2}\right)$$

and therefore (2.9a) applies and (2.9b) is invalid.

Case $M \neq 0$

Differentiating (2.6) gives

$$\frac{d^2M}{ds^2} = \frac{dQ}{ds} + \frac{1}{r}\,\frac{dT}{ds}$$

$$= -w - \frac{M}{r^2}, \text{ using (2.4) and (2.5).}$$

Differentiating (2.5) gives

$$\frac{d^2T}{ds^2} = -\frac{1}{r}\,\frac{dM}{ds} = -\frac{Q}{r} - \frac{T}{r^2}, \text{ using (2.6),}$$

$$= -\frac{T}{r^2}\left(1 + r\,\frac{Q}{T}\right),$$

and since for the case $M \neq 0$, (2.7) applies, Q may be eliminated from this equation:

$$\frac{d^2T}{ds^2} = -\frac{T}{r^2\alpha^2}\,.$$

Substituting these values in the inequality (2.8):

$$\alpha^2\left\{M\left(-w - \frac{M}{r^2}\right) + \left(Q + \frac{T}{r}\right)^2\right\} + T\left(-\frac{T}{\alpha^2 r^2}\right) + \left(-\frac{M}{r}\right)^2 < 0$$

Substituting $Q = (\frac{1}{\alpha^2} - 1)\frac{T}{r}$ from (2.7):

$$-\alpha^2 Mw + (1-\alpha^2)\frac{M^2}{r^2} < 0,$$

or $M\{(1-\alpha^2)M - \alpha^2 wr^2\} < 0.$

If $M < 0$, then $(1-\alpha^2)M \leq 0$ (as $\alpha \leq 1$), and

$$-\alpha^2 wr^2 < 0 \quad \text{if } w > 0;$$

hence $M\{(1-\alpha^2)M - \alpha^2 wr^2\} \nless 0$ if $M < 0$.

If $M > 0$, then

$$(1-\alpha^2)M - \alpha^2 wr^2 < 0$$

or $M < wr^2 (\frac{\alpha^2}{1-\alpha^2})$.

Hence for the inequality to be true:

$$wr^2 (\frac{\alpha^2}{1-\alpha^2}) > M > 0 \quad \ldots\ldots\ldots\ldots\ldots\ldots \quad (2.10)$$

The rule for the formation of a free hinge as derived by Johansen is as follows:

In Fig. 2.3 a section of the arc of a circular bow girder is shown. If a free hinge is to occur at F, then if $w \neq 0$ equation (2.10) requires that the resultant Q of the internal forces in the hinge must cut AB. If w = 0 at F, AB = 0, and Q must cut OB produced, as required by equation (2.9b).

For the case w = 0, the hinge must consequently be in pure torsion.

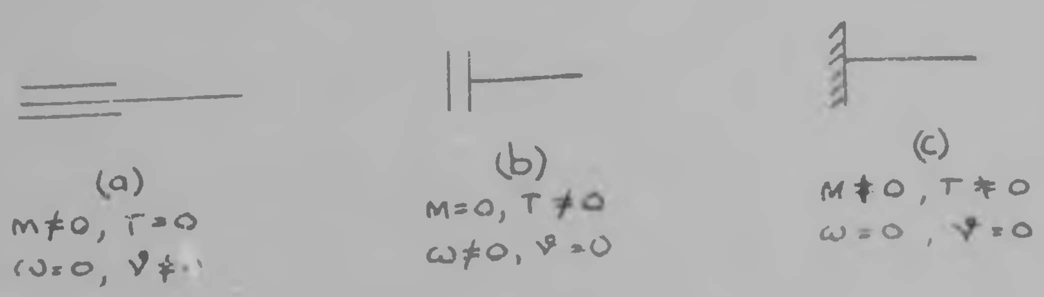

FIGURE 3.1

FIGURE 3.2

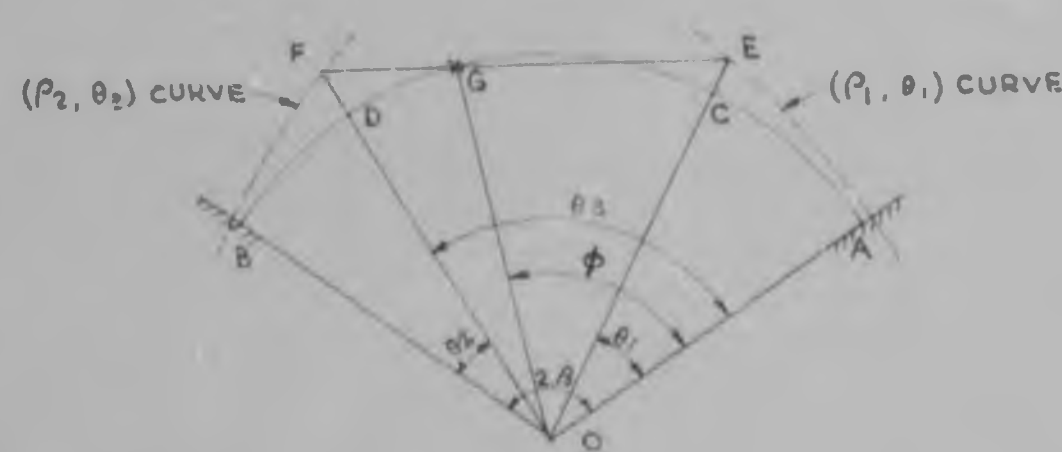

FIGURE 3.3

X = POINT LOAD

CHAPTER 3

SINGLE CONCENTRATED LOAD

3.1 Introduction

The notation used for the supports is the same as that used by Johansen: the three types of support illustrated in Fig. 3.1 are self-explanatory where ω, ν are the rotations of the girder at the support about the bending and torsional axes respectively.

The general principles for the calculation of single, concentrated collapse loads have been developed by Johansen[3] and extended by Boulton and Boonsukha[4]. Johansen has dealt with a central load only as the algebra becomes tedious in more complicated cases and has considered the three support types in Fig. 3 (a), (b) and (c). Boulton and Boonsukha have introduced trial - and - error graphical procedures for calculation when the load is at any point on the girder for the fully fixed case shown in Fig. 3.1 (c). The present chapter is aimed at developing the graphical method into a mathematical form suitable for a trial - and - error solution, using digital computers and also at extending the solution for the type of support reaction shown in Fig. 3.1 (a) to the case with a point load at any point on the arc.

The comparison of the results obtained from the study of reaction types (a) and (c) forms the basis of the final section of this chapter which deals with cases of intermediate fixity. Certain conclusions useful for design purposes will be given.

3.2 Fully Fixed Case

Collapse can occur in three modes, depending on the value of $a = \frac{T_p}{M_p}$. The position of the hinges is as shown in Fig. 3.2. The approximate direction of the axes of rotation of the hinges is indicated by arrows; the rotations are clockwise when viewed in the direction of the arrows.

Mode 1 occurs at small values of α, that is, when the torsional strength is small compared to the bending strength, and consists of four hinges, two fixed hinges at the supports and two free hinges on the arc on either side of the point load. The free hinges must be in pure torsion as demonstrated in the previous chapter. Mode 2 consists of two fixed hinges and one free hinge, and occurs at intermediate values of α. In mode 3 there are three fixed hinges, at the supports and at the load. This mode occurs when the torsional strength is high.

Modes 1 and 2 are too complicated algebraically for direct solution: for these, the graphical method of Boulton and Boonsukha will be described, and extended to a form soluble by electronic computer techniques.

Mode 1 - Low Torsional Strength In this mode (referring to Fig. 3.3) plastic hinges form at A, B, C and D. As the load W is concentrated at G, the hinges at C and D must be free hinges, and therefore in pure torsion.

The shear force, bending moment and torque at supports A and B may be represented by the single forces R_1 at E on OC produced and R_2 at F on OD produced respectively. Clearly, E, G and F must be colinear. This method of representing the support reactions will be adopted throughout the present work.

Johansen has deduced an equation which gives the locus of a reaction point (F or E in Fig. 3.3), if there is a fixed hinge at the support to which it corresponds, and a free hinge in pure torsion at a point where the radius through the reaction point intersects the girder. To illustrate this, the equation of the locus of E will be found, given that there are hinges at A and C.

If O E = ρ_1 and if the angle A O E is θ_1 as shown, then for a plastic hinge at A:

$$\alpha^2 R_1^2 \rho_1^2 \sin^2 \theta_1 + R_1^2 (r - \rho_1 \cos \theta_1)^2 = T_p^2,$$

from the yield criterion (2.2), and since

$$M_1 = R_1 \rho_1 \sin \theta_1 \text{ and } T_1 = R_1 (r - \rho_1 \cos \theta_1).$$

For a plastic hinge at C (in pure torsion):

$$R_1(\rho_1 - r) = T_p.$$

The two equations may be combined:

$$\frac{T_n^2}{R_1^2} = \alpha^2\rho_1^2 \sin^2\theta_1 + (r - \rho_1 \cos\theta_1)^2$$
$$= (\rho_1 - r)^2,$$

or $$2\rho_1 r(1 - \cos\theta_1) = (1 - \alpha^2)\rho_1^2 \sin^2\theta_1$$
$$= \rho_1^2 (1 - \alpha^2)(1 - \cos^2\theta_1).$$

Cancelling ρ_1 $(1 + \cos\theta_1)$ from each side, and solving for ρ_1:

$$\rho_1 = 2r/(1 - \alpha^2)(1 + \cos\theta_1) \quad \ldots\ldots\ldots \quad (3.1)$$

Hence the locus (ρ_1, θ_1) of R_1 at E depends only on r and α.

In essence, the graphical procedure previously referred to is as follows:
The bow girder centre line, with given central angle 2β is plotted out to a large scale. For any value of α, curves at each support can be plotted, which give the locus of possible reaction points, as shown in Fig. 3.3.

A trial position for the point E is selected on the curve (ρ_1, θ_1). The position of F is then fixed since E G F is a straight line and since F is on a curve similar to the curve for E. The values of R_1 and R_2 are given by the basic equations:

$$R_1 + R_2 = W \quad \ldots\ldots\ldots\ldots\ldots\ldots\ldots \quad (3.2)$$

and $$R_1 l_1 = R_2 l_2 \quad \ldots\ldots\ldots\ldots\ldots\ldots\ldots\ldots \quad (3.3)$$

where l_1 = EG and l_2 = FG, which are found by scaling.

The condition which finally fixes the values of θ_1 and θ_2 (= the angle B O F), is that the hinges A and C form at the same values of M_p and T_p as those at B and D. This is true if:

$$(\rho_1 - r) R_1 = (\rho_2 - r) R_2 = T_p \ldots\ldots\ldots\ldots \quad (3.4)$$

For any position of the load, there is a unique solution, depending on the value of α.

The refinements of the graphical method may be found in the paper by Boulton and Boonsukha[4]. In the present work, polar co-ordinates are used since a quicker solution in terms of machine time on the electronic computer is obtained. A solution was first obtained using a rectangular system, and the results of the two methods were found to correspond exactly. In Fig. 3.3, O is the pole, and OA the polar axis.

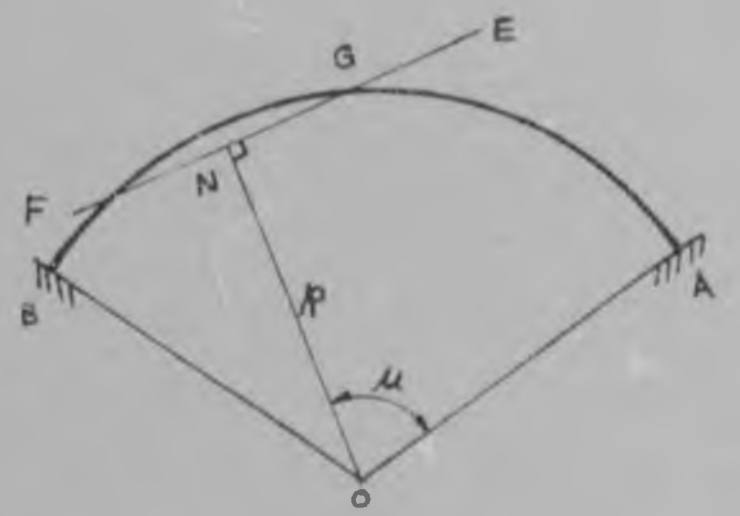

FIGURE 3.4

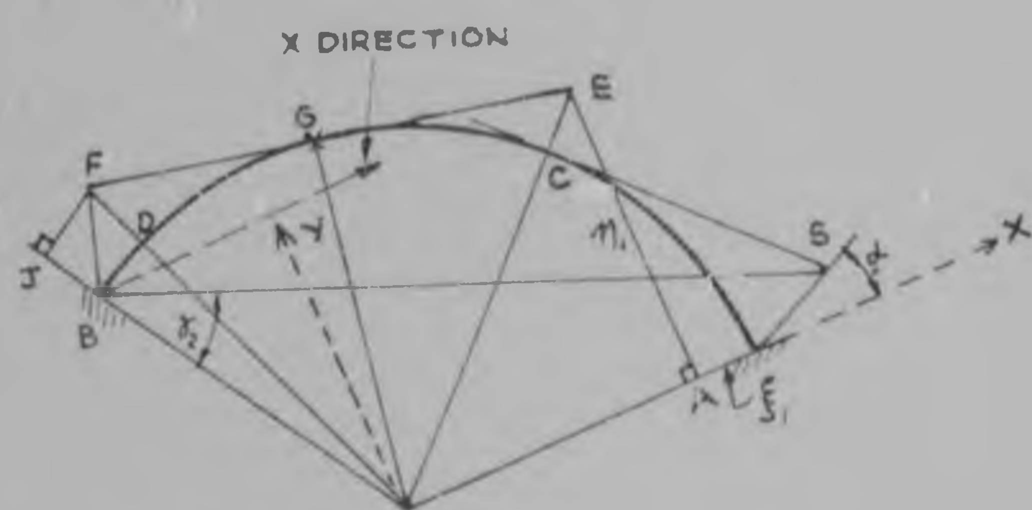

FIGURE 3.5

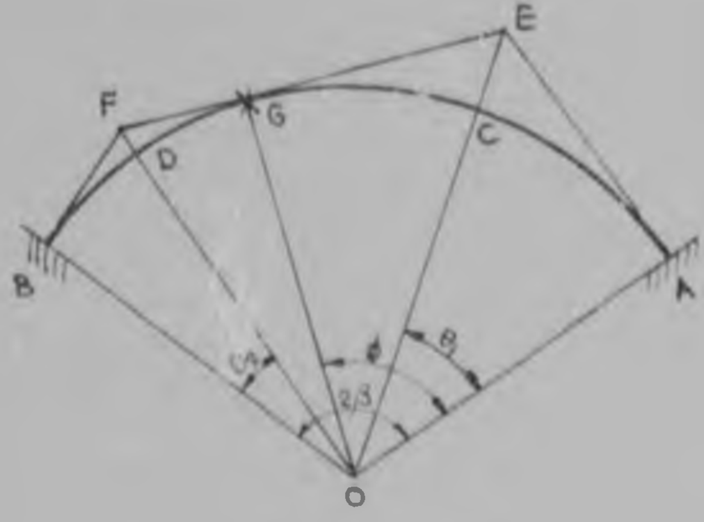

FIGURE 3.6

Referring to Fig. 3.3, the equation of the locus of E (ρ_1, θ_1) is the parabola of equation (3.1):

$$\rho_1 = 2r/(1 - \alpha^2)(1 + \cos\theta_1).$$

Since E, G and F are the colinear, the solution clearly requires the intersection of straight line EG with another parabola of the same shape as that given by equation (3.1), but with OB as axis instead of OA. The equation of the second parabola (ρ_2, θ_3), where θ_3 = the angle AOF, is given by the rotation of the axis of the parabola (3.1) through an angle 2β. Hence the equation of the locus of F(ρ_2, θ_3) is given by

$$\rho_2 = 2r/(1 - \alpha^2)(1 + \cos\theta_2) \quad \ldots\ldots\ldots\ldots \quad (3.5)$$

where $\theta_2 = 2\beta - \theta_3$.

The equation of the line EGF is of the form

$$r = p/\cos(\theta - \mu) \quad \ldots\ldots\ldots\ldots\ldots\ldots\ldots\ldots \quad (3.6)$$

where (r, θ) are the polar co-ordinates of any point on the line, and the point N(p, μ) is such that ON is normal to EGF (see Fig. 3.4).

The trial - and - error method requires an initial estimate of the size of θ_1 and, using equation (3.1), ρ_1 is obtained. Using these estimated co-ordinates of E (ρ_1, θ_1) and the given co-ordinates of G (r_{cg}, ϕ_{cg}), the line EGF is fixed i.e. constants p and μ can be calculated by substitution of the known values in equation (3.6). (The reason for the use of the co-ordinates (r_{cg}, ϕ_{cg}) will be clear in Chapter 4; for this chapter, r_{cg} = r, the radius of the bow girder).

Hence,

$$r_{cg} = p/\cos(\phi_{cg} - \mu)$$

and, $$\rho_1 = p/\cos(\theta_1 - \mu)$$

Therefore

$$\rho_1/r_{cg} = \frac{\cos\mu\ \cos\phi_{cg} + \sin\mu\ \sin\phi_{cg}}{\cos\mu\ \cos\theta_1 + \sin\mu\ \sin\theta_1}$$

$$= \frac{\cos\phi_{cg} + \tan\mu\ \sin\phi_{cg}}{\cos\theta_1 + \tan\mu\ \sin\theta_1}.$$

Solving for $\tan\mu$,

$$\tan\mu = \frac{\cos\phi_{cg} - (\rho_1/r_{cg})\cos\theta_1}{(\rho_1/r_{cg})\sin\theta_1 - \sin\phi_{cg}} \quad \ldots\ldots \quad (3.7)$$

The distance p may now be solved for using either of the initial simultaneous equations.
Hence,

$$p = r_{cg}\cos(\phi_{cg} - \mu) \quad \ldots\ldots\ldots\ldots\ldots\ldots \quad (3.8)$$

The solution now requires the co-ordinates of F, which are given by the intersection of the line EGF and the parabola of equation (3.5).

If the intersection point is denoted by (ρ_2, θ_3) with respect to the polar co-ordinate system, from (3.6),

$$\rho_2 = {}^{p}/_{\cos(\theta_3 - \mu)},$$

and from (3.5),

$$\rho_2 = {}^{2r}/_{(1-\alpha^2)\{1 + \cos(2\beta - \theta_3)\}}.$$

Using these two equations to solve for θ_3, i.e. eliminating ρ_2:

$$p(1-\alpha^2)\{1 + \cos(2\beta - \theta_3)\} = 2r\cos(\theta_3 - \mu)$$

or $$p(1-\alpha^2)(1 + \cos 2\beta\cos\theta_3 + \sin 2\beta\sin\theta_3) = 2r(\cos\theta_3\cos\mu + \sin\theta_3\sin\mu).$$

Hence,

$$\cos\theta_3\{p(1-\alpha^2)\cos 2\beta - 2r\cos\mu\} + \sin\theta_3\{p(1-\alpha^2)\sin 2\beta - 2r\sin\mu\} = -p(1-\alpha^2)$$

or $\quad T\cos\theta_3 + U\sin\theta_3 = V,$

where $\quad T = (1-\alpha^2)\cos 2\beta - 2r\cos\mu,$

$\quad U = p(1-\alpha^2)\sin 2\beta - 2r\sin\mu,$

and $\quad V = p(1-\alpha^2).$

Hence $\quad T + U\tan\theta_3 = V\sec\theta_3.$

Therefore

$$(T + U\tan\theta_3)^2 = V^2(1 + \tan^2\theta_3)$$

i.e. $$(U^2 - V^2)\tan^2\theta_3 + 2UT\tan\theta_3 + T^2 - V^2 = 0,$$

which is a quadratic in $\tan\theta_3$ of the form

$$A\tan^2\theta_3 + B\tan\theta_3 + C = 0 \quad \ldots\ldots\ldots \quad (3.9)$$

where

$$A = U^2 - V^2 = - p^2(1-\alpha^2)^2 \cos^2 2\beta - 4\, rp(1-\alpha^2) \sin 2\beta \sin\mu + 4\, r^2 \sin^2 \mu \quad \text{..........} \quad (3.10a)$$

$$B = 2UT = 2\{p(1-\alpha^2) \sin 2\beta - 2\, r \sin\mu\} \{p(1-\alpha^2) \cos 2\beta - 2r \cos\mu\} \quad \text{..................} \quad (3.10b)$$

and

$$C = T^2 - V^2 = - p^2(1-\alpha^2)^2 \sin^2 2\beta - 4\, rp(1-\alpha^2) \cos 2\beta \cos\mu + 4\, r^2 \cos^2 \mu \quad \text{.........} \quad (3.10c)$$

Hence
$$\tan\theta_3 = \frac{- B \pm \sqrt{B^2-4AC}}{2A} \quad \text{.................} \quad (3.11)$$

The straight line EGF intersects the parabola of equa[illegible].5) twice, given by the two solutions in equation [illegible]11), and inspection (see Fig. 3.3) shows that the greater angle is the required solution. When the central angle of the bow girder is less than 180^o, it is clear by inspection that $V>0$ and therefore $A = U^2 - V^2$ is negative. Hence the larger angle given by (3.11) corresponds to the negative sign before the square root.

As in the graphical procedure described, the final solution is obtained when the hinges at A and C occur at the same values of M_p and T_p as those at B and D. The equations (12), (13) and (14) are used in this step and the equations for the collapse load are easily deduced as:

$$\left(\frac{Wr}{M_p}\right)_1 = \frac{\alpha(\ell_1 + \ell_2)}{\ell_2 (\rho_1 - 1)} \quad \text{....................} \quad (3.12a)$$

$$\left(\frac{Wr}{M_p}\right)_2 = \frac{\alpha(\ell_1 + \ell_2)}{\ell_1 (\rho_2 - 1)} \quad \text{....................} \quad (3.12b)$$

where

$$\ell_1 = EG = \{\rho_1{}^2 + r_{cg}{}^2 - 2\rho_1 r_{cg} \cos(\emptyset-\theta_1)\}^{\frac{1}{2}} \quad (3.13a)$$

$$\ell_2 = FG = \{\rho_2{}^2 + r_{cg}{}^2 - 2\rho_2 r_{cg} \cos(2\beta-\emptyset-\theta_2)\}^{\frac{1}{2}} \quad \text{......} \quad (3.13b)$$

Details of the computer programme used for the calculation are given in the Appendix. The values obtained for the collapse load are in the dimensionless form Wr/M_p. Each value of Wr/M_p, for any given value of 2β and $P\emptyset$, depends only on α. Hence the results may be plotted in a dimensionless form, as were the results obtained graphically by Boulton and Boonsukha.

Imegwu[6] has described a method, also using an electronic computer, which gives a simpler solution, in that θ_1 is obtained directly in terms of θ_2. Some results published by Imegwu were checked and the results were found to agree almost exactly.

<u>Mode 2 - Moderate Torsional Strength</u>. For girders with the load placed unsymmetrically, at intermediate values of α, collapse by mode 2 occurs; in this mode the hinge at D disappears. A description of the transition from mode 1 to mode 2 is given in Chapter 5.

The failure mode now consists of hinges at A, B and C, the hinge at C being in pure torsion (see Fig. 3.5). The geometrical condition is imposed that the three axes of rotation of the hinges must intersect in one point S, as has been proved in section 2.3. The free plastic hinge occurs on the longer arc measured from the point load at G to the supports. The graphical method devised by Boulton and Boonsukha for mode 2 is similar to that for mode 1; a trial position θ_1 is selected, which fixes the position of E which is on the parabola defined by equation (3.1). As before, the line EGF is now fixed. The position of F is determined by the condition that the axes of rotation of the hinges intersect in S. The point S is obtained by the intersection of the tangent at C and the line AS which is defined by

$$\tan \gamma_1 = {}^{T_1}/_{\alpha^2 M_1} = {}^{R\xi_1}/_{\alpha^2 R\eta_1} = {}^{\xi_1}/_{\alpha^2\eta_1}, \text{ from equation (2.3)}$$

where γ_1 is the angle between OA produced and the axis of rotation AS, and $\xi_1 = AH$, $\eta_1 = EH$; EH is perpendicular to the radius OA.

Hence $\tan \gamma_2$ may be easily found graphically as γ_2 is the angle between the radius OB and BS. Now

$${}^{T_2}/_{M_2} = \alpha^2 \tan \gamma_2$$

which defines the slope of BF.

The condition which finally fixes the correct trial value of θ_1 is that the hinges at A and C occur at the same value of T_2 as the hinge at B, i.e. the equations

$$R_1(\rho_1 - r) = T_p \quad \ldots\ldots\ldots\ldots\ldots\ldots\ldots \quad (3.14a)$$

$$\alpha^2 R_2^2 \eta_2^2 + R_2^2 \xi_2^2 = T_p^2 \quad \ldots\ldots\ldots\ldots \quad (3.14b)$$

are satisfied.

For the numerical trial - and - error solution, the rectangular co-ordinate system OXY (see Fig. 3.5) has been used. The locus of E, as before, is defined by equation (3.1):

$$\rho_1 = 2r/(1 - \alpha^2)(1 + \cos \theta_1)$$

The Cartesian co-ordinates of E are given by

$$x_E = \rho_1 \cos \theta_1 \quad \ldots\ldots\ldots\ldots\ldots\ldots\ldots\ldots \quad (3.15a)$$

$$y_E = \rho_1 \sin \theta_1 \quad \ldots\ldots\ldots\ldots\ldots\ldots\ldots\ldots \quad (3.15b)$$

The equation of AS is

$$y = (\tan \gamma_1)(x - r)$$

$$= \frac{\xi_1}{\alpha^2 \eta_1} (x - r),$$

i.e. $$y = \frac{r - x_E}{\alpha^2 y_E}(x - r).$$

The equation of BS is

$$y - r \sin \theta_1 = -\frac{x_E}{y_E} (x - r \cos \theta_1).$$

The co-ordinates of S are given by the intersection of AS and BS. Hence:

$$\frac{x_S}{r} = \frac{\alpha^2(\frac{x_E}{r} \cos \theta_1 + \frac{y_E}{r} \sin \theta_1) + 1 - \frac{x_E}{r}}{1 - \frac{x_E}{r} (1 - \alpha^2)}, \quad ..(3.15a)$$

and using the equation for AS:

$$\frac{y_S}{r} = \frac{1 - {x_E}/r}{\alpha^2 \, {y_E}/r} (\frac{x_S}{r} - 1) \quad \ldots\ldots\ldots\ldots\ldots\ldots \quad (3.16b)$$

The angle γ_2 between the lines OB and SB is given by

$$\tan \gamma_2 = \frac{m_{SB} - m_{OB}}{1 + m_{SB}\, m_{OB}}$$

where m_{OB} and m_{SB} are the slopes of OB and SB respectively.

Since $m_{OB} = \tan 2\beta$

and $$m_{SB} = \frac{y_B - y_S}{x_B - x_S},$$

$$\tan \gamma_2 = \frac{\frac{x_S}{r}\sin 2\beta - \frac{y_S}{r}\cos 2\beta}{1 - \frac{x_S}{r}\cos 2\beta - \frac{y_S}{r}\sin 2\beta} \quad \ldots \quad (3.17)$$

The slope of BF is given by $\tan \delta_1$, δ_1 being the angle between BF and the X-direction. Now

$$\delta_1 = 2\beta - (\pi/2 - \delta_2) \quad \ldots\ldots\ldots\ldots\ldots\ldots\ldots \quad (3.18)$$

where δ_2 is the angle BFJ, and

$$\delta_2 = \text{arc} \tan (\alpha^2 \tan \gamma_2). \quad \ldots\ldots\ldots\ldots\ldots \quad (3.19)$$

The co-ordinates of F are found by the intersection of BF and EG. The equation of EG is given by

$$\frac{y}{r} = \left(\frac{\frac{y_E}{r} - \frac{r_{cg}}{r}\sin \phi_{cg}}{\frac{x_E}{r} - \frac{r_{cg}}{r}\cos \phi_{cg}}\right)\frac{x}{r} + \frac{r_{cg}}{r}\sin \phi_{cg}$$
$$- \left(\frac{\frac{y_E}{r} - \frac{r_{cg}}{r}\sin \phi_{cg}}{\frac{x_E}{r} - \frac{r_{cg}}{r}\cos \phi_{cg}}\right)\cos \phi_{cg} \quad \ldots \quad (3.20)$$

the polar co-ordinates defining the point G are (r_{cg}, ϕ_{cg}): for this chapter $r_{cg} = r$. The reason for this notation will be clear in Chapter 4.

The equation of BF is

$$y = (\tan \delta_1)x + \sin 2\beta - \tan \delta_1 \cos 2\beta \quad \ldots \quad (3.21)$$

Having determined the co-ordinates of F by the method given in the Appendix, the equations for the conditions (3.14) are to be derived. The first part of (3.14) reduces (as before) to:

$$\left(\frac{W_r}{M_p}\right)_1 = \frac{(\ell_1 + \ell_2)}{\ell_2(\rho_1 - 1)}, \quad \ldots\ldots\ldots\ldots\ldots\ldots \quad (3.22a)$$

and the second part reduces to:

$$\left(\frac{W_r}{M_p}\right)_2 = \frac{\alpha(\ell_1 + \ell_2)}{\ell_1(\alpha^2 n_2^2 + \ell_2^2)^{\frac{1}{2}}} \quad \ldots\ldots\ldots\ldots\ldots \quad (3.22b)$$

Where $\alpha^2 n_2^2 + \ell_2^2 = \alpha^2\, \overline{BF}^2 \cos^2 \delta_2 + \overline{BF}^2 \sin^2 \delta_2$

$$= (\alpha^2\cos^2\delta_2 + \sin^2\delta_2)\{(x_F - \cos 2\beta)^2 + (y_F - \sin 2\beta)^2\} \quad \ldots \quad (3.23)$$

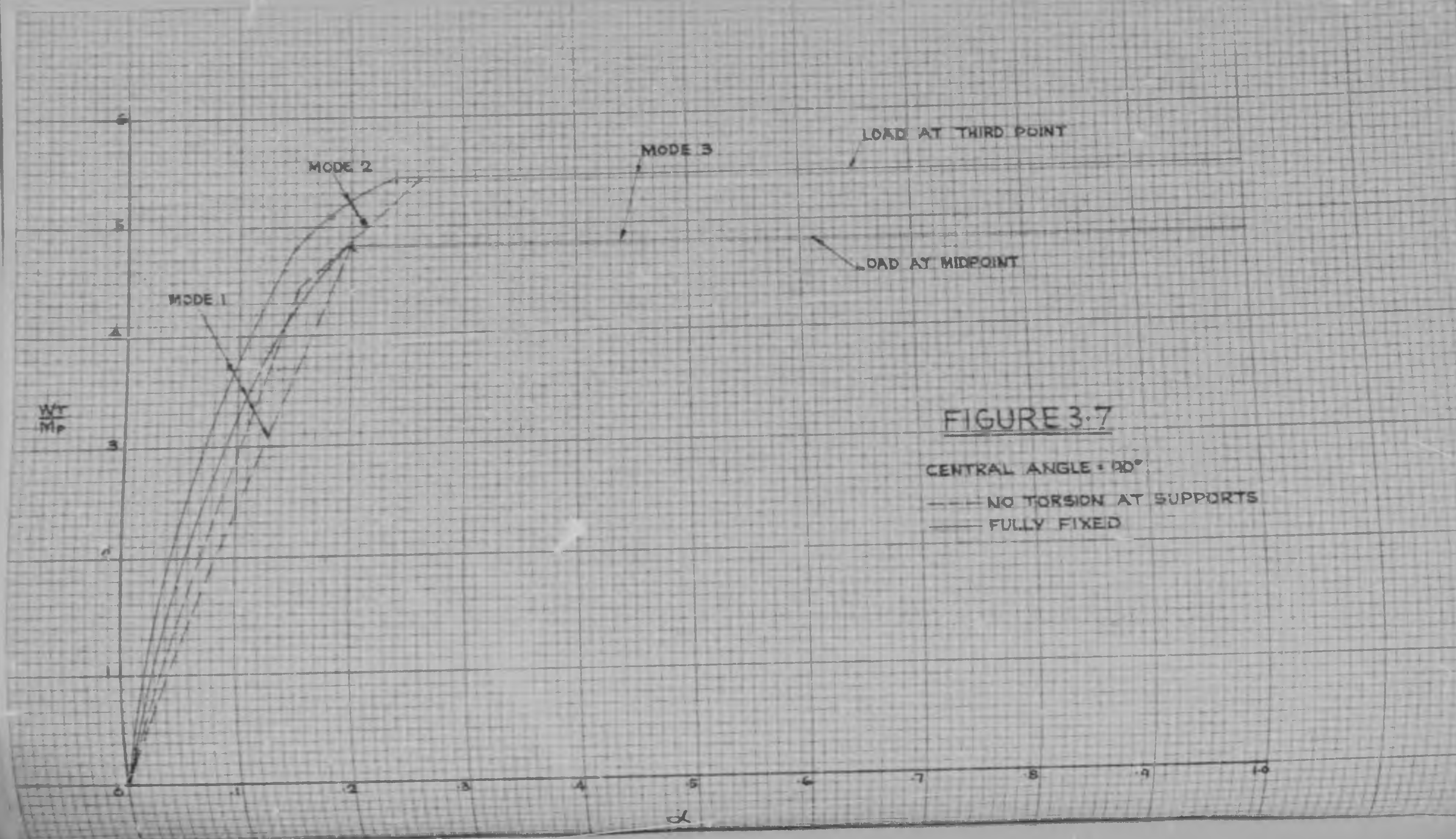
LOAD AT THIRD POINT
MODE 3
MODE 2
MODE 1
LOAD AT MIDPOINT
$\frac{WT}{M_P}$
α
0
·1
·2
·3
·4
·5
·6
·7
·8
·9
1·0
1
2
3
4
5
6
CENTRAL ANGLE = 120°
NO TORSION AT SUPPORTS
FULLY FIXED

FIGURE 3·7

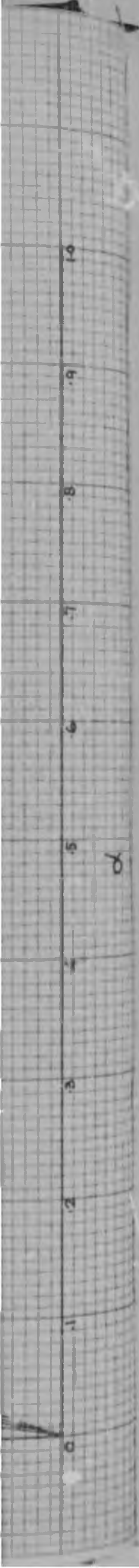
1.0
.9
.8
.7
.6
.5
α
.4
.3
.2
.1
0

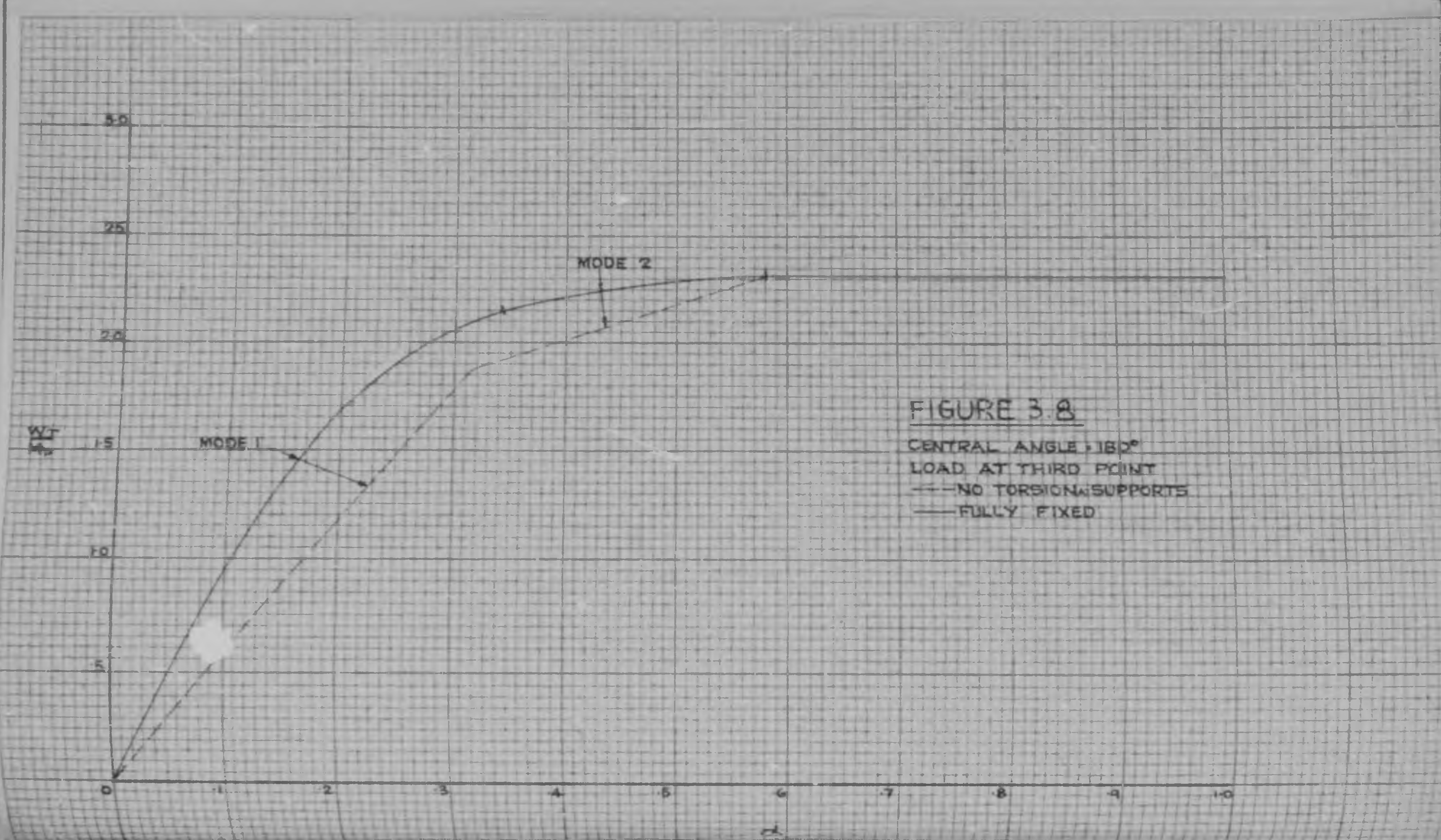

FIGURE 3.8

CENTRAL ANGLE = 180°
LOAD AT THIRD POINT
– – – NO TORSION AT SUPPORTS
——— FULLY FIXED

and

$$\ell_1 = EG = \{\rho_1^2 + r_{cg}^2 - 2\rho_1 r_{cg} \cos(\emptyset - \theta_1)\}^{\frac{1}{2}} \quad ..(3.24a)$$

$$\ell_2 = FG = \{\rho_2^2 + r_{cg}^2 - 2\rho_2 r_{cg} \cos(2\beta - \emptyset - \theta_2)\}^{\frac{1}{2}} \quad .....(3.24b)$$

When the equations (3.22a) and (3.22b) are simultaneously satisfied, the solution is complete.

Details of the solution using the computer are given in the Appendix.

Imegwu[6] has given a solution using a computer which is different from the solution described here. Almost exact agreement was obtained between results published by Imegwu and results obtained from computation by the present method.

Mode 3 - High Torsional Strength. This mode occurs at large values of α and consists of three hinges in pure bending at A, G and B in Fig. 3.6. The axes of rotation at A, G and B intersect in one point O. The solution is comparatively simple and has been derived by Johansen[3] as:

$$\frac{Wr}{Mp} = \cot(\beta - \emptyset/2) + \cot \emptyset/2 \quad ....(3.25)$$

The necessary condition for the solution is that a plastic hinge does not form at E, or

$$\alpha > \tan\frac{\theta_1}{2} = \tan(\beta/2 - \emptyset/4) \quad ....(3.26)$$

In Fig. 3.7 and 3.8 some complete solutions are shown for bow girders with central angles of 90° and 180°. The values of collapse load are, as already mentioned, in the dimensionless form $\frac{Wr}{Mp}$; for any given central angle 2β and loading point $\emptyset$, the graphs give solutions for any torsional strength. The values of α range from zero to 1.00, the maximum value.

The curves show how the collapse load varies with change in α. The transition from mode 1 to mode 2 is smooth, whereas the transition from mode 2 to mode 3 is not, except for girders with a central angle of 180°. It can be shown that a smooth transition takes place from mode 2 to a mode with hinges at A and B, that is, with AB as axis of rotation. However, for $2\beta < 180^\circ$ such a mode cannot develop, as the calculated values of moment and torque at the load point violate the yield

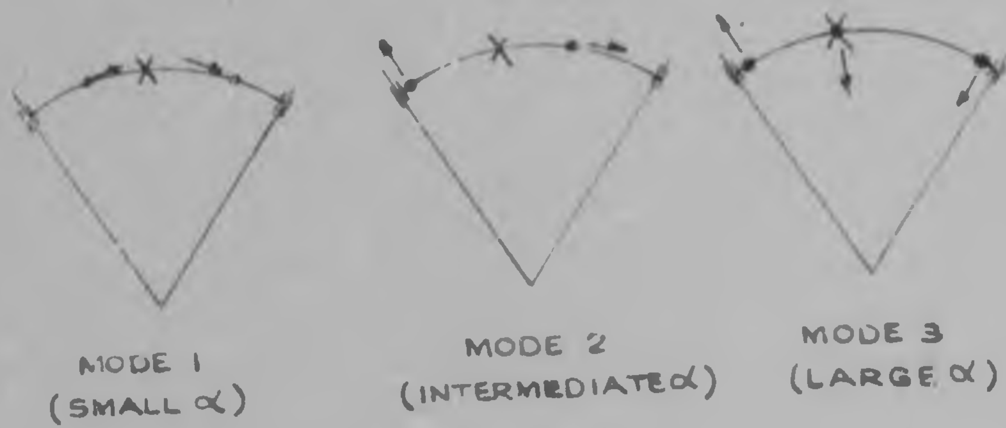

FIGURE 3.9

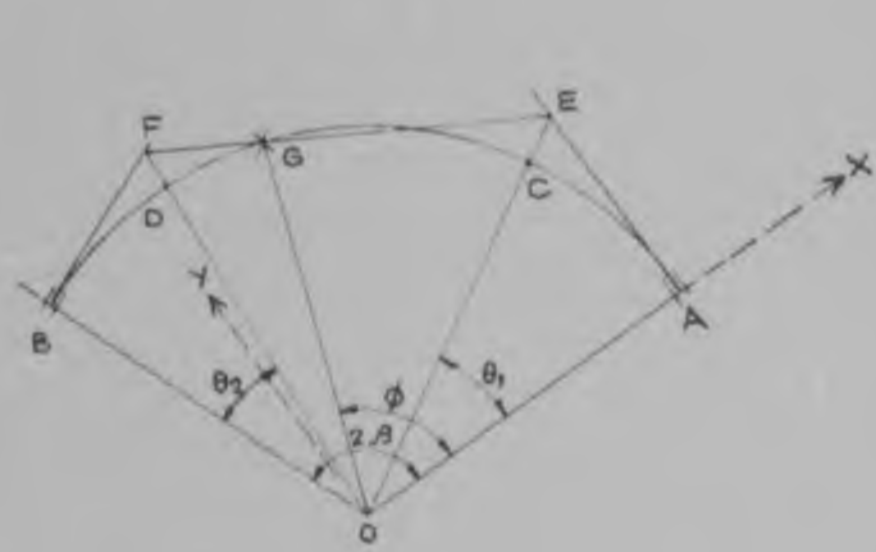

FIGURE 3.10

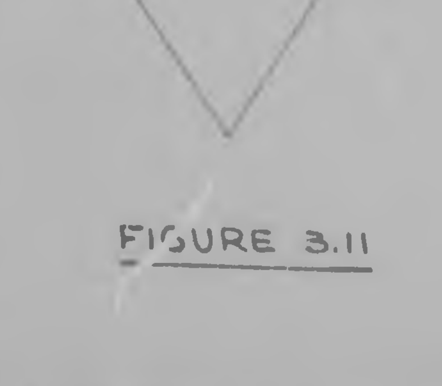

FIGURE 3.11

criterion. For $2\beta = 180^\circ$, the two- and three-hinge modes coincide. For $2\beta > 180^\circ$, it is possible that collapse can take place about a common axis joining the supports.

3.3 No Torsion at Supports

As previously mentioned, this case has been dealt with by Johansen for a single load on the centre of the girder: in the present section the solution is extended for the load at any point on the girder.

The collapse modes are analogous to those for the fully fixed case and will be designated modes 1, 2 and 3. In the present investigation modes 1 and 2 have been solved numerically using a digital computer.

In Fig. 3.9 the possible modes are shown. In mode 1 free hinges occur in pure torsion as shown; in mode 2 a hinge in pure torsion and a hinge in pure bending occur as shown. Mode 3 is identical to the mode 3 for the fully fixed case. The approximate direction of the axes of rotation at the hinges is shown.

It may sometimes happen that the free hinge and the bending hinge at the support occur at the same value of α: for this value of α modes 1 and 2 are combined, but this does not invalidate any of the following solutions.

<u>Mode 1 - Low Torsional Strength</u>. Since there is no torsion at the supports, the reaction points R_1 and R_2 at E and F respectively always fall on the tangents at A and B (see Fig. 3.10). For mode 1 failure, hinges in pure torsion occur at C and D, and the yield criterion is not exceeded at any other point on the girder. In the following a trial - and - error solution similar to that obtained in the last section and using an electronic computer is developed.

The co-ordinates of E with respect to the rectangular co-ordinate system OXY are $(r, r \text{ Tan } \theta_1)$ and G has co-ordinates $(r \cos \phi, r \sin \phi)$. The straight line EG is given by:

$$\frac{y - r \tan \theta_1}{r \sin \phi - r \tan \theta_1} = \frac{x - r}{r \cos \phi - r}.$$

Since the slope of BF is $- \cot 2\beta$ and the co-ordinates of B are $(r \cos 2\beta, r \sin 2\beta)$, the equation of BF is

$$y - r \sin 2\beta = - \cot 2\beta(x - r \cos 2\beta).$$

The co-ordinates of the intersection point F of these two lines are given by:

$$\frac{x_F}{r} = (\cos \phi - 1) \operatorname{cosec} 2\beta - \tan \theta_1 \cos \phi$$

and $$\frac{y_F}{r} = \frac{\operatorname{cosec} 2\beta(\sin \phi - \tan\theta_1) + \cot 2\beta(\tan\theta_1 \cos\phi - \sin\phi)}{\sin \phi - \tan \theta_1 + (\cos \phi - 1) \cot 2\beta}$$

Hence,

$$\tan (2\beta - \theta_2) = {}^{y_F}/_{x_F}$$

or

$$\tan(2\beta - \theta_2) = \frac{\operatorname{cosec} 2\beta(\sin\phi - \tan\theta_1) + \cot 2\beta(\tan \theta_1 \cos\phi - \sin\phi)}{(\cos \phi - 1) \operatorname{cosec} 2\beta - \tan \theta_1 \cos \phi + \sin \phi} \quad \ldots\ldots\ldots\ldots\ldots \quad (3.27)$$

The equations which give the final solution are

$$R_1(\rho_1 - r) = T_p \quad \ldots\ldots\ldots\ldots\ldots\ldots\ldots\ldots \quad (3.28a)$$

and $$R_2(\rho_2 - r) = T_p \quad \ldots\ldots\ldots\ldots\ldots\ldots\ldots\ldots \quad (3.28b)$$

If $\ell_1 = EG$ and $\ell_2 = FG$, $R_1\ell_1 = R_2\ell_2$ where $R_1 + R_2 = W$.

Since $\rho_1 = r \sec \theta_1$

and $\rho_2 = r \sec \theta_2$,

equations (3.28a) and 3.28b) reduce to

$$\left(\frac{Wr}{M_p}\right)_1 = \left(\frac{\alpha}{\sec \theta_1 - 1}\right)\left(\frac{\ell_1 + \ell_2}{\ell_2}\right) \quad \ldots\ldots\ldots\ldots\ldots \quad (3.29a)$$

$$\left(\frac{Wr}{M_p}\right)_2 = \left(\frac{\alpha}{\sec \theta_2 - 1}\right)\left(\frac{\ell_1 + \ell_2}{\ell_1}\right) \quad \ldots\ldots\ldots\ldots\ldots \quad (3.29b)$$

where

$$\ell_1 = EG = \rho_1^2 + r^2 - 2\rho_1 r \cos (\phi - \theta_1) \quad \ldots\ldots \quad (3.30a)$$

and $$\ell_2 = FG = \rho_2^2 + r^2 - 2\rho_2 r \cos (2\beta - \phi - \theta_2) \ldots \quad (3.30b)$$

Mode 2 - Moderate Torsional Strength. This mode occurs when α is too large for the formation of the free hinge at D, and a hinge in pure bending at B occurs; the support B is nearer to the load than the support A.

The equations developed in the preceding section all apply except for (3.28b) of the simultaneous yield equations (3.28) which become

$R_1(\rho_1 - r) = T_p$, as before,

and $R_2 \, r \tan \theta_2 = M_p$.

Hence the equations corresponding to (3.29) are

$$\left(\frac{Wr}{M_p}\right)_1 = \left(\frac{\alpha}{\sec \theta_1 - 1}\right)\left(\frac{\ell_1 + \ell_2}{\ell_2}\right) \quad \ldots\ldots\ldots\ldots\ldots \quad (3.31a)$$

$$\left(\frac{Wr}{M_p}\right)_2 = \cot \theta_2 \left(\frac{\ell_1 + \ell_2}{\ell_1}\right) \quad \ldots\ldots\ldots\ldots\ldots\ldots \quad (3.31b)$$

Mode 3 - High Torsional Strength. This mode is identical to mode 3 for the fully fixed case, and the equations (3.25) and (3.26) apply.

Some solutions for the no-torsion case can be seen in Figs. 3.7 and 3.8. The solution is composed of a succession of straight lines.

3.4 No Bending at Supports

This has not been solved in the general case in this work, as it is not of great practical importance.

Johansen has given a solution for a point load at the centre of the girder. In Fig. 3.11 a bow girder is shown with load at the centre. Since there is no bending moment at the supports, the reactions R_1 and R_2 must lie on the radii at A and B produced, at E and F respectively. Plastic hinges can form at A, B and G only; the hinges at A and B must be in pure torsion. For the central load, the hinge at B must be in pure bending. For the point load at any point on the girder, the same principles apply, except that a hinge forming at G would not necessarily be in pure bending.

3.5 Effect of Lack of Torsional Restraint

It can be seen from Figs. 3.7 and 3.8 that for a bow girder with a single concentrated load and a given central angle and loading position, the value of $\frac{Wr}{M_p}$ depends on α only; it is also evident that if α is above a certain value, collapse occurs by mode 3 whether the supports are torsionally restrained or not. From this it is clear that in the design of a bow girder, if a mode 3 failure is anticipated, an increase of torsional strength relative to bending strength does not increase the strength of the bow girder; a further conclusion is that the provision of an end connection designed to resist torsion does not increase the ultimate strength of the bow girder.

For cases of mode 1 and mode 2 failure, the collapse load depends on the value of α, and the provision of torsional strength at the support does increase the collapse load. In cases of partial fixity, where there is some torsional movement of the support, greater deflections than for the fully fixed case will result; the ultimate load will be unaffected if there is enough torsion at the supports to cause full plastic hinges to form at the supports. If, on the other hand, the torsional support movement is sufficient to allow the formation of free hinges on the arc without fixed hinges at the supports, the ultimate load will be less than for the fully fixed case.

It has been observed from the tests in Chapter 6 that, at large deflections, the collapse load tends to decrease. If torsional restraint is not provided for girders with low α, the effects of changes in geometry and instability would tend to be more marked.

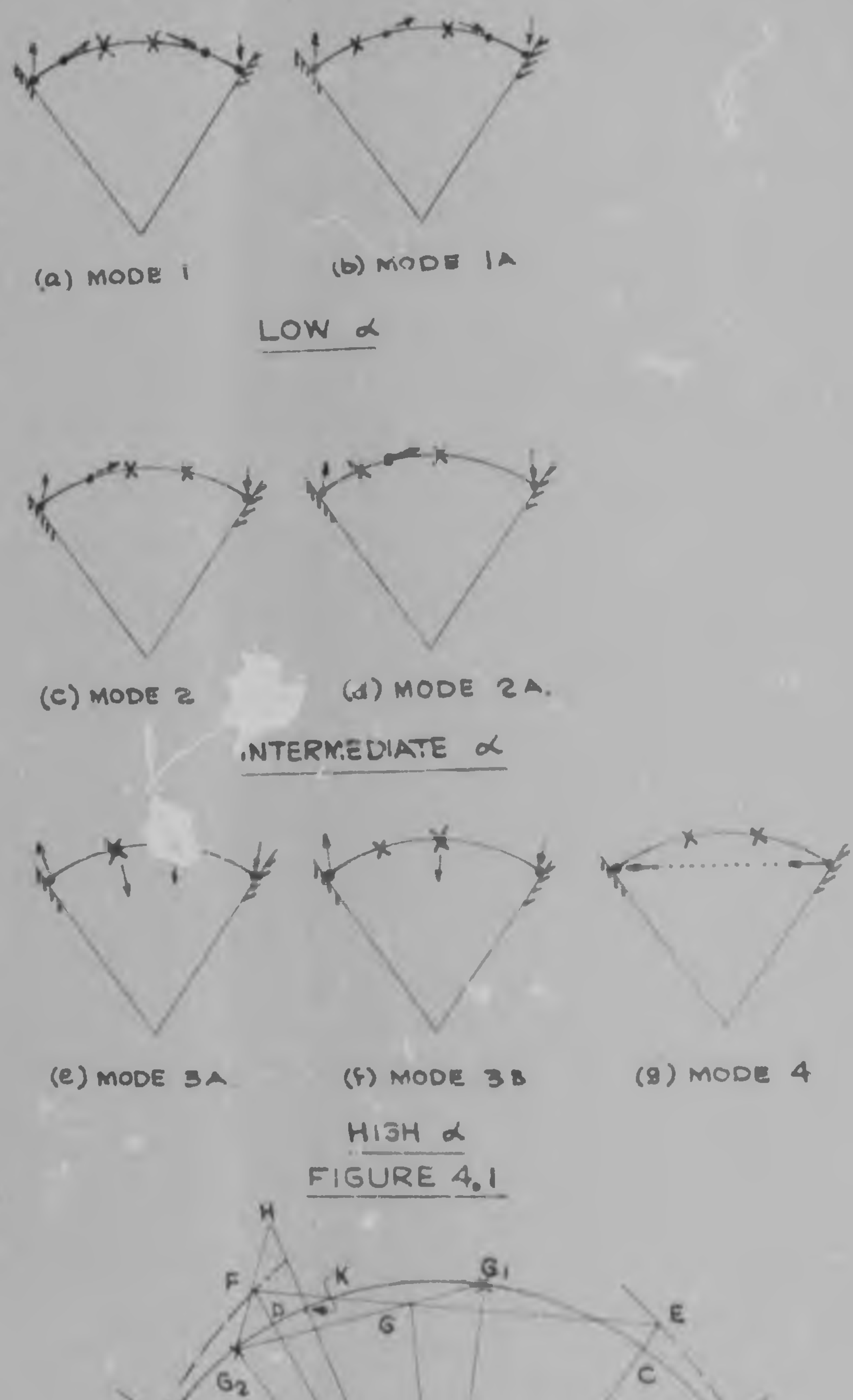

FIGURE 4.1

FIGURE 4.2

CHAPTER 4

TWO CONCENTRATED LOADS

4.1 Introduction

In this chapter, all the possible modes of failure for a circular girder fully fixed at the supports and loaded with two concentrated loads are investigated. Almost all of the solutions require the use of an electronic computer; some of the solutions are based directly on the results of the preceding chapter.

The effect of lack of torsional restraint at the supports is discussed, and in the final section some suggestions for the calculation of collapse loads of a girder loaded with several concentrated loads are made.

4.2 The Fully Fixed Case

There are various modes of failure for two concentrated loads: the modes are designated 1, 1A, 2, 2A, 3A, 3B and 4, and are analagous to those for a single concentrated load with the exception of mode 4. The modes are illustrated in Fig. 4.1.

The modes which can occur at low values of α are shown in Fig. 4.1 (a) and (b), and involve the formation of two free hinges. The main difference from the mode 1 of Chapter 3 is that one of the free hinges can occur between the two concentrated loads.

In the modes which occur at intermediate values of α, the possibility also exists of a hinge occurring between the two point loads, as shown in Fig. 4.1 (c) and (d).

When the results are plotted as $\frac{Wr}{M_p}$ against α, the transition from modes 1, 1A, 2 or 2A is a smooth one to a mode with two hinges at the supports as was the case for the single concentrated loads. The two-hinge mode is designated mode 4, and is illustrated in Fig. 4.1 (g). There are, as for the single load case, certain "foreign" modes, designated 3A and 3B, which correspond to the mode 3 of the previous chapter. The modes are illustrated in Figs 4.1 (e) and (f), and involve the formation of fixed hinges, at the supports and at the loads. When plotted on the curves mentioned above, the transition from lower modes to modes 3A and 3B is not necessarily a smooth one.

Modes 1, 1A - Low Torsional Strength. The conditions for mode 1A to be possible will first be considered.

In Fig. 4.2, G_1 and G_2 are the positions of the loads W_1 and W_2 respectively. The position of the centre of gravity of the loads W_1 and W_2 is at G. The angles ϕ_1, ϕ_2 and ϕ_{cg} are measured from OA to OG_1, OG_2 and OG respectively. The symbol r_{cg} designates the distance OG. Clearly EGF must be a straight line.

Johansen has shown that it is impossible for two free hinges to exist on the same unloaded beam section. In mode 1A failure, it is assumed that one hinge occurs between the loads. Assuming the hinge on $G_1 G_2$ to be near to G_2, i.e., that the reaction R_2 must be between G_1 and G_2, then the force acting on any cross-section of the member between G_1 and G_2 will be the resultant of W_2 and R_2, i.e. R_2-W_2, and is assumed to act upwards at H. This implies $R_2 > W_2$, which is true if R_2 lies between G_1 and G_2. Under these conditions the hinge will form at K, the intersection point of OH with the centre-line of the girder. The condition for a plastic hinge at K is

$$\overline{HK}\,(R_2-W_2) = T_p \quad \ldots\ldots\ldots\ldots\ldots\ldots \quad (4.1)$$

For a hinge at the support

$$a^2 R_2^2\, \eta_2^2 + R_2\, \xi_2^2 = T_p^2, \quad \ldots\ldots\ldots\ldots \quad (4.2)$$

where ξ_2 and η_2 have the same meaning as in the previous chapter.

The distance G_2H may be found by taking moments about the perpendicular to G_2H at G_2, i.e.,

$$\overline{G_2H} = \frac{R_2}{R_2-W_2}\,(\overline{FG_2}) \quad \ldots\ldots\ldots\ldots\ldots\ldots \quad (4.3)$$

If $OF = \rho_2$, $OH = \rho_3$ and θ_2 = the angle BOF, then by the cosine rule

$$\rho_3^2 = \overline{OG_2}^2 + \overline{G_2H}^2 - 2\,\overline{OG_2}\cdot\overline{G_2H}\cos(OG_2H).$$

By the sine rule, and as the angle $G_2OF = \theta_2 - 2\beta + \phi_2$,

$$\sin(OG_2H) = \frac{\rho_2 \sin(\theta_2 - 2\beta + \phi_2)}{\overline{FG_2}}.$$

Substituting this and $\overline{OG_2} = r$ in the above equation:

$$\rho_3^{\ 2} = r^2 + \overline{G_2H}^2 - 2r\ .\ \overline{G_2H}\ \{1 - \frac{\rho_2^{\ 2}\ \sin^2(\theta_2 - 2\beta + \phi_2)}{\overline{FG_2}^{\ 2}}\}^{\frac{1}{2}}.$$

Substituting from (4.3) for $\overline{G_2H}$:

$$\rho_3^{\ 2} = r^2 + (\frac{R_2}{R_2 - W_2})^2\ \overline{FG_2}^{\ 2} - \frac{2rR_2}{R_2 - W_2}\ \{\overline{FG_2}^{\ 2} - \rho_2^{\ 2}\ \sin^2(\theta_2 - 2\beta + \phi_2)\}^{\frac{1}{2}}.$$

Since $\overline{FG_2}^{\ 2} = \rho_2^{\ 2} + r^2 - 2\rho_2\ r\ \cos\ (\theta_2 - 2\beta + \phi_2)$,

$$\frac{\rho_3^{\ 2}}{r^2} = 1 + (\frac{R_2}{R_2 - W_2})^2\ \{\frac{\rho_2^{\ 2}}{r^2} + 1 - 2\frac{\rho_2}{r}\ \cos(\theta_2 - 2\beta + \phi_2)\}$$

$$- \{\frac{2\ R_2}{R_2 - W_2}\}\{\frac{\rho_2^{\ 2}}{r^2}\ \cos^2(\theta_2 - 2\beta + \phi_2) - \frac{2\rho_2}{r}\cos(\theta_2 - 2\beta + \phi_2) + 1\}^{\frac{1}{2}}$$

or

$$\frac{\rho_3^{\ 2}}{r^2} = 1 + (\frac{R_2}{R_2 - W_2})^2 (\frac{\rho_2^{\ 2}}{r^2} + 1 - \frac{2\rho_2}{r}\ \cos(\theta_2 - 2\beta + \phi_2))$$

$$- \{\frac{2\ R_2}{R_2 - W_2}\}\{\frac{\rho_2}{r}\ \cos\ (\theta_2 - 2\beta + \phi_2) - 1\}\ \ ....\ (4.4)$$

Since $\overline{HK} = \rho_3 - r$, the value of ρ_3 from (4.4) could be substituted in (4.1) and combined with (4.2) to give a new equation to replace equation (3.5) of the previous chapter, which gives the equation of the locus of possible reaction points if there is a fixed hinge at the support and a free hinge on the span.

However, if $(\theta_2 - 2\beta + \phi_2)$ is small, so that $\cos(\theta_2 - 2\beta + \phi_2)$ is nearly equal to unity, then

$$\frac{\rho_3^{\ 2}}{r^2} = \{(\frac{R_2}{R_2 - W_2})(\frac{\rho_2}{r} - 1) - 1\}^2$$

or $$\frac{\rho_3}{r} - 1 = (\frac{R_2}{R_2 - W_2})(\frac{\rho_2}{r} - 1),$$

and equation (4.1) becomes

$$R_2(\frac{\rho_2}{r} - 1) = \frac{T_p}{r},$$

which is the condition for a free hinge on the arc opposite the reaction point, as if the girder was loaded with a single concentrated load at the centre of gravity of the two concentrated loads.

Hence it may be stated:

(i) if mode 1 in Fig. 4.1(a) occurs, the locus of reaction points is the same as for the single concentrated load.

(ii) if the free hinge occurs between the point loads and the position of the hinge is such that R_2 is close to W_2, with the result that the angle $(\theta_2 - 2\beta + \phi_2)$ is small, the locus of reaction points is almost the same as for the single concentrated load.

(iii) if $(\theta_2 - 2\beta + \phi_2)$ is not small, the locus of reaction points must be derived using equations (4.1), (4.2) and (4.4).

The present work is confined to the solutions of cases (i) and (ii), and it has been found that the solution (iii) is not often necessary.

For the two solutions (i) and (ii), all the equations of the mode 1 solution for a single concentrated load may be used, if the two loads W_1 and W_2 are replaced by a load $(W_1 + W_2)$ at a point with polar co-ordinates (r_{cg}, ϕ_{cg}) with respect to CA, that is, by replacing the two loads by a single one at the centre of gravity. As the position of the load in Chapter 3 was at a point (r_{cg}, ϕ_{cg}) the same computer programme has been used for the present solution. Details of this programme are given in the Appendix.

Modes 2 and 2A - Moderate Torsional Strength. The failure by mode 2 illustrated in Fig. 4.1 (c) is similar to the single load case. If the two loads acting are W_1 and W_2 and if these loads are replaced by a single load $(W_1 + W_2)$ acting at centre of gravity of the two loads, specified by the polar co-ordinates (r_{cg}, ϕ_{cg}) then the equations derived in Chapter 3 for the single concentrated load apply. Hence the computer programme used for the single concentrated load may be used. Details of the computer programme are given in the Appendix.

Mode 2A, shown diagrammatically in Fig. 4.1 (d), is an unlikely failure mode. In this mode one free hinge is assumed to occur between the two loads. In the transition from mode 1A to mode 2A, the hinge on the shorter arc, measured from the centre of gravity of the loads to the supports, disappears first. Since the hinge between loads is usually on the shorter arc, the mode 2 failure is most common.

Mode 2A could occur if $W_2 \gg W_1$ and, referring to Fig. 4.2, G is close to G_2. Since the position of the free torsion hinge in this mode is different from the position given by the mode 2 solution, the condition that the three hinges must intersect in one point requires calculation of the new position of the torsion hinge, involving the use of equations (4.1), (4.2) and (4.4).

The failure by mode 2A has not been worked out in detail in this investigation.

Modes 3A and 3B - High Torsional Strength. In failure by mode 3A, fixed plastic hinges occur at both loads and at the supports. A solution is easily obtained if the loading is symmetrical. However, the more general problem of unsymmetrical loading has been worked out in such a form as to be solved using an electronic computer.

As before, W_1 and W_2 act at G_1 and G_2 respectively, which are defined in position by polar co-ordinates (r, ϕ_1) and (r, ϕ_2) with respect to OA. The centre of gravity of the loads, the point G, is defined in position by co-ordinates (r_{cg}, ϕ_{cg}). The reaction R_1 acts at E, and R_2 acts at F.

Plastic hinges form at A, G_1, G_2, and B. It can be shown that E and F usually lie on the bisector of the angles AOG_1 and BOG_2, respectively. For the formation of hinges at A and G_1, the yield criterion must be satisfied at these points. If the line EL is perpendicular to OA, and if ξ_1 = AL and η_1 = EL, then the bending moment and torque at A are given by

$$M_A = R_1 \eta_1$$

and $$T_A = R_1 \xi_1 .$$

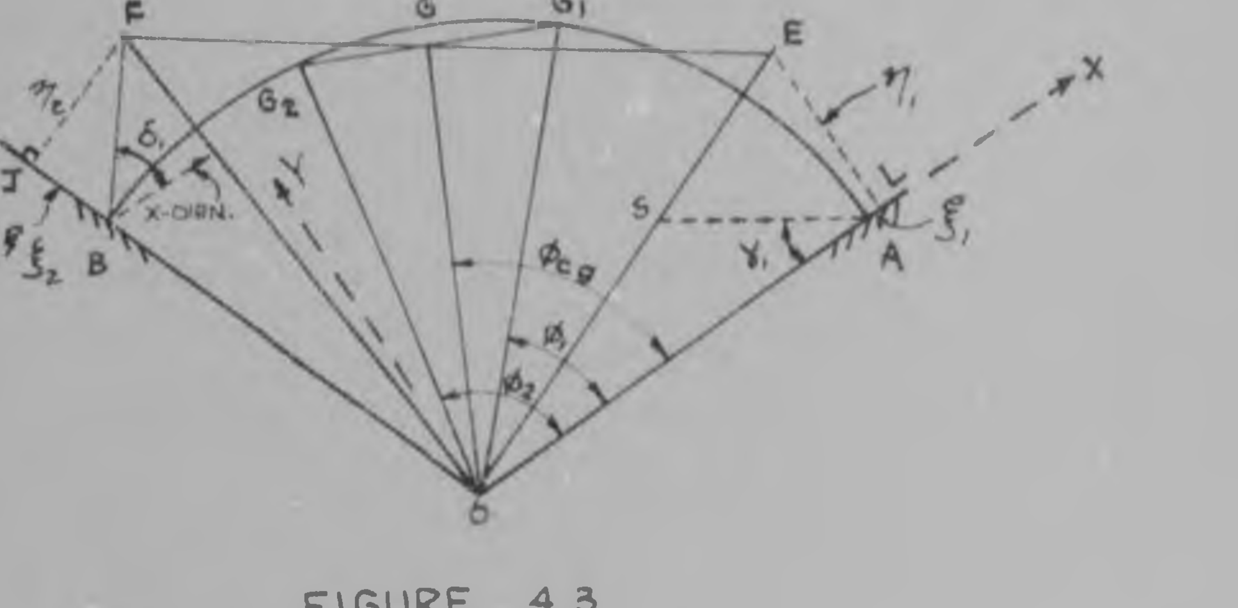

FIGURE 4.3

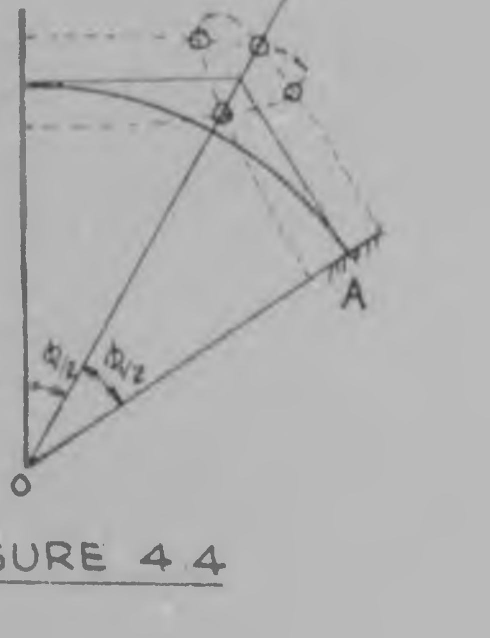

FIGURE 4.4

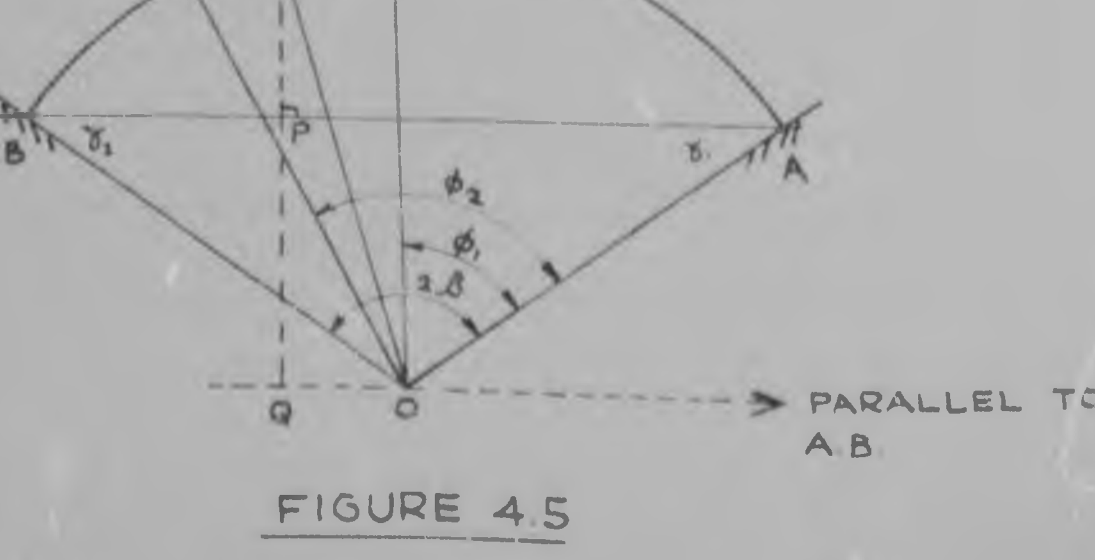

FIGURE 4.5

The yield criterion at A becomes:

$$R_1^2(\alpha^2\eta_1^2 + \xi_1^2) = T_p^2$$

or $$\alpha^2\eta_1^2 + \xi_1^2 = (\frac{T_p}{R_1})^2.$$

This equation represents an ellipse, and for any given values of α and R_1, an ellipse can be plotted with axes along the radius and tangent at A; such an ellipse gives the locus of the point E for the formation of a hinge at A. An identical ellipse can be drawn with the radius and tangent at G_1 as axes. The intersection points of the ellipses give the possible positions of E, as shown in Fig. 4.4. As the failure mode usually occurs at large values of α, the ellipses are in most cases nearly circular and the intersection points on the bisector of angles AOG_1 and BOG_2 are the correct ones; this case only is considered here. The correctness of this assumption must be checked for any particular case.

The method of solution is to try a value of ρ_1 = OE; then, since E has rectangular co-ordinates ($\rho_1 \cos \phi_1/2$, $\rho_1 \sin \phi_1/2$) and G has co-ordinates ($r_{cg} \cos \phi_{cg}$, $r_{cg} \sin \phi_{cg}$) with respect to OXY, the equation of the straight line EG is given by

$$\frac{y - y_{cg}}{y_E - y_{cg}} = \frac{x - x_{cg}}{x_E - x_{cg}} \quad \ldots\ldots\ldots\ldots\ldots\ldots \quad (4.5)$$

OF is given by

$$y = \tan (\beta + \frac{\phi_2}{2})\, x \quad \ldots\ldots\ldots\ldots\ldots\ldots\ldots \quad (4.6)$$

F is found by the intersection of these two straight lines, as described in the Appendix.

If ξ_1, η_1, ξ_2 and η_2 have the same meaning as before, and if ρ_2 = OF,

$$\rho_2 = (x_F^2 + y_F^2)^{\frac{1}{2}}, \quad \ldots\ldots\ldots\ldots\ldots\ldots\ldots \quad (4.7)$$

$$\xi_1 = r - x_E, \quad \eta_1 = y_E, \quad \ldots\ldots\ldots\ldots\ldots\ldots \quad (4.8)$$

$$\xi_2 = r - \rho_2 \cos (\beta - \frac{\phi_2}{2}) \text{ and } \eta_2 = \rho_2 \sin(\beta - \frac{\phi_2}{2}) \ldots (4.9)$$

If EG = ℓ_1 and FG = ℓ_2,

$$\ell_1 = \{(x_E - x_{cg})^2 + (y_E - y_{cg})^2\}^{\frac{1}{2}} \quad \text{......} \quad (4.10a)$$

and

$$\ell_2 = \{(x_F - x_{cg})^2 + (y_F - y_{cg})^2\}^{\frac{1}{2}} \quad \text{......} \quad (4.10b)$$

The two simultaneous equations to be satisfied for the final solution are:

$$\left(\frac{Wr}{Mp}\right)_1 = \frac{\alpha\,(\ell_1 + \ell_2)}{\ell_2(\alpha^2 n_1^2 + \ell_1^2)^{\frac{1}{2}}} \quad \text{...............} \quad (4.11a)$$

and

$$\left(\frac{Wr}{Mp}\right)_2 = \frac{\alpha\,(\ell_1 + \ell_2)}{\ell_1(\alpha^2 n_2^2 + \ell_2^2)^{\frac{1}{2}}} \quad \text{...............} \quad (4.11b)$$

In mode 3B, hinges form at A, G_1 and B. For this to happen, the loading must obviously be unsymmetrical, and the axes of rotation of the hinges must intersect in one point S (see Fig. 4.3). If the assumption is made (as for mode 3A) that the point E is on the bisector of angles AOG_1, then S must fall on the line EO, or EO produced.

Now $\tan \gamma_1 = \dfrac{y_S}{r-x_S}$,

and $\tan \dfrac{\phi_1}{2} = \dfrac{y_S}{x_S}$.

Eliminating y_S from these two equations,

$$x_S = \frac{r \tan \gamma_1}{\tan \frac{\phi_1}{2} + \tan \gamma_1} \quad \text{..................} \quad (4.12)$$

and the second of the two equations may be used to solve for y_S:

$$y_S = x_S \tan {}^{\phi_1}/_2 \quad \text{.....................} \quad (4.13)$$

The equation for $\tan \gamma_2$, where γ_2 is the angle between OB and BS has been determined in Chapter 3 in the section on mode 2 collapse as

$$\tan \gamma_2 = \frac{\frac{x_S}{r} \sin 2\beta - \frac{y_S}{r} \cos 2\beta}{1 - \frac{x_S}{r} \cos 2\beta - \frac{y_S}{r} \sin 2\beta} \quad \text{.......} \quad (3.17)$$

The equations (3.18) and (3.19) of chapter 3 for the angles δ_1 and δ_2 also apply in this case and are repeated for convenience:

$$\delta_1 = 2\beta - \frac{\pi}{2} + \delta_2 \quad \ldots\ldots\ldots\ldots\ldots\ldots\ldots \quad (3.18)$$

$$\delta_2 = \text{arc tan } (\alpha^2 \tan \gamma_2) \quad \ldots\ldots\ldots\ldots\ldots\ldots \quad (3.19)$$

Equation (4.5) of this chapter for EG still applies, and DF is given by (3.21) of Chapter 3:

$$y = (\tan \delta_1)\, x + \sin 2\beta - \tan \delta_1 \cos 2\beta \; .. \quad (3.21)$$

The co-ordinates of F are given by the intersection of these two straight lines. The distances ρ_2, ξ_2 and η_1 may be found using equations (4.7), (4.8) and 4.9) of this chapter. Also, if θ_3 = the angle AOF,

$$\theta_3 = \text{arc tan } ({}^{y_F}/x_F) \quad \ldots\ldots\ldots\ldots\ldots\ldots \quad (4.14)$$

$$\xi_2 = \rho_2 \cos (2\beta - \theta_3) - r \quad \ldots\ldots\ldots\ldots\ldots \quad (4.15)$$

and $$\eta_2 = \rho_2 \sin (2\beta - \theta_3) \quad \ldots\ldots\ldots\ldots\ldots\ldots \quad (4.16)$$

Equations (4.10) give values for ℓ_1 and ℓ_2, and (4.11a) and (4.11b) are the final simultaneous equations required for complete solution.

<u>Mode 4 - Large Torsional Strength</u>. As illustrated in Fig. 4.1 (g), in this mode there is a hinge at each support, and the axis of rotation is, for both hinges, a line joining the supports. Referring to Fig. 4.5, the centre of gravity of the loads is at G (r_{cg}, ϕ_{cg}) with respect to OA.

Clearly $\gamma_1 = \gamma_2 = \frac{\pi}{2} - \beta = \gamma$, where γ_1 and γ_2 are the angles OAB and OBA respectively; for both hinges,

$$\tan \gamma = \tan \left(\frac{\pi}{2} - \beta\right) = \frac{T}{\alpha^2 M} \quad \ldots\ldots\ldots\ldots\ldots \quad (4.17)$$

Taking moments about AB, and since $W_1 + W_2 = W$:

$$W \cdot \overline{GP} = 2(M \cos \gamma + T \sin \gamma)$$
$$= 2(M \sin \beta + T \cos \beta),$$

where GP is perpendicular to AB.

IF OQ is parallel to AB, and GQ perpendicular to OQ, the angle OGQ is equal to $\phi_{cg} - \beta$, and $\overline{GP} = \overline{GQ} - \overline{PQ}$. Hence $\overline{GP} = r_{cg} \cos (\phi_{cg} - \beta) - r \cos \beta$

Therefore,

$$W \{r_{cg} \cos (\phi_{cg} - \beta) - r \cos \beta\} = 2(M \sin \beta + T \cos \beta) \; \ldots\ldots\ldots \quad (4.18)$$

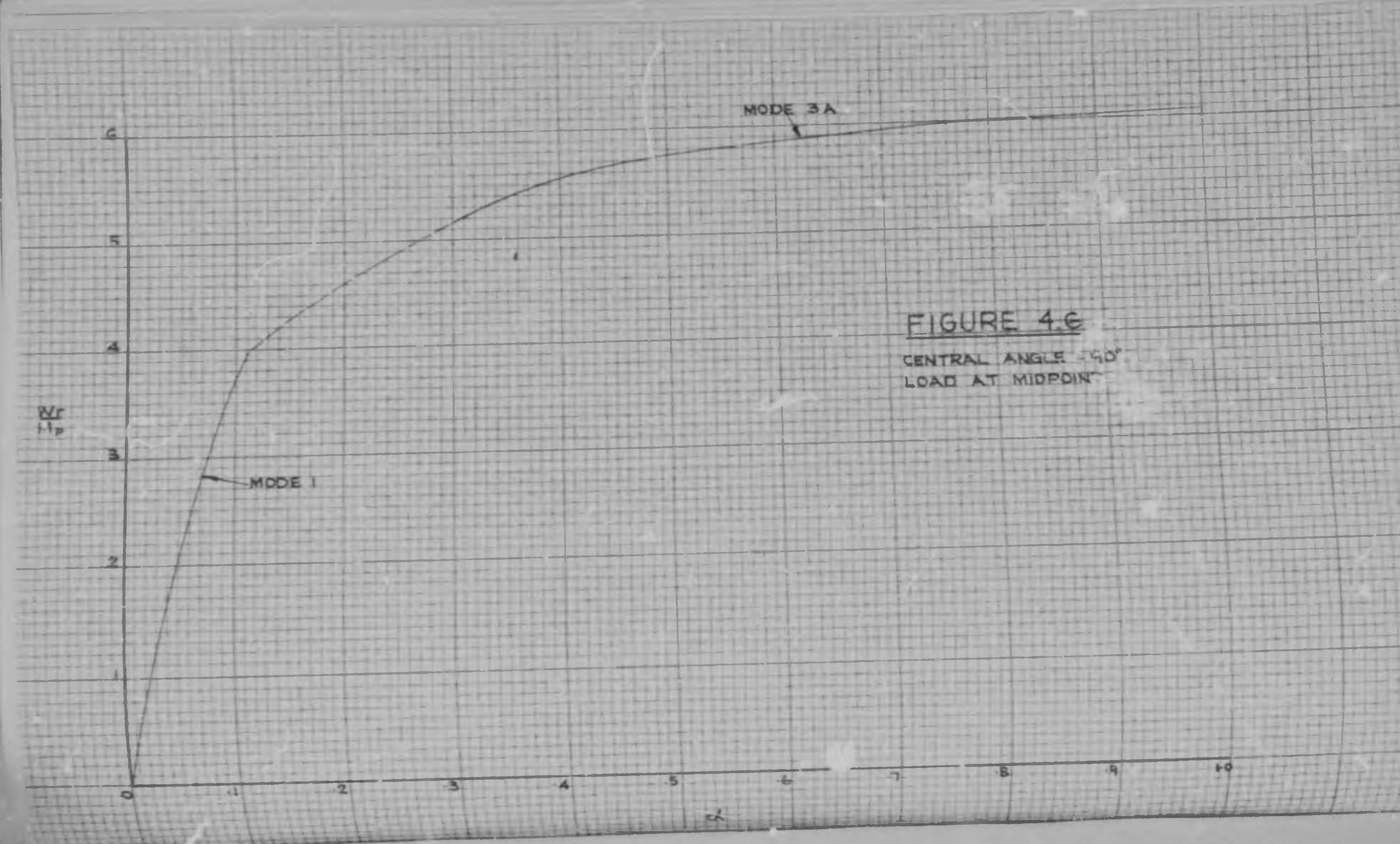
FIGURE 4.6
CENTRAL ANGLE 90°
LOAD AT MIDPOINT
MODE 3A
MODE 1
Wr/Mp
0
·1
·2
·3
·4
·5
·6
·7
·8
·9
1·0
1
2
3
4
5
6
α

Using equation (4.17) and the yield criterion $\alpha^2 M^2 + T^2 = T_p^2$,

$$\alpha^2 M^2 + \alpha^4 M^2 \cot^2 \beta = T_p^2 .$$

Solving for M:

$$M = \frac{T_p}{\alpha(1+\alpha^2 \cot^2 \beta)^{\frac{1}{2}}} .$$

Substituting this value for M and $T = \alpha^2 M \cot\beta$ in (4.18):

$$W\{ r_{cg} \cos(\phi_{cg}-\beta) - r\cos\beta\}$$
$$= 2\{ \frac{T_p \sin\beta}{\alpha(1+\alpha^2 \cot^2\beta)^{\frac{1}{2}}} + \frac{\alpha^2 T_p \cot\beta\cos\beta}{\alpha(1+\alpha^2 \cot^2\beta)^{\frac{1}{2}}} \} .$$

Therefore,

$$\frac{Wr}{T_p} = \frac{2(\sin\beta + \alpha^2 \cos\beta\cot\beta)}{\alpha(1+\alpha^2\cot^2\beta)^{\frac{1}{2}}\{\frac{r_{cg}}{r}\cos(\phi_{cg}-\beta) - \cos\beta\}} \quad (4.19a)$$

and hence

$$\frac{Wr}{M_p} = \frac{2\sin\beta\,(1+\alpha^2\cot^2\beta)^{\frac{1}{2}}}{\frac{r_{cg}}{r}\cos(\phi_{cg}-\beta) - \cos\beta} \quad \ldots\ldots\ldots\ldots (4.19b)$$

The occurrence of this mode of failure is possible when the centre of gravity of the loads is comparatively close to the line joining the supports.

A typical result for a bow girder with the central angle equal to 90° and with loads symmetrically placed at 22½° from the axis of symmetry is plotted in Fig. 4.6. The broken line on the curve represents an approximate result, obtained graphically, corresponding to mode 3A failure when the reaction points are not on the bisector of AOG_1 (Fig. 4.4). This case has not been dealt with analytically in the previous sections.

4.3 Effect of Lack of Torsional Restraint

It is apparent from Fig. 4.6 and other results obtained that the form of the solution for two concentrated loads is similar to that for a single concentrated load. For low values of α, the effect of changes in torsional strength on the collapse load is considerable, while for high values of α small changes in torsional strength have a negligible effect on the collapse load. During collapse at high values of α, the value of torsion in combined hinges is generally small compared with the value of bending moment, and the amount of energy absorbed in torsion during failure is small compared with the energy absorbed in bending.

Hence the conclusions reached in section 3.5 for single loads also apply here; namely that an increase in torsional strength of the beam has a negligible effect on the ultimate load for high values of α, and that at these high values of α the provision of torsional restraint at the supports has a small effect on the collapse load.

4.4 Girders with Several Concentrated Loads

For small α, the probable failure modes are similar to those for the two concentrated loads, that is, the modes 1, 1A, 2 and 2A or similar modes are the most likely to occur. The suggested approach is to replace the several concentrated loads with a single load at the centre of gravity of the loads and then to solve as a mode 1 or mode 2 failure. The position of the free hinges can then be compared with positions of the point loads and an amended solution carried out using equations (4.1), (4.2) and (4.4) to take into account the effect of the concentrated loads on the hinge positions. This approach is tedious and an easier solution might be obtained using the approach adopted by Imegwu.

The higher modes for girders with several concentrated loads could be solved using the methods outlined in the previous sections: the correct configuration of hinges could be found by trial depending on the position of the concentrated loads.

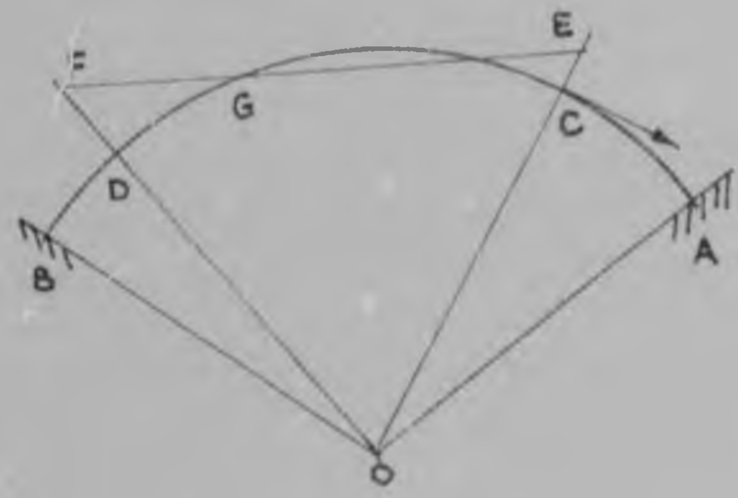

FIGURE 5.1

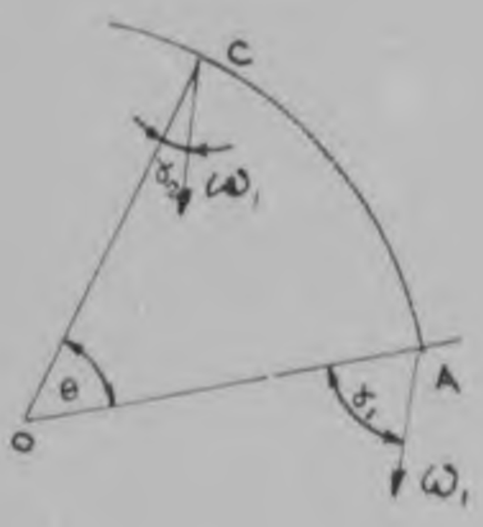

FIGURE 5.2

CHAPTER 5

A KINEMATIC APPROACH

5.1 Introduction

The methods of analysis described in the previous chapters are based essentially on a static approach, and can yield incorrect results if it is not ensured that the rotations of the hinges are compatible with the directions of the moments and torques. An example is the partial collapse of a girder with a single point at G, shown in Fig. 5.1. Johansen has demonstrated that collapse with hinges at C, G and D is impossible. This is proved as follows:

The reaction R_1 at E causes a torque acting on the section of the girder CGDE at C directed as indicated by the arrow in Fig. 5.1. (Rotations are clockwise when viewed in the direction of the arrows). If a plastic hinge were to form at C, then the rotation of CGD with respect to AC (which can be regarded as rigid) would be in the opposite direction to the moment vector shown. This would cause the load at G to move upwards and increase its potential energy. The same reasoning can be applied to the formation of a hinge at D, irrespective of the direction or amount of rotation at a possible hinge at D.

Hence the partial collapse by the formation of hinges at C, G and D is impossible, since the static and geometric conditions are in conflict.

The method proposed in this chapter is aimed at the calculation of collapse loads by equating the energy absorbed in the hinges during plastic deformation with the loss in potential energy by the load during collapse.

In the following complete solutions will be given in some simple cases; methods of approach will be suggested for some more complicated cases. It is suggested that use of the minimum principle may be made in complicated cases; by the minimum principle it is meant that the collapse loads obtained using the kinematic method are either greater or equal to the exact collapse load.

Imegwu[6] has described a method similar to that suggested above; use has been made of the minimum principle. The work by Imegwu was published after completion of the present investigation.

5.2 Basic Principles

Energy absorbed in a plastic hinge subjected to combined bending and torsion. Consider a hinge on a circular beam subjected to combined bending and torsion: the rotation ω during plastic flow of the hinge is about an axis at an angle γ to the radius at the hinge.

If a moment M and torque T act at the hinge, then the energy absorbed in the hinge during plastic deformation is:

M x Rotation about bending axis + T x Rotation about torsional axis

$= M\omega\cos\gamma + T\omega\sin\gamma$.

Using the yield criterion (2.2) and the equation (2.3), the following results may be easily deduced:

$$M = T_p/\alpha(1 + \alpha^2\tan^2\gamma)^{\frac{1}{2}},$$

and $$T = T_p\,\alpha\tan\gamma/(1 + \alpha^2\tan^2\gamma)^{\frac{1}{2}}.$$

Substituting for M and T in the above equation, the energy absorbed in the hinge is

$$\frac{T_p\,\omega\cos\gamma}{\alpha(1 + \alpha^2\tan^2\gamma)^{\frac{1}{2}}} + \frac{T_p\,\omega\alpha\tan\gamma\sin\gamma}{(1 + \alpha^2\tan^2\gamma)^{\frac{1}{2}}}$$

$$= \frac{T_p\,\omega\cos\gamma}{\alpha}(1 + \alpha^2\tan^2\gamma)^{\frac{1}{2}}$$

$$= M_p\,\omega\cos\gamma(1 + \alpha^2\tan^2\gamma)^{\frac{1}{2}} \quad \ldots\ldots\ldots\ldots \quad (5.1)$$

Rotation of rigid segments. During collapse, the portions of the bow girder between hinges have been considered as rigid. In Fig. 5.2 a segment of a circular girder is shown: the end A is subjected to a rotation ω, about the axis at an angle γ_L to the radius at A. The angle subtended at the centre of the circular segment AC is θ.

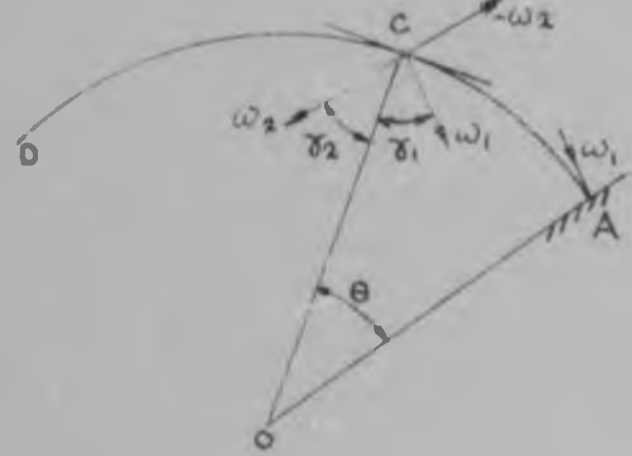

FIGURE 5.3

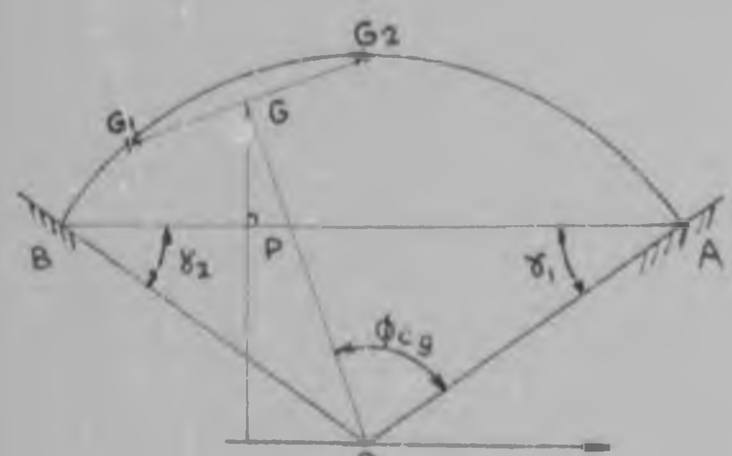

FIGURE 5.4

If the segment AC is rigid, then the rotation at the end C is equal in magnitude and in the same direction as at the end A.

By simple geometry,

$$\gamma_1 = \gamma_2 + \theta$$

or $$\gamma_2 = \gamma_1 - \theta \quad \ldots\ldots\ldots\ldots\ldots\ldots\ldots\ldots \quad (5.2)$$

Conditions for the existence of a hinge in pure torsion. Fig. 5.3 shows a portion of a circular bow girder, with a hinge at C in pure torsion.

The absolute rotations of the segments AC and CD are ω_1 and ω_2 and are about the axes at angles γ_1 and γ_2 respectively to the radius at C.

The twisting which occurs at C due to plastic deformation is the vectorial difference between the absolute rotations of the segments AC and CD, i.e., if the discontinuity at C is $\Delta\omega$, then

$$\Delta\omega = \vec{\omega}_1 - \vec{\omega}_2 .$$

Since the hinge at C is in pure torsion, the bending rotation is zero,

i.e. $$\omega_1 \cos\gamma_1 = \omega_2 \cos\gamma_2 \quad \ldots\ldots\ldots\ldots\ldots\ldots \quad (5.3)$$

and $$\Delta\omega = \omega_1 \sin\gamma_1 + \omega_2 \sin\gamma_2 \quad \ldots\ldots\ldots\ldots \quad (5.4)$$

for the directions shown.

5.3 Examples of Application

Mode 4 Collapse. In this section, the mode 4 collapse of the Chapter 4 will be deduced. The collapse mode is illustrated in Fig. 5.4: the girder is loaded at G_1 and G_2 with loads W_1 and W_2 respectively. Hinges form at A and B and collapse takes place about an axis joining A and B. The mode can only occur when the centre of gravity is fairly close to the supports, or possibly for girders with central angle $2\theta > 180^\circ$.

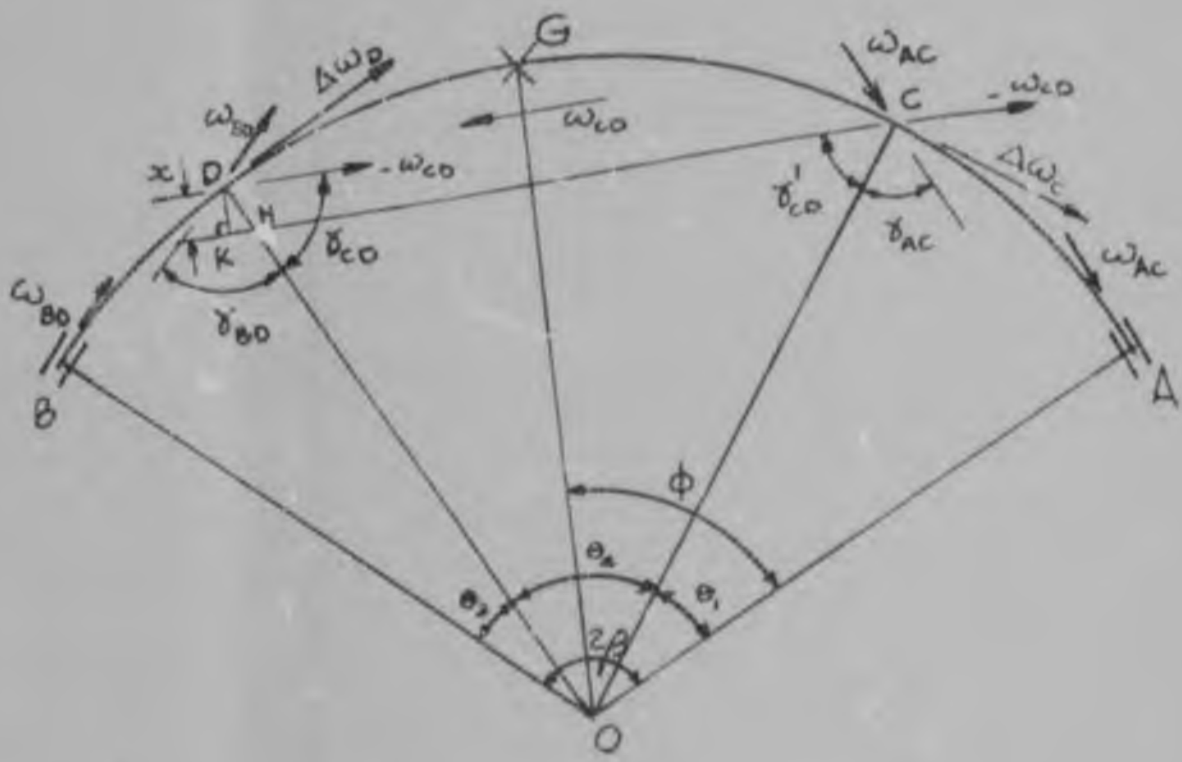
G
ωAC
C
-ωCO
ΔωD
ωBD
ωCO
x
D
-ωCO
H
K
γCO
γ'CO
γAC
ΔωC
ωAC
ωBD
γBD
B
A
φ
θ4
θ2
θ1
2β
O

FIGURE 5.5

If G is the centre of gravity of the loads, and if during plastic collapse a rotation $\Delta\omega$ takes place, then the point G moves downwards a distance $(\Delta\omega)\,(\overline{GP})$, where $\overline{GP} = r_{cg} \cos(\phi_{cg} - \beta) - r \cos\beta$.

The energy absorbed in each hinge is given by equation (5.1) and is

$$M_p \Delta\omega \cos\gamma \,(1 + \alpha^2 \tan^2 \gamma)^{\frac{1}{2}}.$$

Clearly in this case $\gamma_1 = \gamma_2 = \frac{\pi}{2} - \beta$.

Hence the virtual work equation may be written:

$$2 M_p \Delta\omega \cos(\pi/2 - \beta)\,(1 + \alpha^2 \tan^2(\pi/2 - \beta))^{\frac{1}{2}} =$$

$$(W_1 + W_2)\Delta\omega\,\{r_{cg}\cos(\phi_{cg} - \beta) - r\cos\beta\}^{\frac{1}{2}},$$

or, since $W_1 + W_2 = W$,

$$\frac{Wr}{M_p} = \frac{2\sin\beta\,(1 + \alpha^2\cot^2\beta)^{\frac{1}{2}}}{\frac{r_{cg}}{r}\cos(\phi_{cg} - \beta) - \cos\beta},$$

which is the same as the result obtained previously.

<u>Collapse with no torsion at the supports - Mode 1</u>.

This is the collapse mode already investigated in section 3.3, and is illustrated in Fig. 5.5; plastic hinges occur at C and D.

Using the equation (5.3) deduced in the previous section, for the existence of a hinge in pure torsion at C and D:

$$\omega_{AC} \cos\gamma_{AC} = \omega_{CD} \cos\gamma^1_{CD} \quad \ldots\ldots\ldots\ldots \quad (5.5)$$

and $$\omega_{BD} \cos\gamma_{BD} = \omega_{CD} \cos\gamma_{CD} \quad \ldots\ldots\ldots\ldots \quad (5.6)$$

where ω_{AC}, ω_{BD} and ω_{CD} are the absolute rotations of the segments AC, BD and CD respectively.

Using now the equation (5.2), and since the angle between the radii and the axes of rotation at the supports is $\pi/2$,

$$\gamma_{AC} = \frac{\pi}{2} - \theta_1$$

and $$\gamma_{BD} = \frac{\pi}{2} - \theta_2$$

From triangle OCH, $\gamma_{CD} + \gamma^1_{CD} + \theta_4 = \pi$,

or $$\gamma^1_{CD} = \pi - \theta_4 - \gamma_{CD}.$$

Substituting these values in equations (5.5) and (5.6):

$$\omega_{AC} \sin \theta_1 = \omega_{CD} \cos (\pi - \theta_4 - \gamma_{CD}) \; .... \quad (5.7)$$

and $$\omega_{BD} \sin \theta_2 = \omega_{CD} \cos \gamma_{CD}. \; .... \quad (5.8)$$

The vertical movement of the points C and D due to the torsional rotations at the supports are $(\sec \theta_1 - 1)\omega_{AC}$ and $(\sec \theta_2 - 1)\omega_{BD}$, assuming the beam to be of unit radius.

Assuming that the supports A and D remain at the same levels during collapse (this does not assume that A and D are on the same level: a small difference will not affect the following equation):

$$(\sec \theta_1 - 1)\omega_{AC} + x\omega_{CD} - (\sec \theta_2 - 1)\omega_{BD} = 0 \; ... \; .... \quad (5.9)$$

where x is the perpendicular distance DK between the straight line CH and a parallel line through D (see Fig. 5.5). The line DH is parallel to the axis of rotation of ω_{CD}.

The distance x is found by consideration of the triangle CKD. The angle KCD is equal to $\frac{\pi}{2} - \frac{\theta_4}{2} - \gamma^1_{CD}$ or $\frac{\theta_4}{2} + \gamma_{CD} - \frac{\pi}{2}$. Hence x is equal to $\overline{CD}$ sin $(\frac{\theta_4}{2} + \gamma_{CD} - \frac{\pi}{2})$, and since $\overline{CD} = 2 \sin \frac{\theta_4}{2}$,

$$x = 2 \sin \frac{\theta_4}{2} \sin (\frac{\theta_4}{2} + \gamma_{CD} - \frac{\pi}{2}).$$

Equation (5.9) becomes:

$$(\sec \theta_1 - 1)\omega_{AC} + 2(\sin \frac{\theta_4}{2} \sin(\frac{\theta_4}{2} + \gamma_{CD} - \frac{\pi}{2})\omega_{CD} - (\sec \theta_2 - 1)\omega_{BD} = 0 \; .... \quad (5.10)$$

From (5.7) and (5.8),

$$\frac{\omega_{AC}}{\omega_{CD}} = \frac{\cos (\pi - \theta_4 - \gamma_{CD})}{\sin \theta_1} \; .... \quad (5.11)$$

and $$\frac{\omega_{BD}}{\omega_{CD}} = \frac{\cos \gamma_{CD}}{\sin \theta_2} \; .... \quad (5.12)$$

Substituting these values in (5.10):

$$\frac{(\sec\theta_1-1)\cos(\pi-\theta_4-\gamma_{CD})}{\sin\theta_1} + 2\sin\frac{\theta_4}{2}\sin\left(\frac{\theta_4}{2}+\gamma_{CD}-\frac{\pi}{2}\right)$$
$$-\frac{(\sec\theta_2-1)\cos\gamma_{CD}}{\sin\theta_2} = 0 \quad \ldots \quad (5.13)$$

Hence, since $\theta_4 = 2\beta-\theta_1-\theta_2$, for any assumed values of θ_1 and θ_2, a value of γ_{CD} may be obtained from equation (5.13). The virtual work equation may now be written down, using equation (5.4) if the vertical displacement Δz of the load W is found. It may be shown by a method similar to that used in deriving equation (5.10) above that:

$$\Delta z = (\sec\theta_1-1)\omega_{AC}+2\left\{\sin\left(\frac{\phi-\theta_1}{2}\right)\sin\left(\gamma_{CD}+\theta_4+\frac{\theta_1}{2}-\frac{\phi_1}{2}-\frac{\pi}{2}\right)\right\}\omega_{CD}$$

Hence the virtual work equation may be written (considering only the energy absorbed in plastic deformation):

$$T_p\{\omega_{AC}\cos\theta_1+\omega_{CD}\sin(\pi-\theta_4-\gamma_{CD})\}+T_p\{\omega_{BD}\cos\theta_2$$
$$+\omega_{CD}\sin\gamma_{CD}\} = W\Delta z \quad \ldots \quad (5.14)$$

By substituting the value of Δz obtained, equations (5.11) and (5.12) can be used to eliminate the rotations from equation (5.14). Hence for the assumed values of θ_1 and θ_2 and the corresponding value of γ_{CD} obtained from (5.13), a value of the collapse load can be obtained.

The above method could be developed to such a form as to yield solutions using the minimum principle; in the present form it can be used to check numerical solutions already obtained.

Collapse with fully fixed supports - Mode 1. This collapse mode has been investigated in section 3.2. For the calculation of the collapse load by the present method, the approach adopted in the section above for the case with no torsion at the supports can be used. The chief difference is that energy absorbed in the hinges at the supports must be included in the virtual work equation; the axis of rotation at the supports is not along the tangent at the supports. Equation (5.1) gives the energy absorbed in a hinge in combined bending and torsion.

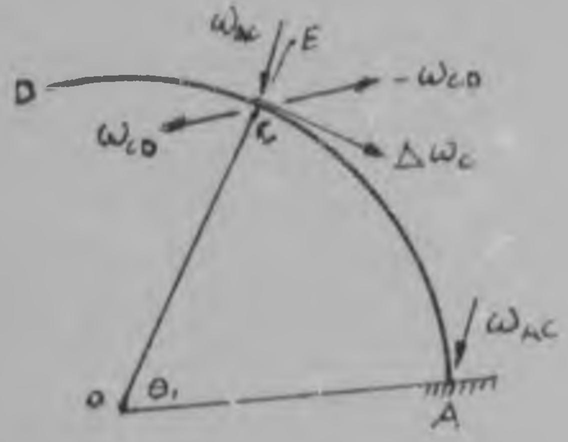

(a)

(b)

FIGURE 5.6

Transition from Mode 1 to Mode 2. The transition from mode 1 to mode 2 failure as the value of α is increased will now be discussed. In Fig. 5.6 (a) a portion of a bow girder with a free hinge at point C on the arc and a fixed hinge at the support is shown. It is assumed that the hinge at C is on the shorter arc measured from the single load to the supports, and would be the hinge to disappear in the transition. The rotational movement of the hinge ($= \Delta\omega_C$) is the vectorial difference between ω_{AC} and ω_{CD}, D being the position of the second free hinge.

If α is increased, the value of ρ corresponding to any particular value of θ in equation (3.1) increases and the (ρ, θ) curves giving possible reaction points at the supports move radially outwards. Since the point load and the reaction points are on the same straight line, the values of θ_1 and θ_2 tend to decrease with an increase in α. Hence the axis of rotation at A will in general tend to move closer to the radius at A as α increases and as the reaction point E (ρ_1, θ_1) moves further from the centre. In certain cases the axis of rotation may cross the radius at the support.

If, at the transition from mode 1 to mode 2, the value of of $\frac{Wr}{M_p}$ corresponding to the transition value of α is the same for both modes, and if the position of the free hinge in the mode 2 solution is the same as for the mode 1 solution, then the direction of ω_{AC} and ω_{CD} must be in the same direction (see Fig. 5.6b). An examination of equation (5.3) shows at this stage that $\omega_{AC} = \omega_{CD}$. Hence there is no torsional rotation at the hinge.

If the computer solutions developed in Chapter 3 are used it is found that values of collapse load can be obtained using the mode 1 solution at values of α exceeding the transition value, and that the values obtained for mode 1 are less than for mode 2. Imegwu[6] explains this by means of a maximum principle:

> "Such ambiguity is easily resolved here and elsewhere by theorem I: the larger load is the required collapsed load".

The Theorem I used by Imegwu is as follows:

"Theorem I. The collapse load is the largest load for which the equations of equilibrium are satisfied while at the same time the structure develops just enough plastic hinges to cause collapse".

This explanation is not satisfactory as it appears to be based on the assumption that there are two possible modes of failure for the bow girder and that the solution corresponding to the larger load is the correct one. Clearly if the equilibrium, yield and mechanism conditions are satisfied for the mode 1 solution, then it must be the correct one.

A suggested answer to the above anomaly is that in the mode 1 computer solutions the direction of the rotation $\Delta\omega_c$ of the torsional hinge for values of α above the transition value is opposite to the direction before the transition. Since the applied torque remains in the same direction, this leads to the contradiction of static and geometric conditions at the hinge as the torque applied to the hinge and the torsional rotation of the hinge would be in opposite directions; solutions could still be obtained using the mode 1 computer solution developed in Chapter 3.

The ideas proposed in this last section are not conclusive as a full mathematical treatment has not been developed.

CHAPTER 6

EXPERIMENTAL INVESTIGATION

6.1 Introduction

The only known results of tests to failure on steel circular-arc bow girders are those by Boulton and Boonsukha[4]. Johansen[3] has described some preliminary tests on circular rings but, unfortunately, the test set-up collapsed before complete failure of the rings took place.

The results of the tests by Johansen showed that the plastic hinges appeared as indicated by the theory and that the deviation of the directions of the axes of rotation from theoretical was slight, but the exact collapse load could not be determined. Boulton and Boonsukha obtained fairly accurate predictions of the collapse load, based on experimentally found values of the full plastic moments in bending and torsion.

In the present work, tests were carried out on eight miniature mild steel bow girders of about 24 inches radius, all subtending a central angle of 90°, and under various loading and end support conditions.

The object of the tests was four-fold:

(i) to investigate the behaviour of the hinges in actual bow girders

(ii) to verify experimentally the conclusions reached in Chapter 3 with regard to the relation between $\alpha = {}^{T_P}/_{M_P}$ and the effect of torsional restraint at the supports of the bow girders

(iii) to verify the results of Chapter 4 in which the existing work was extended to the calculation of collapse loads for the case of two concentrated loads

(iv) to calculate, in addition, elastic deflections for two of the eight tests.

The specimens were of three different cross-sections, giving three different values of α. The values of T_p and M_p were determined experimentally in control tests, from which the torsional and bending rigidities were also obtained for the prediction of elastic deflections.

The statistical deviation of the control test results from the mean was determined where possible so that the difference between the predicted and actual collapse loads could be viewed in relation to the variation in strength of the metal.

6.2 Preparation of Specimens and Description of Apparatus

Preparation of Test Specimens. The three cross-sections used are designated A, B and C. In Table 6.1 details of the specimens are shown.

Table 6.1

Symbol	Cross-section	Shape	No.	Final Measured Radius (Mean)	Maximum Deviation from Measured Radius
A	1"x1"	Square	2	24.00"	.10"
B	$1\frac{1}{2}$"x$\frac{5}{8}$"	Rectangular	2	24.65"	.10"
C	$1\frac{1}{2}$"x$\frac{3}{16}$"	Rectangular	4	23.55"	.06"

The girders were cold bent to a 2 foot radius, and cut to the correct lengths for a 90° arc. Arms for the end fixing arrangement, the latter described in a later section, were then welded on the ends of the girders. The arms were designed to remain elastic throughout the tests, and were at an angle of 45° to the tangent to the axis of the bow girder at the supports (see Fig. 6.5). The welds were double bevel butt welds and were made so as to ensure that the thickened portion at the weld was stronger than the girder section.

The girders were then annealed by heating to 920°C, soaking for at least one hour per inch of cross-section, and then removing from the furnace at below 600°C, and cooling in the air. Millscale resulting from the heat treatment was removed by sand blasting.

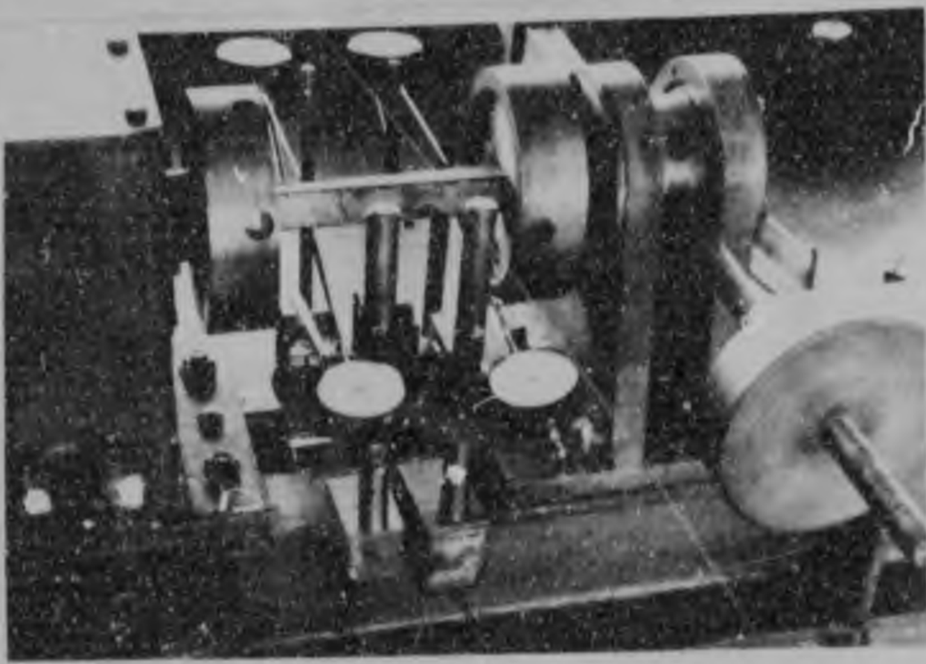

FIGURE 6.1

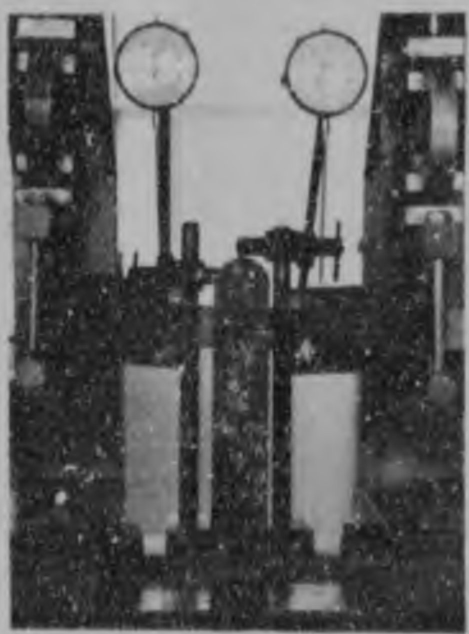

FIGURE 6.2

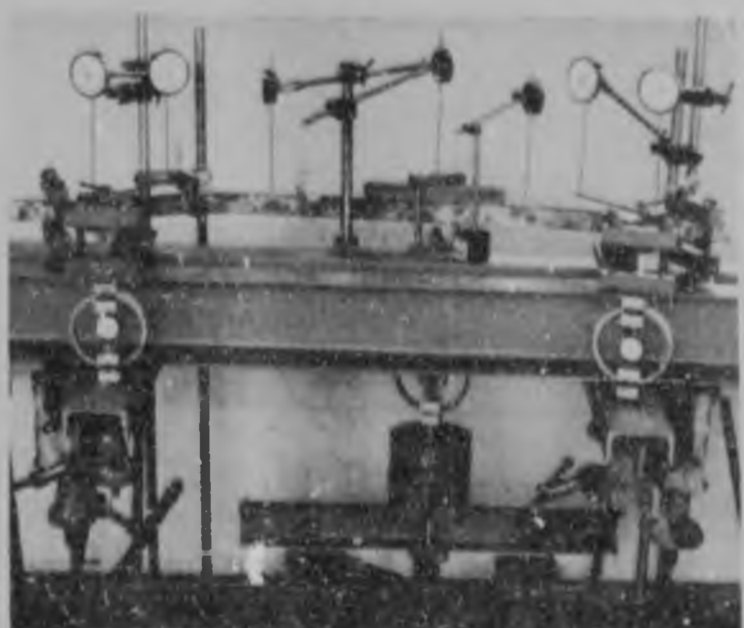

FIGURE 6.3

The radii of the girders were measured before and after heat treatment. The radii for the various sections were not exactly the same, but for a particular section the radius was found to be nearly constant. The heat treatment caused distortion of the 'C' girders, and they were bent back to a true radius. This unfortunately must have caused some localised strain hardening, and will be taken into account in the discussion of the results. The final measured radii and the maximum deviations from the measured values are given in Table 6.1.

Before testing the girders were cleaned and coated with Stresscoat ST 1208, a brittle coating, for the purpose of detecting the position and spread of the hinges. It was found in the control tests that the coating flaked from the metal surface during plastic flow, and not at elastic strains.

Control Tests. For the 'A' and 'C' sections, five straight lengths for the torsion and five for the bending tests were prepared, while for the 'B' section, three of each were prepared. The specimens were subjected to the same heat treatment and sand blasting as were the bow girders.

The torsion tests were carried out in a torsion testing machine in which the torque was measured by the force exerted at a known distance along a lever arm which acted on a platform scale. The rotation measurements were made directly on the specimens using two sets of dial deflection gauges at a known distance apart on the section, as can be seen in Fig. 6.1. The torque applied was constant over the length of the specimen.

The bending tests were done on simply supported lengths, the deep narrow 'B' and 'C' sections being clamped between plates for part of their length to prevent buckling, as shown in Fig. 6.2. The reactions were measured by previously calibrated proving rings, and deflections were read on dial deflection gauges.

The errors in readings of bending moment and torque were small compared with the standard deviations of the control values.

FIGURE 6.4

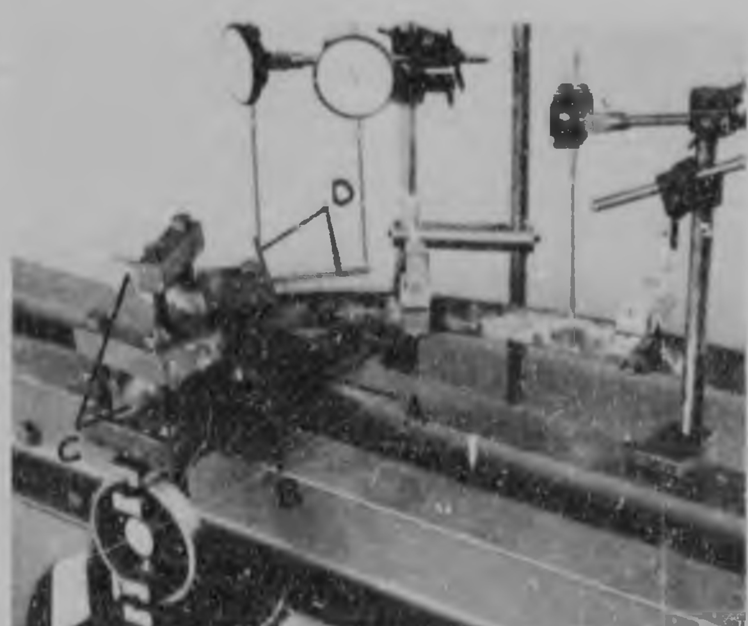

FIGURE 6.5

FIGURE 6.6

FIGURE 6.7

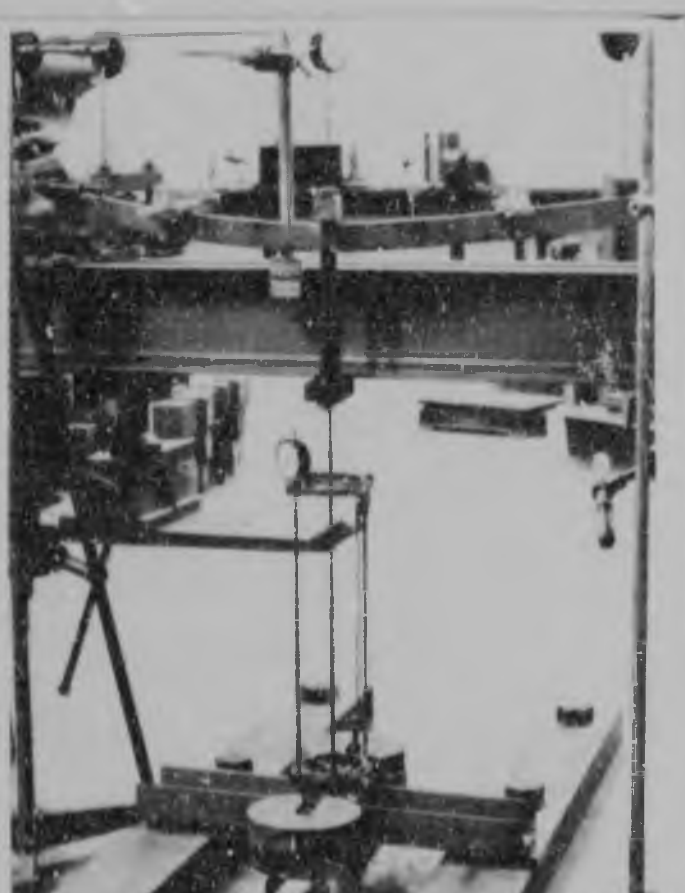

Bow Girder Tests. The general arrangement of typical tests can be seen in Figs. 6.3 and 6.4. The girders were supported on a test bed and loaded through a calibrated loading device and a screw jack anchored to the test floor.

The supports of the bow girders consisted of two-way cylindrical bearings A (see Fig. 6.5), the bases of which were bolted to the test bed. Plates B were clamped to the top and bottom of the lever arms C at the supports: the plates were bolted together to form a unit with the lever arms. The bottom plate served as a bearing plate and ensured that the reaction acted at the desired section of the bow girder. The torsional and bending rotations of the supports were measured by the deflections of the ends of arms D secured to the top plate (Fig. 6.5).

The moments and torques at the supports were measured by calibrated proving rings coupled to the girder lever arms through ball connections: the rotational movement of the supports was controlled by jacks connected to the proving rings (see Fig. 6.6).

The loading devices were designed to give an accuracy of about ± 2 per cent at the 5 per cent level of significance. The two devices used were:

(i) a 5 mm. prestressing wire fitted with a Macklow-Smith type extensometer of 16 inch gauge length (see Fig. 6.7). This was used for the tests on 'A' and 'B' sections, but the accuracy obtained was not sufficient for the 'C' sections, which had a rather lower collapse load

(ii) a proving ring which had a range large enough and the required degree of sensitivity for the 'C' tests.

Both devices were calibrated using dead load, but on the device (i) it was found that torsional effects due to the inertia of the dead load influenced the readings considerably. During the actual tests torsion in the device would be caused by the friction on the grips at the ends of the tensioned prestressing wire. To overcome this, a thrust race was incorporated in the device, which for practical purposes eliminated torsional effects. Re-calibration was carried out by setting up the prestressing wire with a calibrated proving ring in order to simulate the test conditions. The test device (ii) showed very slight sensitivity to applied torsion, and the dead load tests were used for the calibration.

It was found that, up to about 70 lb., there was a deviation from linearity in both gauges because of effects such as slackness in the prestressing wire in the case of the device (i). Hence in the girder tests the loading up to 70 lb. was applied by means of accurately known dead load, and thereafter measured by the loading devices. In the calibration the readings below 70 lb. were ignored.

The proving rings used for the measurements of support moments and torques were also calibrated using dead load (the gauge (i) was calibrated against one of these proving rings).

The data from all these calibrations were analysed on the University IBM 1620 computer using the IBM Regression Analysis Programme No. 6.0.001 which gave the calibration constants and standard deviations using a least squares analysis. The results of this analysis yielded the following standard deviations:

Device (i) : S.D. = 12.75 lb.
Device (ii) : S.D. = 3.12 lb.

Assuming the population to be normally distributed, the limits at the 5 per cent level of significance are:

Device (i) : $\pm$ 26.2 lb.
Device (ii) : $\pm$ 6.8 lb.

The tests were carried out by applying a certain deflection to the loading point, and measuring the load. This deflection was effected by means of the screw at the top of the prestressing wire (Fig. 6.7), and by the screw jack situated under the proving ring (Fig. 6.4). Once plastic flow had started, the apparatus was left until the difference between two successive readings at 15 minute intervals was negligible. The dead load for initial loading can be seen clearly in each case. The thrust bearing mentioned was placed under the channel supporting the dead load (Fig. 6.7).

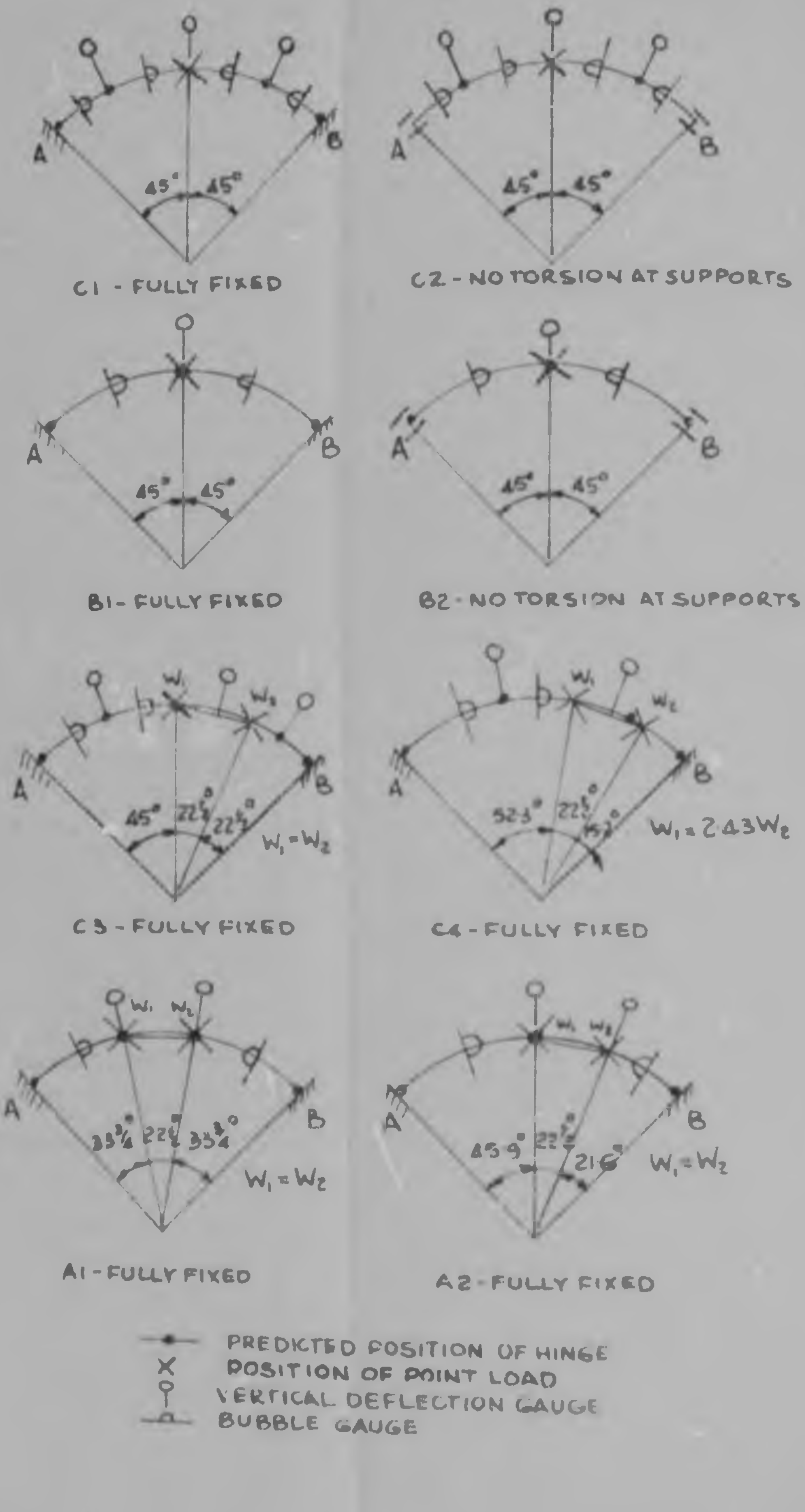

A
B
45°
C1 - FULLY FIXED
C2 - NO TORSION AT SUPPORTS
B1 - FULLY FIXED
B2 - NO TORSION AT SUPPORTS
W1
W2
22½°
W1 = W2
C3 - FULLY FIXED
52.5°
15°
W1 = 2.43W2
C4 - FULLY FIXED
33¾°
W1 = W2
A1 - FULLY FIXED
45.9°
21.6°
A2 - FULLY FIXED
PREDICTED POSITION OF HINGE
POSITION OF POINT LOAD
VERTICAL DEFLECTION GAUGE
BUBBLE GAUGE

FIGURE 6.8

The single or double point loads were applied by means of balls fitting into slightly punched recesses on the girder. For the double point load the loads were applied by dividing a single known load by means of a simply supported bar. The load was applied to the bar through a greased cylindrical bearing. The bar applied the load to the girder through balls at the two required points. This can be seen in Fig. 6.3.

The purpose of the deflection measurements was to calculate, where possible, the rotations at the plastic hinges. To this end, vertical deflection readings were taken at the points of application of the loads and at the predicted free hinge points. Vertical rods were placed between the deflection gauges and the points where deflections were measured in order to eliminate the effects of lateral movement of the girders during the tests. Rotations of the sections were measured by means of bubble slope gauges placed, where possible, midway between successive plastic hinges (as predicted).

6.3 Scope of Tests

The eight tests conducted do not represent an exhaustive investigation of the objects (i), (ii) and (iii) as set out in 6.1, but an attempt was made to cover as many aspects as possible.

The eight tests all yielded results of value for the object (i), that is, the investigation of the yield criterion. The objects (ii) and (iii) were covered by four tests each; for the object (ii) the two "B" cross-sections and two of the "C" cross-sections were used, and are denoted C1, C2, B1 and B2 (see Fig. 6.8). The loads in these tests were centrally placed. The tests C1 and B1 were conducted under conditions of full fixity at the supports, i.e., the rotations of the support were eliminated after each loading by adjustment of the jacks connected to the support lever arms. Test C2 was carried out with torsion at the supports as near zero as possible until the collapse load was reached, at which stage the torsional rotation of the supports was stopped, in an attempt at causing the load to increase to the fully fixed value. Test B2 was conducted with no torsion at supports. Since the moments measured at supports during

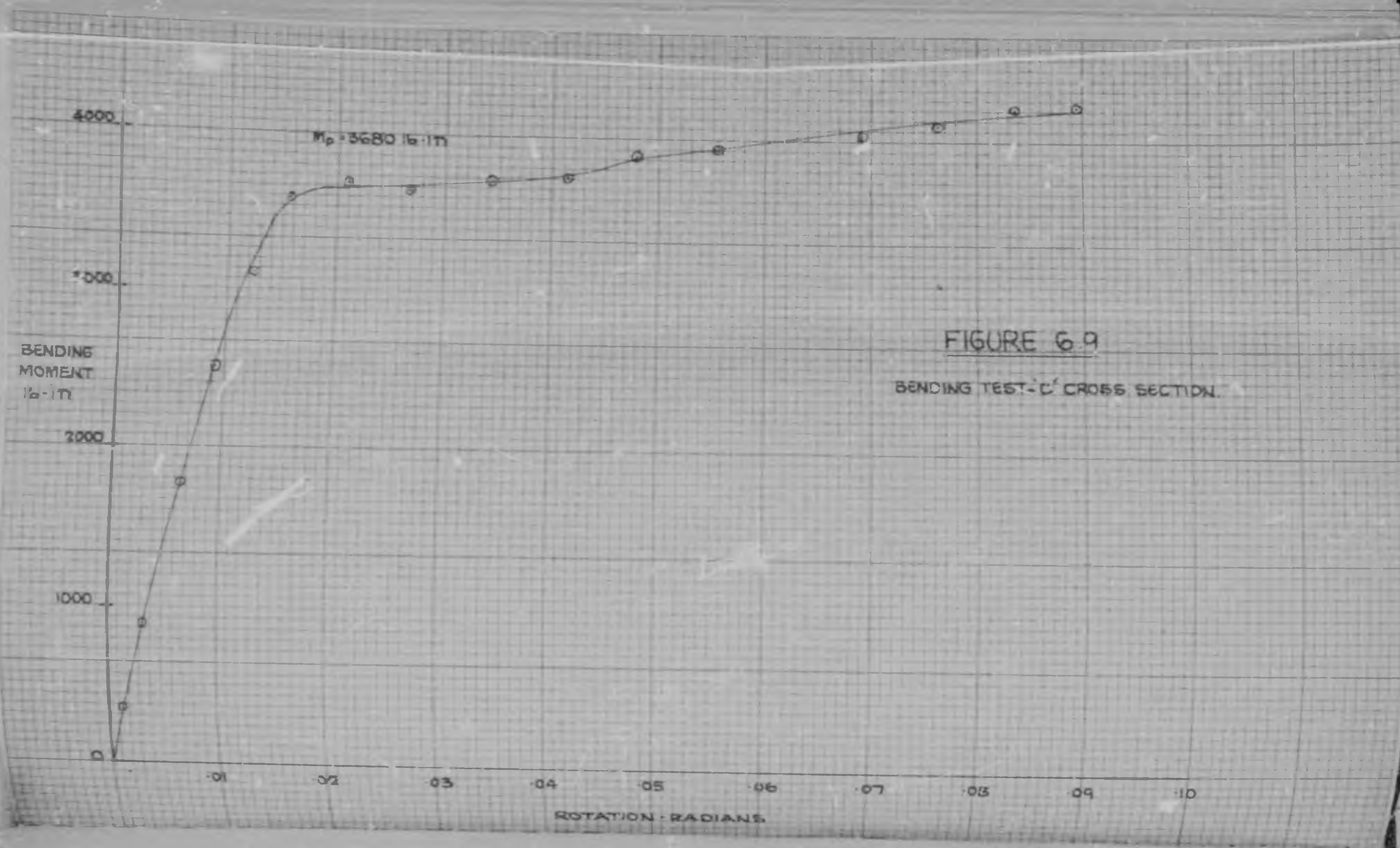

FIGURE 6.9

BENDING TEST:- 'L' CROSS SECTION.

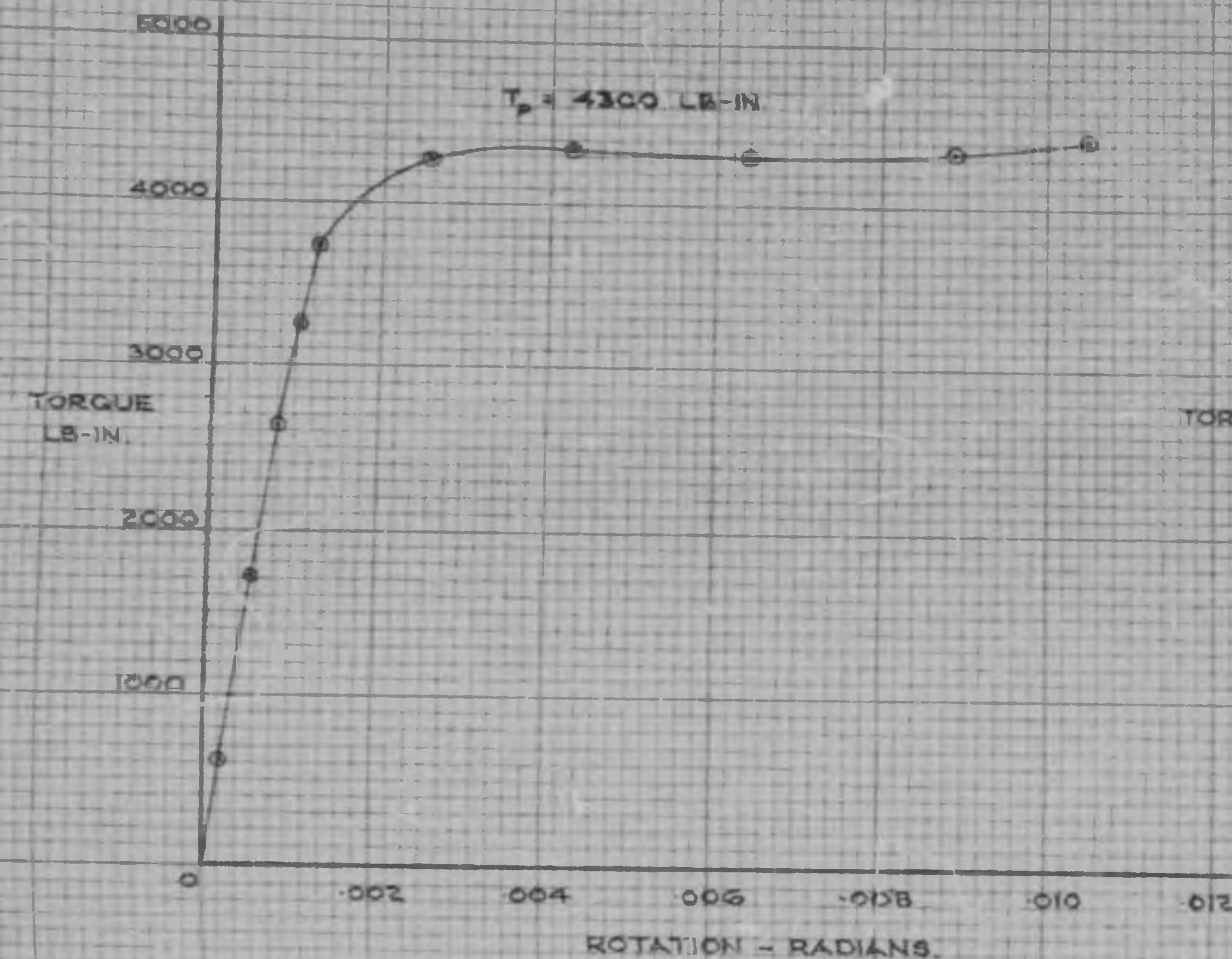

FIGURE 6·10

TORSION TEST – 'A' CROSS-SECTION.

the tests were at 45° to the tangent to the axis at the supports, the moments measured by the proving rings were adjusted until they were as nearly equal as possible in order to effect the no-torsion support condition. The "C" tests (α = .1265) corresponded to mode 1 failure of Chapter 3.2 and 3.3. In the "B" tests (α = .224) the value of α is theoretically just above the transition (at α = .200) from mode 1 to mode 3 (see Fig. 3.7).

The remaining four tests were all conducted under fully-fixed support conditions with two concentrated loads. The tests C3 and C4 were arranged so as to verify failure by modes 1 and 1A, as described in Chapter 4. The "A" tests - A1 and A2 - were designed to verify failure by modes 3A and 3B respectively. The loads in test C3 were equal and placed at quarter points, as shown in Fig. 6.8. In test C4, the loads were unsymmetrically placed as shown in Fig. 6.8, and were such that $W1/W2 = 2.43$. This was the best practical arrangement which gave, theoretically, the mode 1A failure (i.e. with a free hinge between the two point loads).

In the test A1 the loads were equal and symmetrical: hence a mode 3A failure was favoured. In the test A2, the loads were equal and unsymmetrically placed and the three-hinge failure mode was predicted.

The arrangement of the deflection gauges is shown in Fig. 6.8.

6.4 Results of Tests and Comparison with Theory

Control Tests. The results of the control tests are given in Table 6.2: the mean values of the full plastic moments in torsion and bending are given, together with the standard deviations in the case of the "A" and "C" cross-sections. The plastic moments were obtained from the torque-rotation and bending moment-rotation graphs; typical graphs are shown in Figs. 6.9 and 6.10. The standard deviation was calculated for the "A" and "C" cross-sections as the number of specimens was five for the determination of each control value, whereas for the "B" cross-section only three specimens were available for each value, which was insufficient for an estimate of the standard deviation. It is seen that the standard

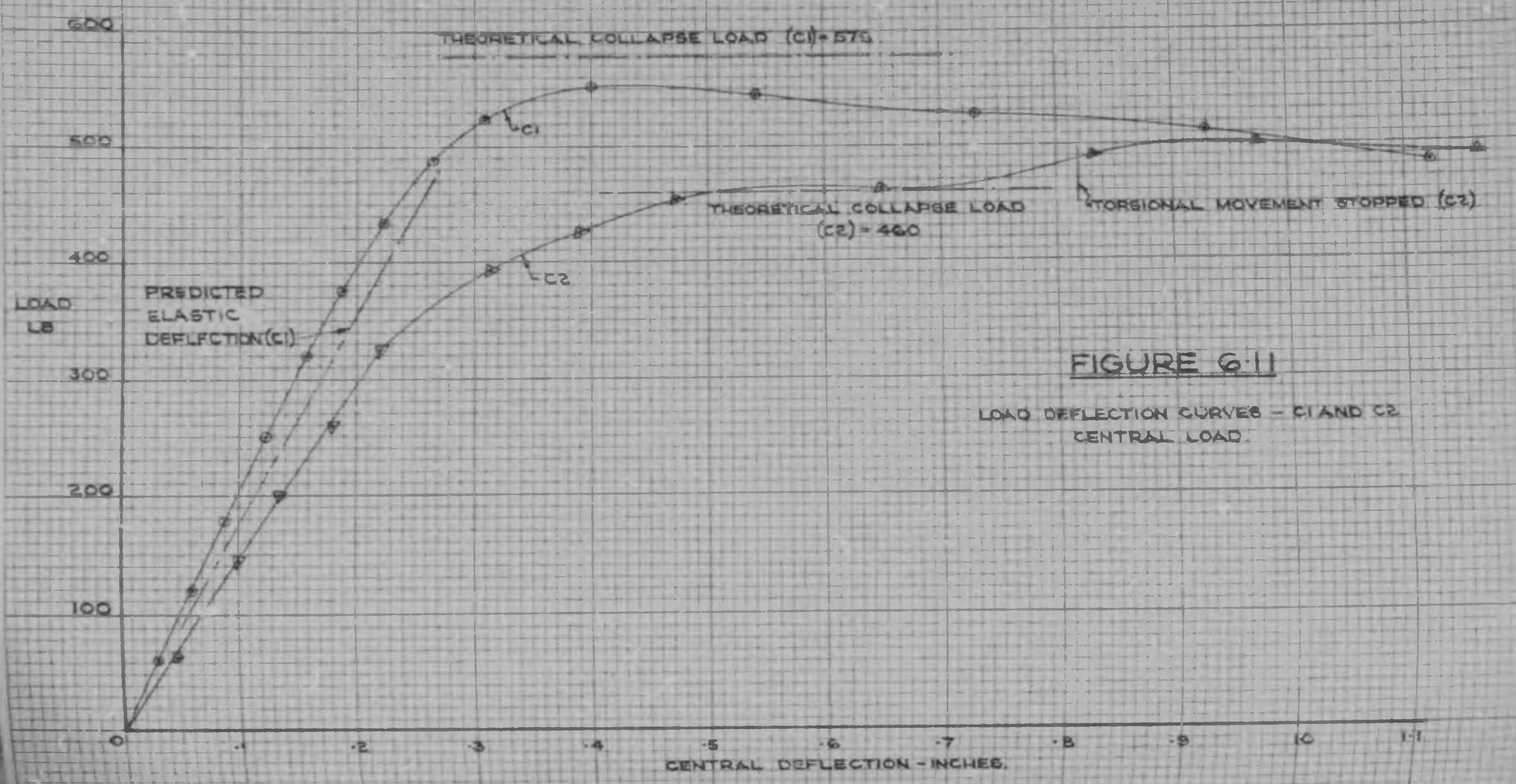

FIGURE 6·11

LOAD DEFLECTION CURVES – C1 AND C2
CENTRAL LOAD.

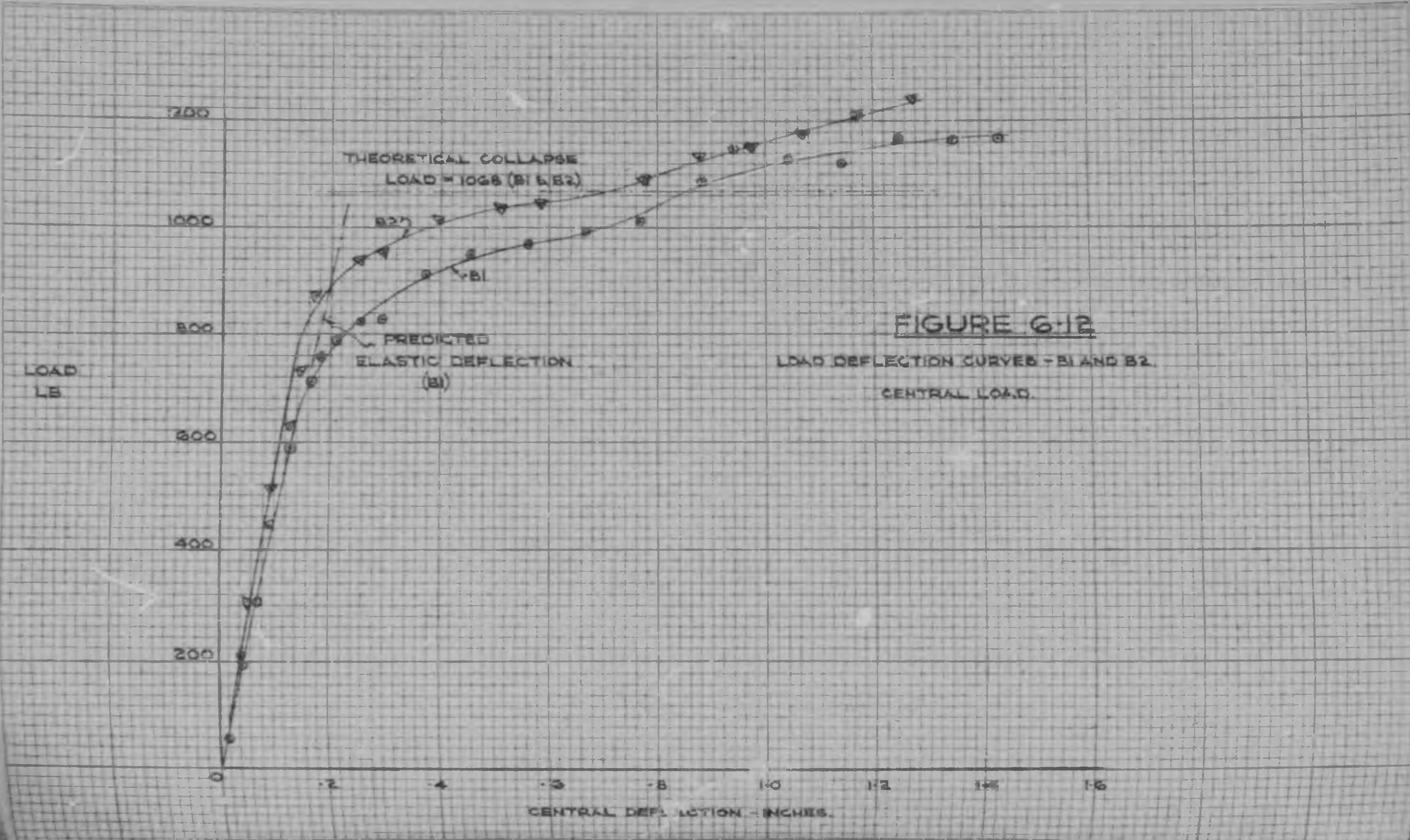

FIGURE 6·12

LOAD DEFLECTION CURVES - B1 AND B2.

CENTRAL LOAD.

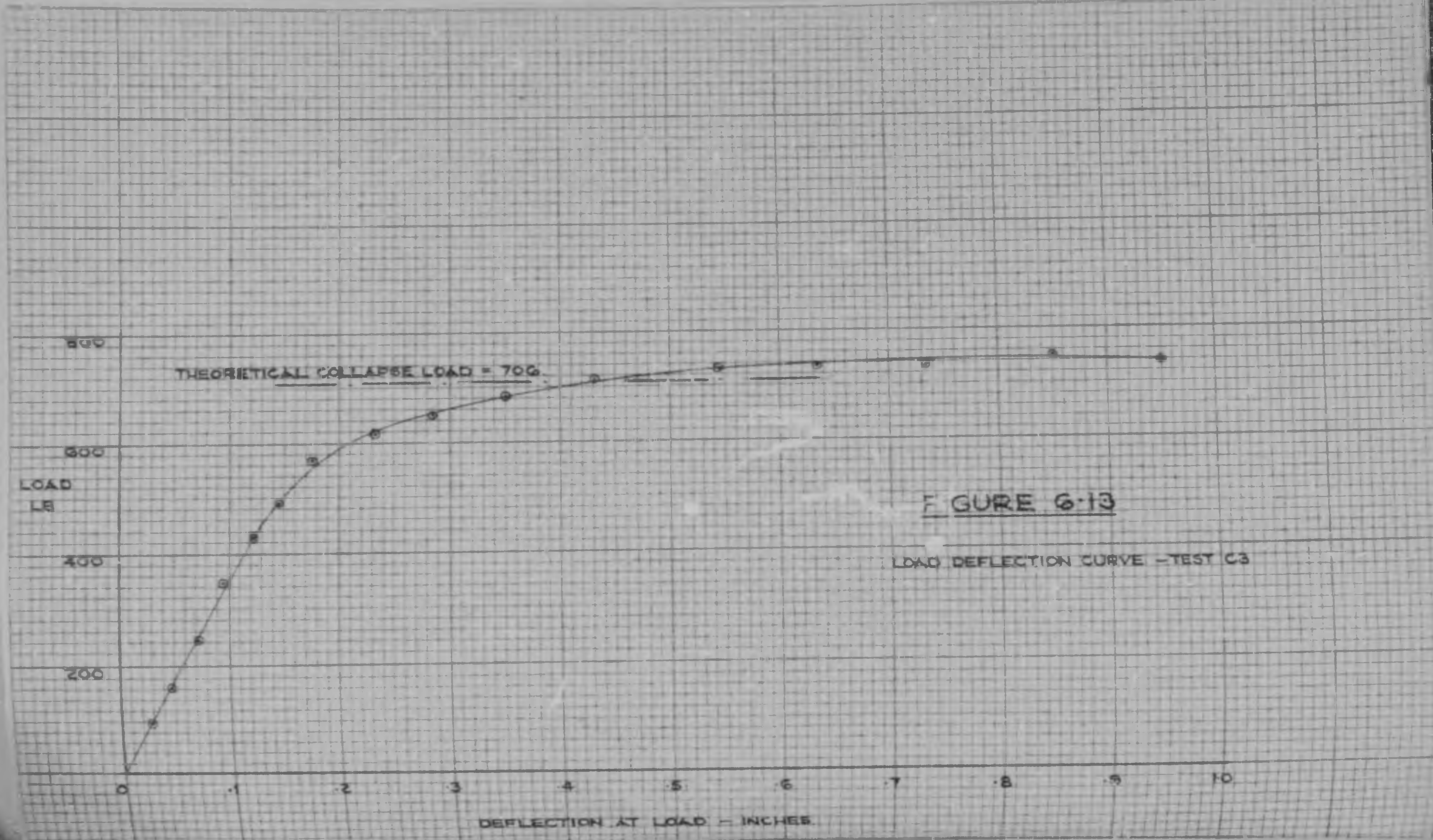

FIGURE 6·13

LOAD DEFLECTION CURVE — TEST C3

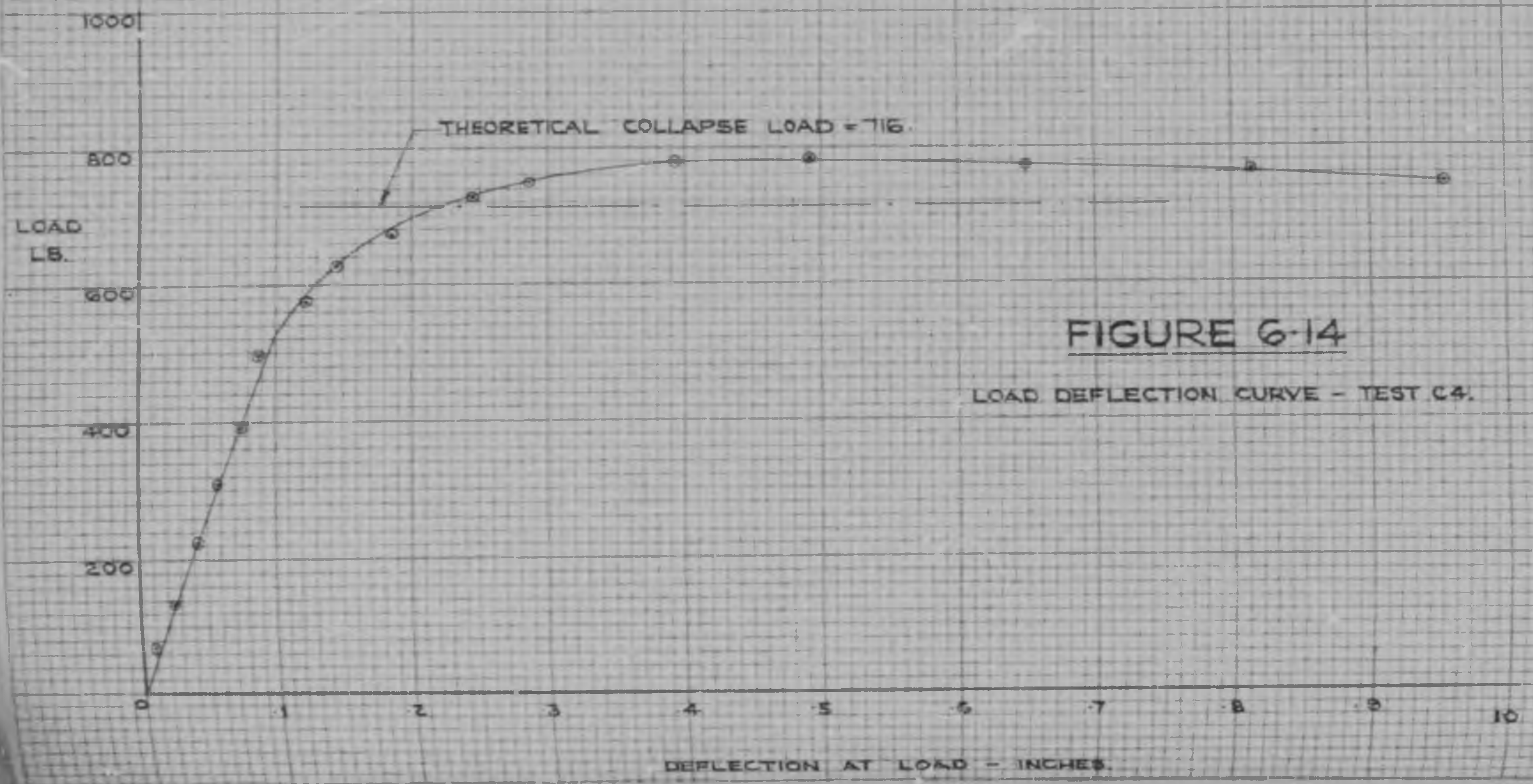

FIGURE 6·14

LOAD DEFLECTION CURVE - TEST C4.

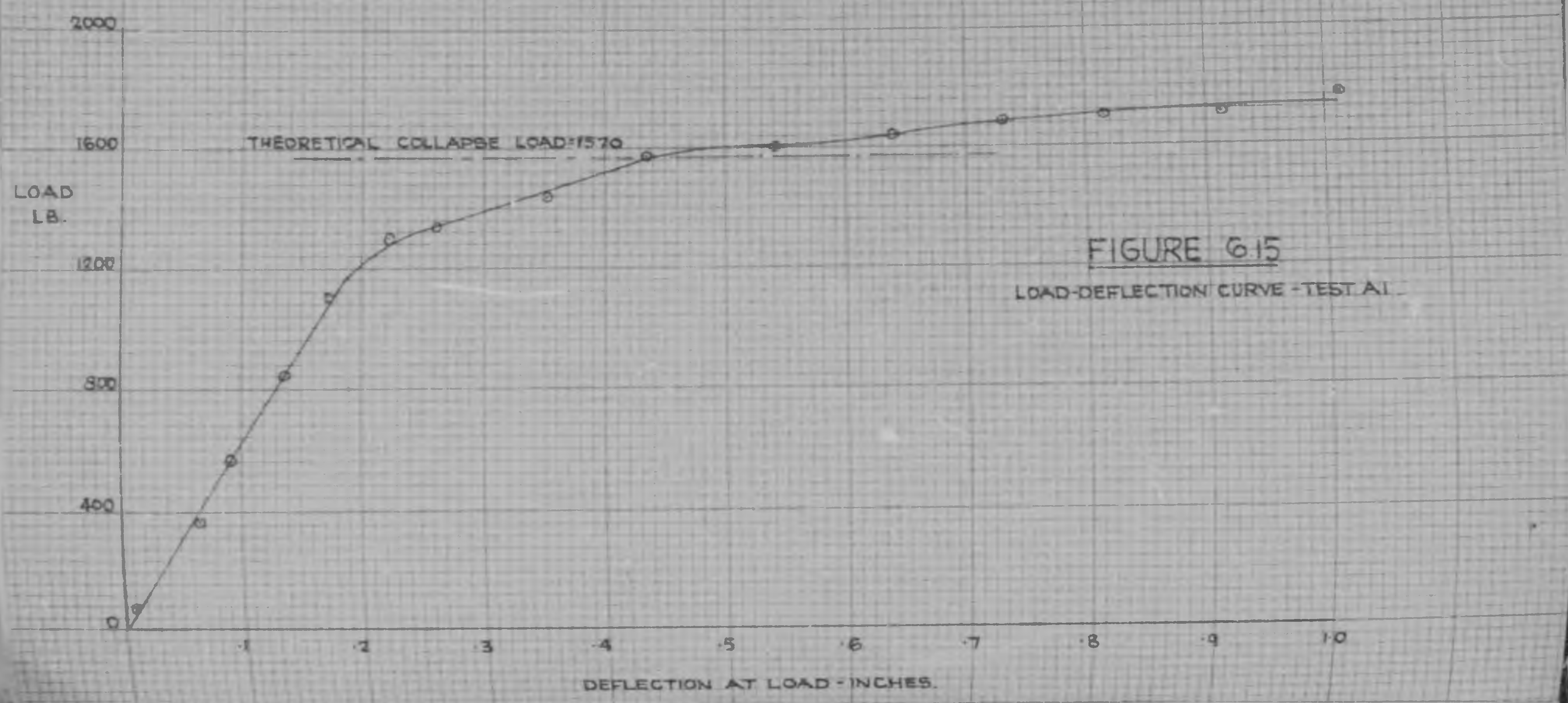

FIGURE 6.15

LOAD-DEFLECTION CURVE - TEST A1.

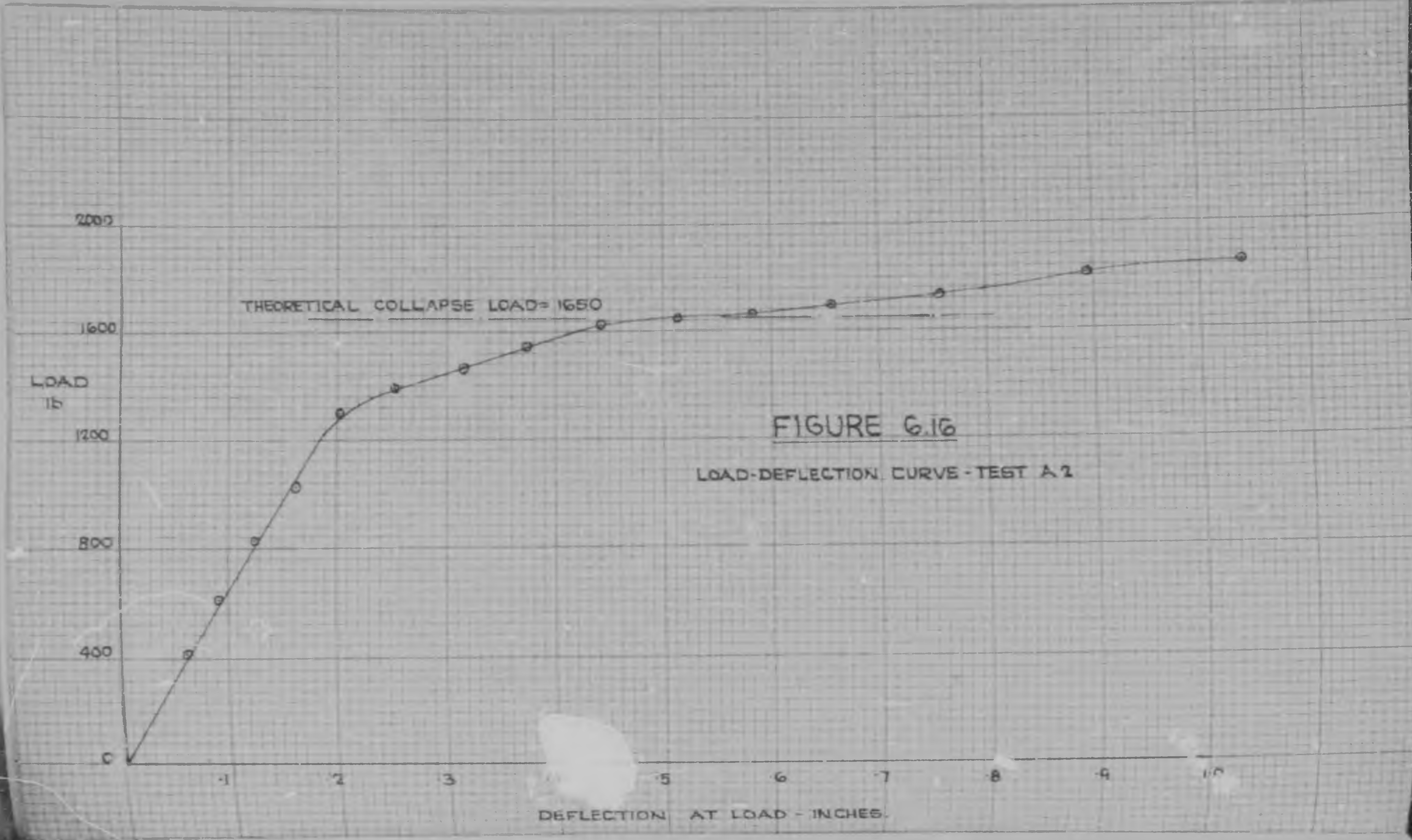

FIGURE 6.16

LOAD-DEFLECTION CURVE - TEST A2

deviation of the "C" results is much higher than the "A" results.

Table 6.2

Section	T_p lb.-in.	Standard Deviation	M_p lb.-in.	Standard Deviation	$\alpha = {}^{T_p}/_{M_p}$
A	4160	81 = 1.9%	6380	85 = 1.3%	.652
B	1220	-	5450	-	.224
C	446	27 = 6%	3526	151 = 4.3%	.1265
	EI lb.-in.^{2}	NJ lb.-in.^{2}	$\gamma = \frac{EI}{NJ}$		
B	8.6×10^6	1.65×10^5	52		
C	2.79×10^6	2.60×10^4	107		

The value of α for each section was calculated from the mean plastic moments; the values of the flexural and torsional rigidities are also given for the "B" and "C" sections (these are the sections for which elastic deflections in the main tests were calculated).

Tests on Miniature Bow Girders. The results will be discussed in the following manner:

firstly, the load-deflection curves for all the tests will be given, with the predicted elastic deflections, the predicted and actual collapse loads, and the position and spread of the plastic hinges;

secondly, the results of the investigation of the yield criterion will be given and,

thirdly, the results of the investigation of the direction of axes of rotation will be discussed.

In Figs. 6.11 to 6.16 the load-deflection curves are plotted. From these graphs the values of the collapse loads have been obtained and are shown with the predicted values in Table 6.3.

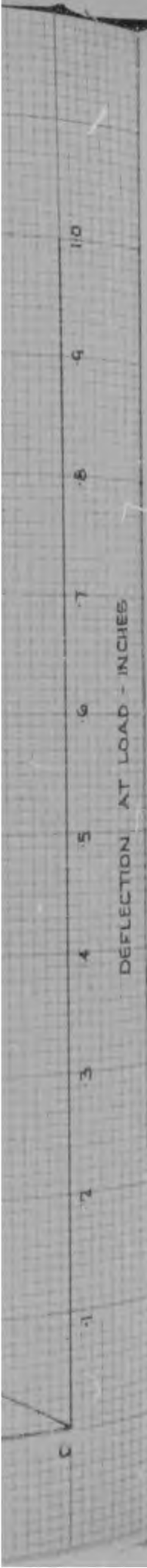

Table 6.3

Test	$\frac{Wr}{M_p}$	W Predicted (lb)	W Actual (lb)	Difference (lb)	Difference %
C1	3.87	578	555 ± 6.8	− 23	− 4.0
C2	3.07	460	465 ± 6.8	+ 5	+ 1.1
B1	4.82	1068	1000 ± 26.2	− 68	− 6.4
B2	4.82	1068	1070 ± 26.2	+ 2	+ 0.2
C3	4.705	706	735 ± 6.8	+ 29	+ 4.1
C4	4.79	716	780 ± 6.8	+ 64	+ 8.9
A1	5.91	1570	1600 ± 26.2	+ 30	+ 1.9
A2	6.21	1650	1660 ± 26.2	+ 10	+ 0.6

The intervals given with the actual collapse loads are the confidence intervals of the loading devices at the 5 per cent level of significance.

The results are in fair agreement with the theoretical collapse loads. In the appraisal of these results two approaches have been used:

(i) a statistical test to determine whether the difference between the actual and predicted collapse loads is significant, and,

(ii) a discussion of each failure load after the yield criterion investigations: deviations of particular values can be interpreted in terms of the measured values of moment and torque in the hinges.

The analysis (i) shows that the average amount by which the measured loads exceeded the predicted loads (.8 per cent) was not significant. This was based on the assumption that the percentage differences (the last column in Table 6.3) were a sample from a normal population and the "Students t" distribution with 7 degrees of freedom was used.

FIGURE 6.17

FIGURE 6.18

On the basis of tests on beams and frames[8], a small increase of experimental over calculated collapse loads would be expected because of strain hardening effects. A further factor that would add to this is that the bending moment-torque interaction equation is a lower bound approximation. On the other hand, in the case of the "C" beams, the failure load decreased as collapse progressed, probably owing to the effect of changes in geometry and instability of the deep narrow sections. Hence an exact agreement between actual and predicted collapse loads would not be expected, since these factors have not been taken into account in the theory.

In the test C2, the load increased slightly after the fixing of the supports, as described in section 6.3, but did not increase to the failure load for the fully fixed case.

The position of the hinges as indicated by flaking of the brittle coating agreed with the theoretical in all cases except in test C2, where in addition to the two free hinges, which occurred as expected, a small amount of plastic flow was evident at the supports before the torsional rotation of the supports was stopped (when there was no torsion at the supports, two free hinges were expected, and plasticity at the supports was only expected after the supports were fully fixed). The positions of the free hinges, taken as the centres of the flaked area on the girder arcs, agreed with the theoretical positions to within two inches; the length of the flaked area of the hinges was from about two inches to about four inches.

Figures 6.17 and 6.18 show the flaking of the brittle coating in tests B1 and C4 respectively, the latter showing formation of a free plastic hinge between the two point loads.

An interesting point which might be of practical importance is that, in the tests C1, C2 and C4, the load decreased after failure had taken place, and did not show the usual increase in load due to strain hardening.

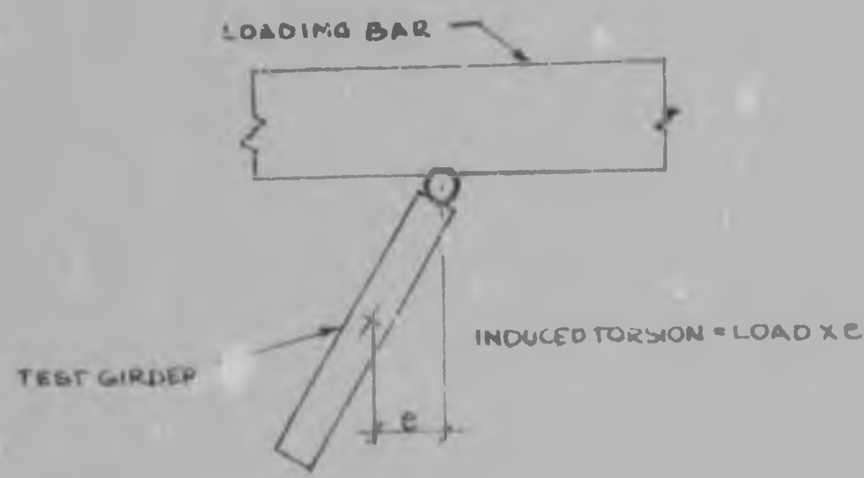

FIGURE 6.19

The explanation for this behaviour is probably that, in the case of the fairly flexible "C" girders, the effect of changes in geometry during collapse is no longer negligible, and that lateral instability of the deep, narrow section affects the load.

The load in the tests was applied to a point on the top edge of the rectangular section. At plastic collapse and therefore at a stage when deformations were large, the section at the load was rotated through quite a large angle and the load consequently induced an additional torque in the beam equal to the product of the load and its eccentricity from the centre of gravity of the section (see Fig. 6.19).

Owing to the induced torsion in the beam, the plasticity at various points in the girder, and the very small resistance of the girder to bending about the vertical axis, it is likely that the lessening of the collapse load of the "C" girders is at least partly a buckling effect; since the point of application of the load would tend to stay in the same vertical line, the girder would tend to buckle outwards at the positions of free hinges.

Further reference will be made to this point in the discussion of torsion in the free hinges.

Elastic deflections of the loading point were calculated for tests B1 and C1, based on the elastic rigidities found from the control tests, and are shown on Figs. 6.11 and 6.12. The agreement with the experimental values was very close in test B1; in test C1 the deflections were slightly less than predicted.

Yield Criterion Investigation. As the bending moment and torque at the supports were measured during the tests, the value of bending moment and torque at any point on the girder could be calculated. The yield criterion has been checked by calculating the bending moment and torque at the hinge, and hence the square root of the left hand side of equation (2.2), i.e., by calculating $(\alpha^2 M^2 + T^2)^{\frac{1}{2}}$. Using the rotation measurements, the rotations corresponding to the values of torque and moment could be calculated for most hinges, except in those cases where due to congestion of

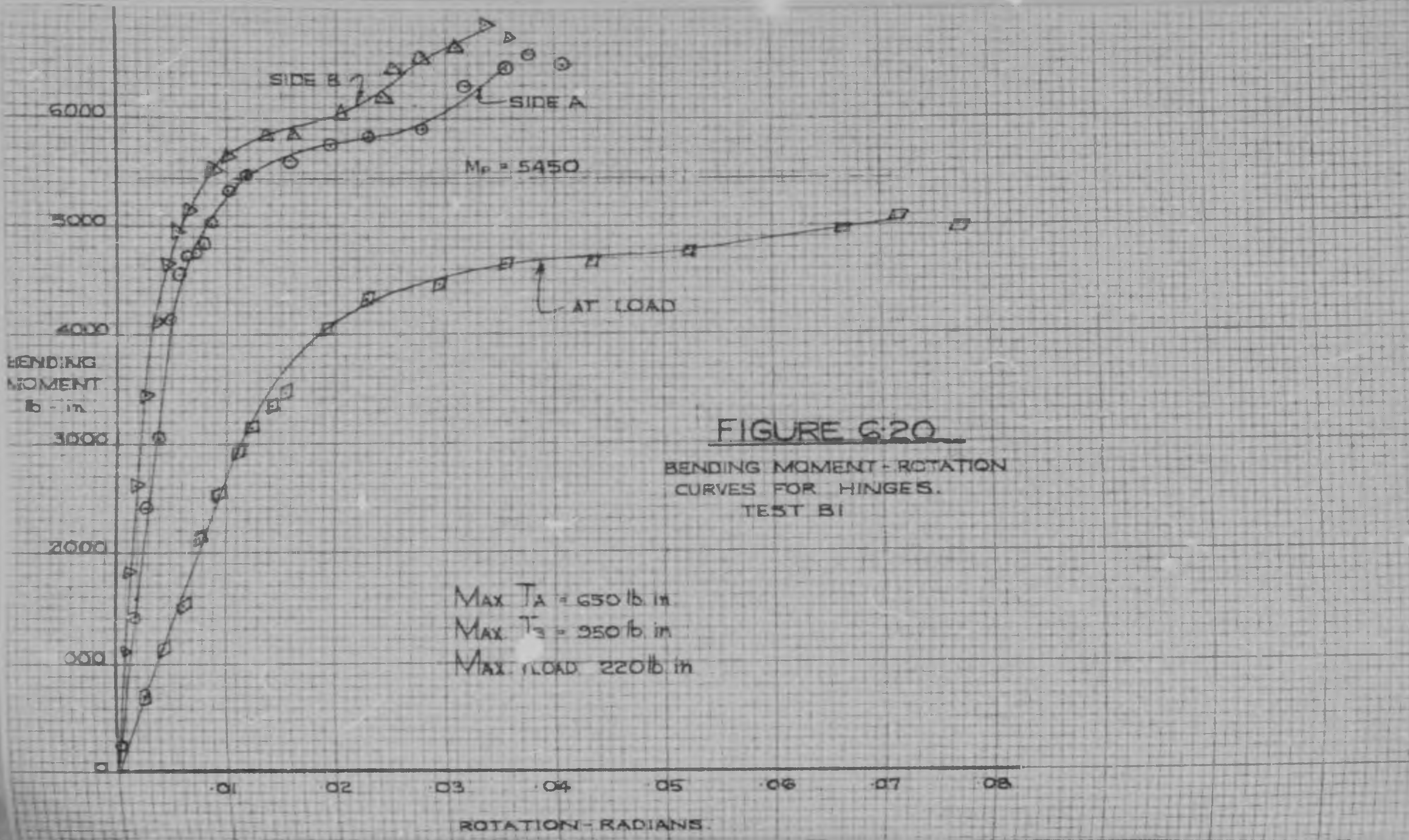

FIGURE 6·20

BENDING MOMENT - ROTATION CURVES FOR HINGES.
TEST B1

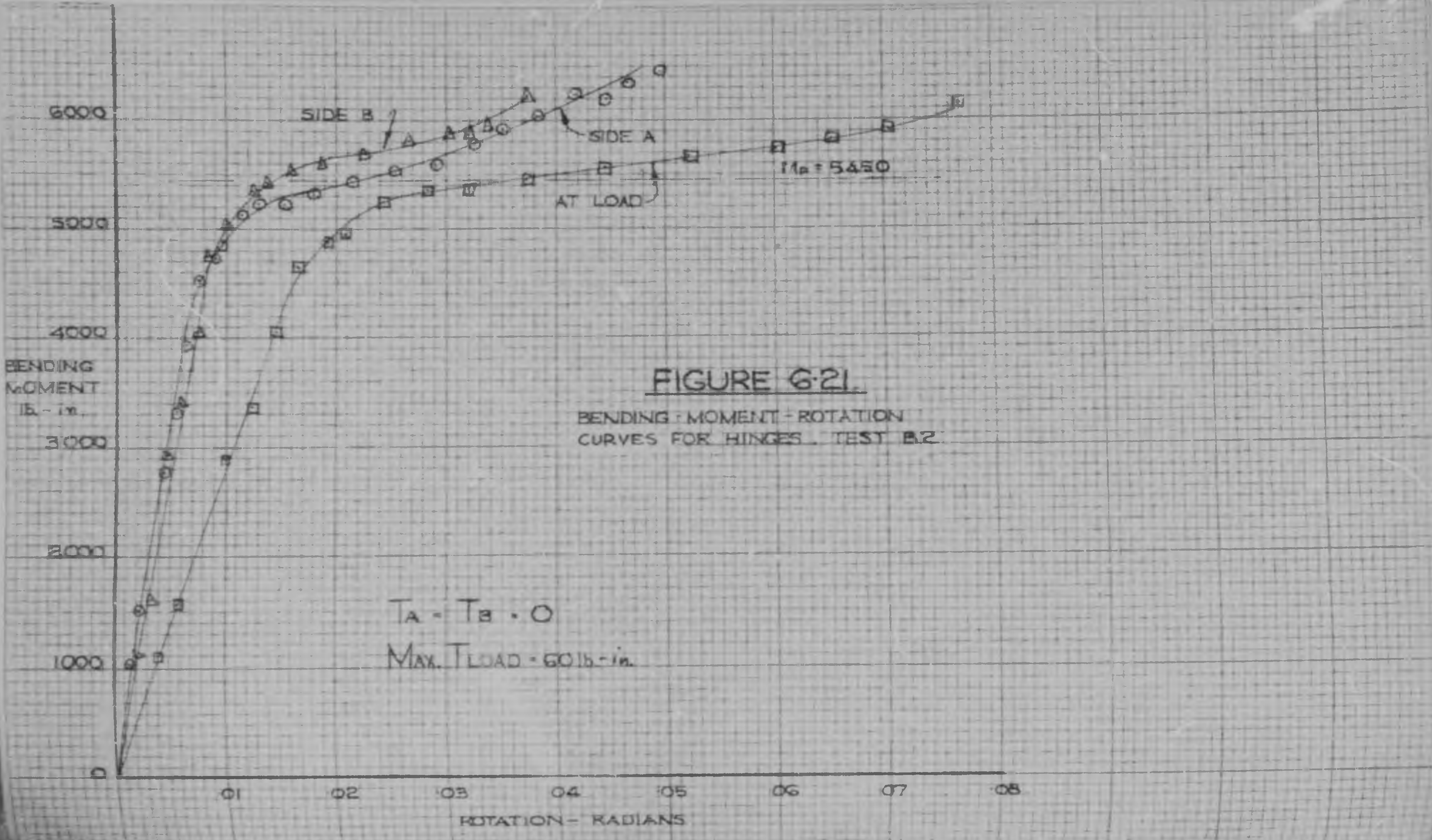

FIGURE 6·21.

BENDING - MOMENT - ROTATION CURVES FOR HINGES. TEST B2.

apparatus, sufficient gauges could not be used. The values of bending moment, torque and $(\alpha^2 M^2 + T^2)^{\frac{1}{2}}$ have been plotted against the bending, torsional and resultant rotation, respectively, at the hinges. In the cases where it was not possible to calculate the rotation, the values of bending moment and torque in a hinge alone do not give much evidence of plastic flow, as it is known that elastic moments and torques remain approximately constant during collapse. It was decided, therefore, to analyse the behaviour of only those hinges for which rotations were available.

As the equation (2.2) represents a theoretical lower bound, it would be expected that the substitution of actual bending moment and torque values would cause $(\alpha^2 M^2 + T^2)^{\frac{1}{2}}$ to exceed T_p by a small amount.

"B" Tests. As predicted, hinges occurred at the supports and at the loading point for both B1 and B2. Theoretically, the hinges are in pure bending. The values of bending moment and bending rotation have been calculated, and are plotted in Fig. 6.20 (test B1) and Fig. 6.21 (test B2). The rotations plotted are the bending rotations of the lengths of beam between the support and central point for the support hinges, and the rotations of the whole arc about the bending axis at the centre for the centre hinge. This is why the rotations at the centre hinges are much larger than at the support hinges. The maximum values of torsion in the hinges are shown on the graphs.

The values of the plastic moment taken from the graphs are shown in Table 6.4.

Table 6.4

Test	Location of Hinge	Plastic Moment		
B1	Support A	5800)	Mean for)	Mean for all
B1	Support B	5800)	B1 = 5370)	tests =
B1	At load	4500)	)	5508
B2	Support A	5600)	Mean for)	
B2	Support B	5850)	B2 = 5650)	
B2	At load	5500)		

The mean value of the plastic moment, i.e., 5508 lb.-in. is very close to the mean value obtained in the control tests (5450 lb.-in.); all the values of plastic moment exceeded the control value except for the value of plastic moment in test B1 at the load. It is clear that the effect of the torsion in the hinges would tend to reduce the average value of plastic moment obtained below the average obtained in the control tests. An investigation reveals that this effect is negligible except in the case of the hinge at support B in test B1, in which case the contribution of torsion to the value of $(\alpha^2 M^2 + T^2)^{\frac{1}{2}}$ is less than ten per cent. The effect of torsion on the plastic moments has therefore been neglected.

An inspection of the collapse loads for B1 and B2 reveals that the girder B1 failed at a value 6.4 per cent less than predicted whereas the failure load for B2 was almost exactly as predicted. The large difference for B1 is mainly due to the extremely small value of plastic moment at the hinge under the load. Since the rotation at the central hinge during plastic deformation is about twice the rotation at the supports, the energy absorbed by the central hinge during plastic collapse is about twice the energy absorbed by the support hinge. Hence the effect on the collapse load of the small value of plastic moment in the central hinge in test B1 is double the effect of the same plastic moment at a support. This low value of plastic moment appears to be a random occurrence (the torsion in the hinge has a negligible effect) and explains the low value of collapse load in test B1.

<u>"C" Tests</u>. The "C" tests all involved the formation of four hinges, namely, two free and two fixed (for test C2, four hinges formed fully only after torsional rotation was stopped at the supports). As has been mentioned, those hinges for which it was not possible to measure the deformations during collapse have not been used in the yield criterion investigation. The hinges that have been considered are: all hinges in C1 and C2, one fixed and free hinge in each of C3 and C4, that is, in all, six fixed hinges (at supports) and six free hinges.

FIGURE 6.22

BENDING MOMENT - ROTATION CURVES - FIXED HINGES AT SUPPORTS. TEST C1.

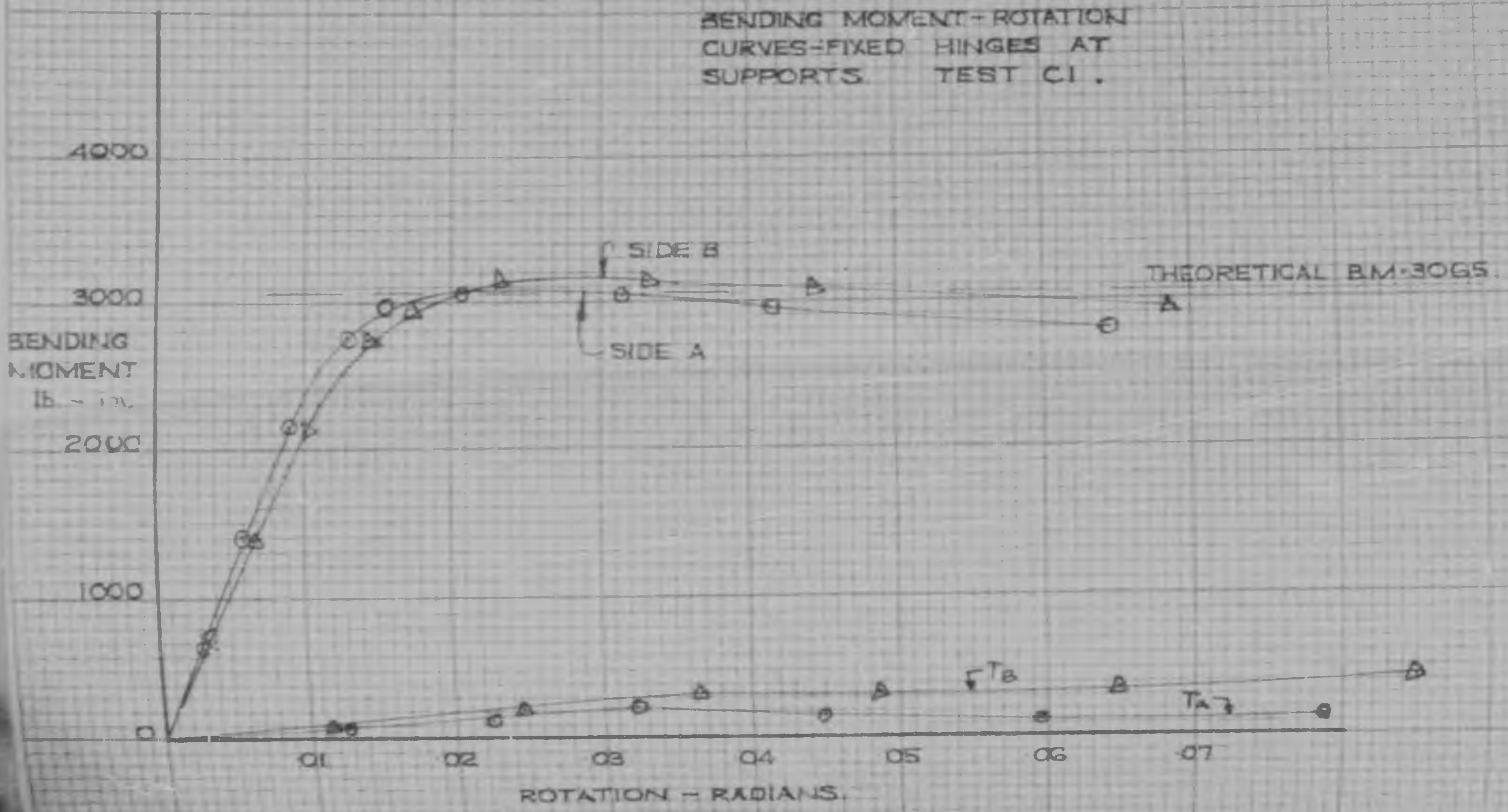

FIGURE C23

TORQUE - ROTATION CURVES

FIXED HINGES AT SUPPORTS

TEST C1

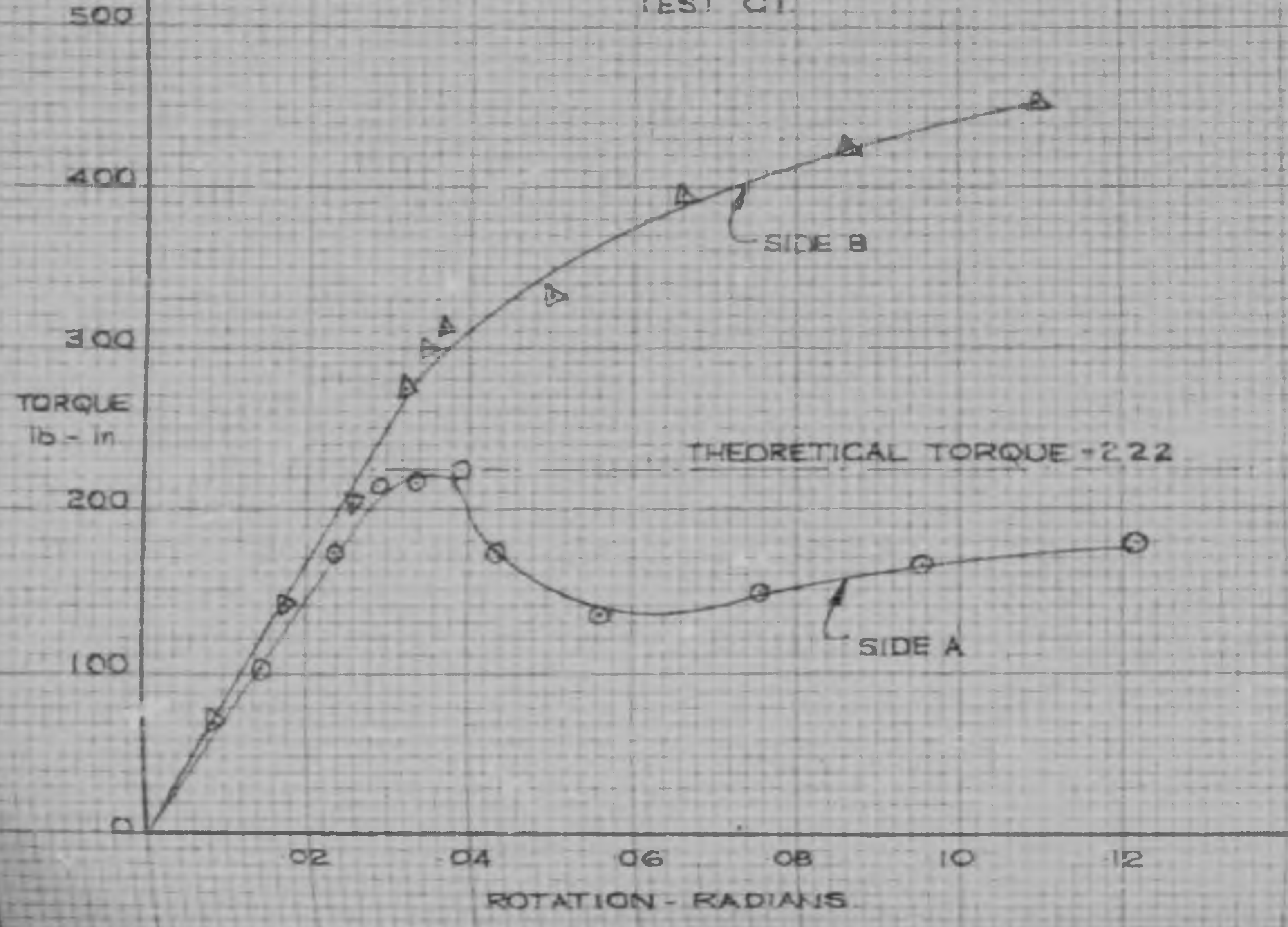

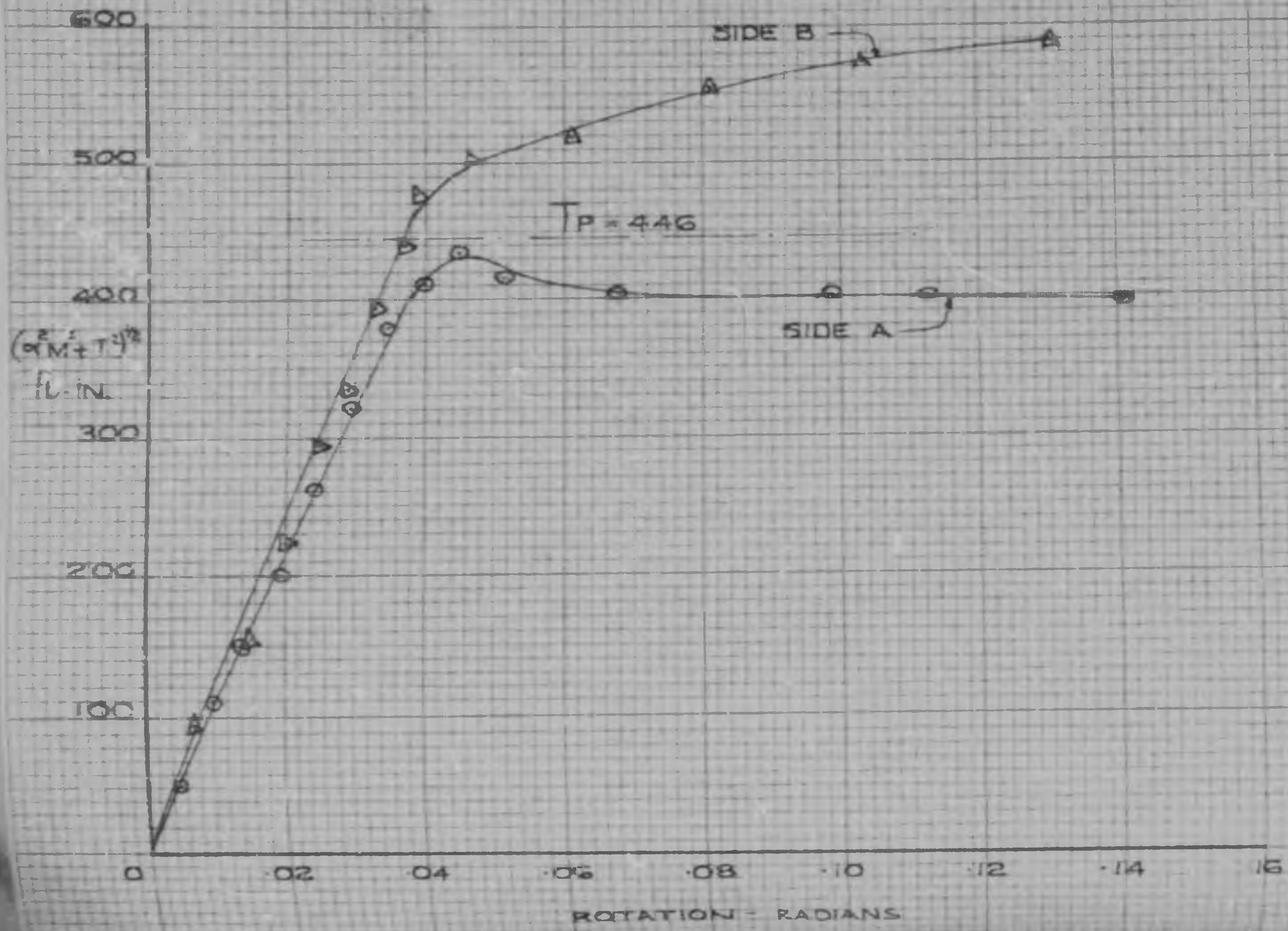

FIGURE 6·24

YIELD CRITERION - FIXED HINGES

TEST C1.

FIGURE 6·25.

BENDING MOMENT – ROTATION CURVES

FIXED HINGES AT SUPPORTS-TEST C2.

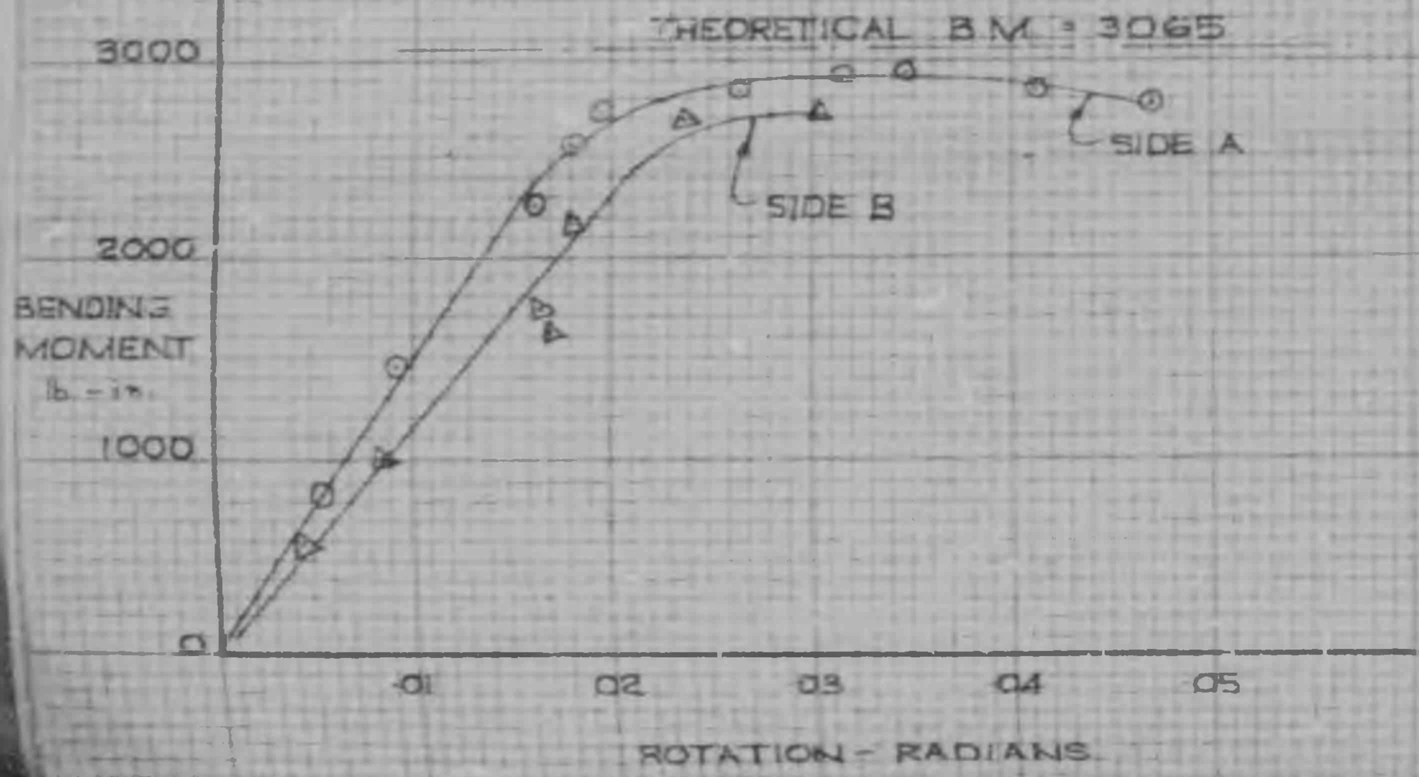

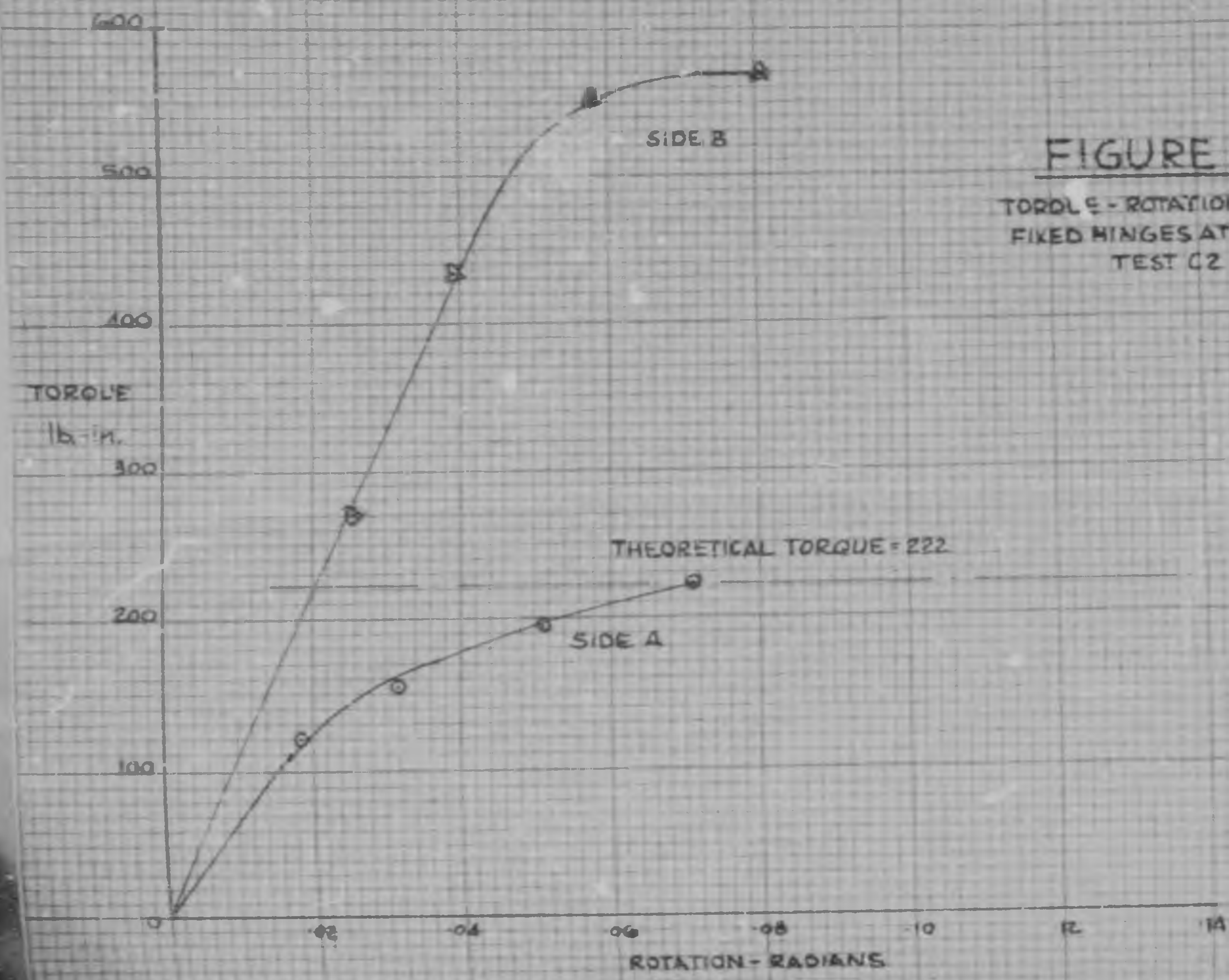

FIGURE 6.26

TORQUE - ROTATION CURVES
FIXED HINGES AT SUPPORTS
TEST C2

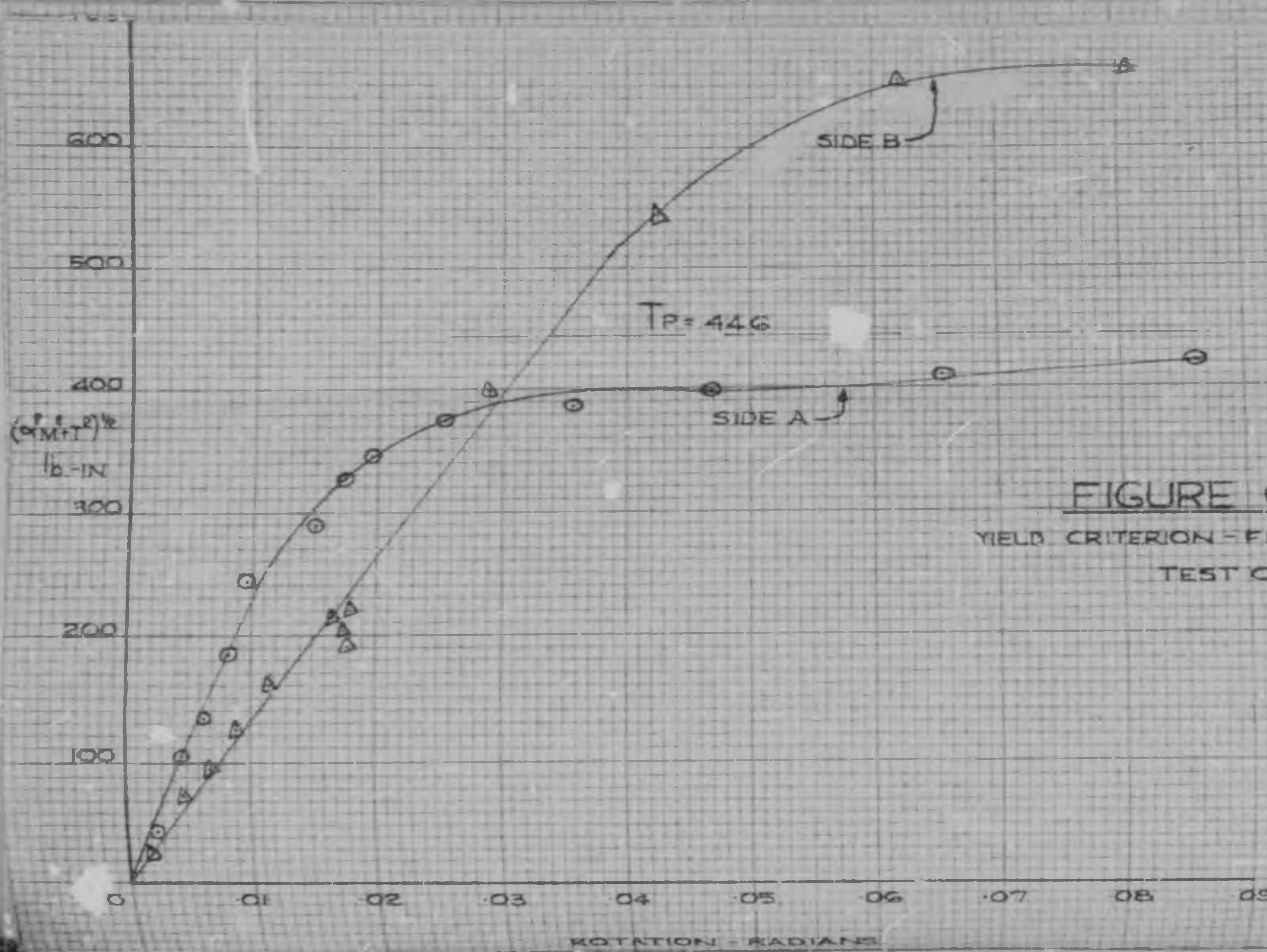

FIGURE 6·27

YIELD CRITERION - FIXED HINGES

TEST C2

FI RE 6.28

BENDING MOMENT ROTATION CURVES

FIXED HINGES AT PORTS

TESTS C3 AND C4

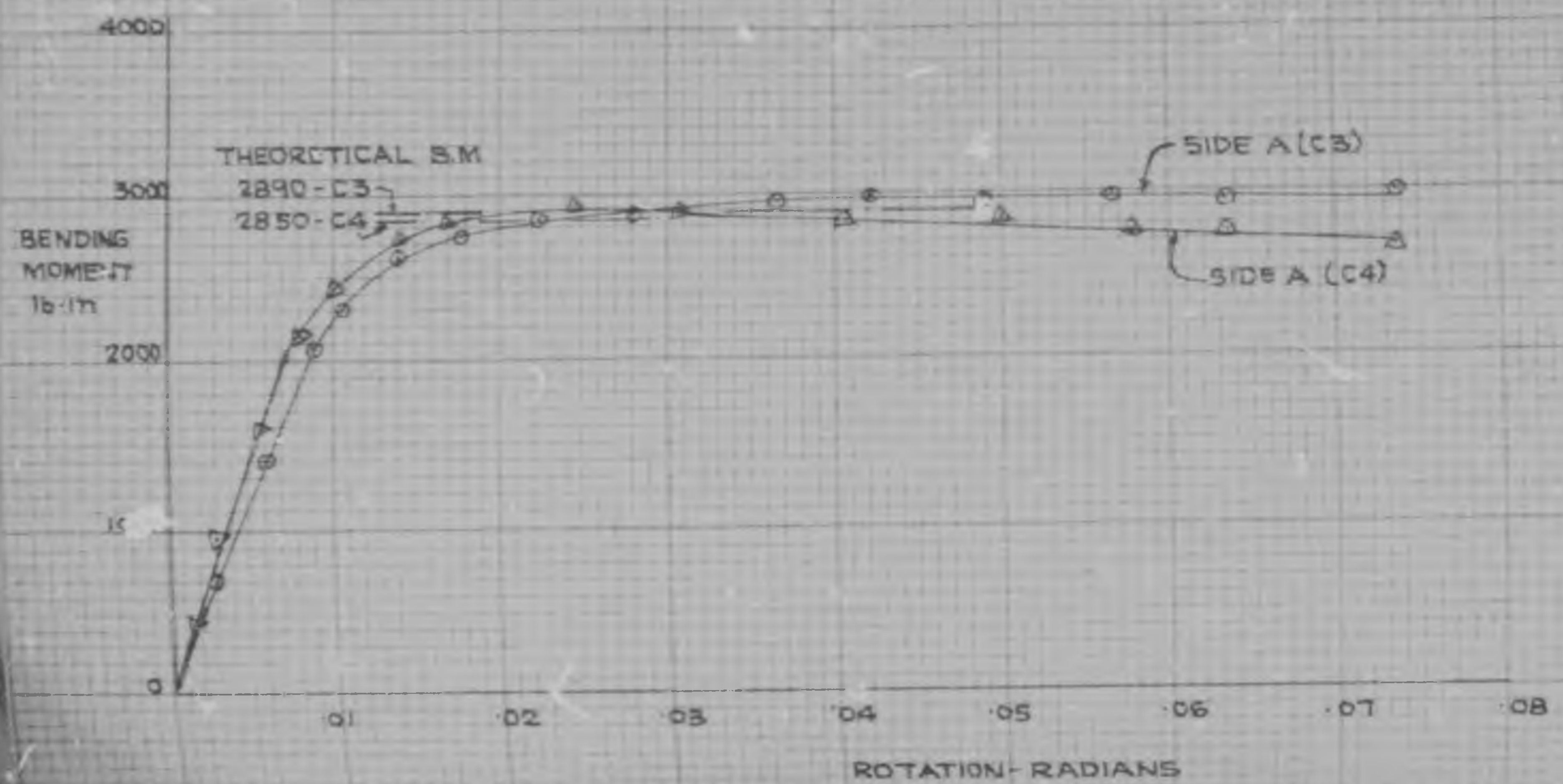

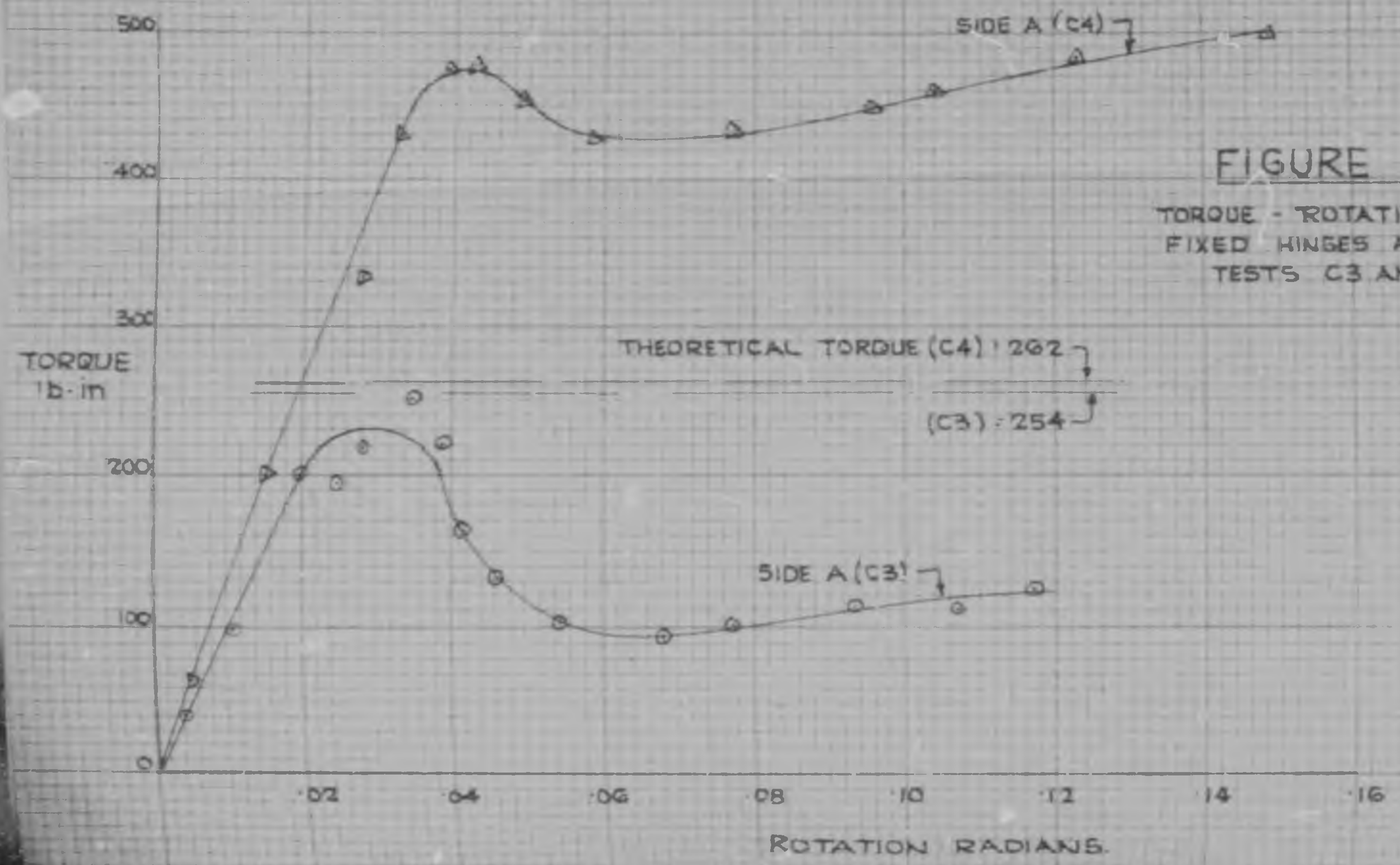

FIGURE 6.29

TORQUE - ROTATION CURVES
FIXED HINGES AT SUPPORTS
TESTS C3 AND C4.

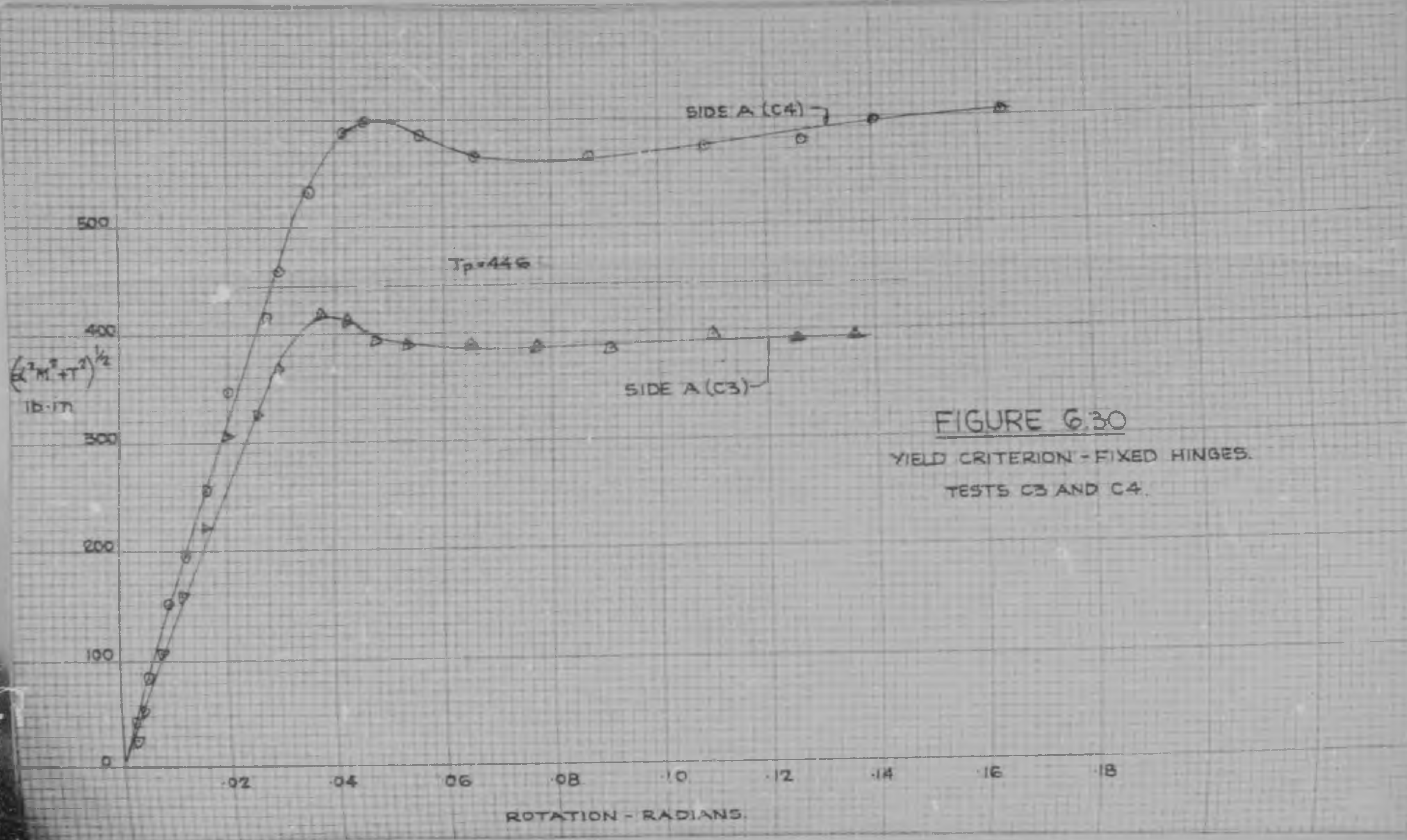

FIGURE 6.30

YIELD CRITERION - FIXED HINGES.

TESTS C3 AND C4.

In Figs. 6.22 to 6.30 the value of bending moment, torque and $(\alpha^2 M^2 + T^2)^{\frac{1}{2}}$ are plotted against the bending, torsional and total rotation of the various fixed hinges, and in Figs. 6.31 to 6.33 the values of torsion in the free hinges are plotted against the torsional rotation of the free hinge. In the case of the latter curves, to facilitate calculation, the positions on the arc for which the values of torsion were calculated were not positions where the bending moment was zero, but were points for which the bending moment was small and had a small effect on the value of torsion. The rotations plotted are the rotations of the lengths of girder between bubble gauges on either side of the free hinges and the lengths from the support to the nearest vertical deflection gauge in the case of the fixed hinges.

The values of $(\alpha^2 M^2 + T^2)^{\frac{1}{2}}$ at full plasticity of the section, taken from the graphs are shown in Table 6.5.

Table 6.5

Test	Location of Hinge	$(\alpha^2 M^2 + T^2)^{\frac{1}{2}}$ lb.-in.	
C1	Support A	405	)
C1	Support B	520	)
C2	Support A	390	)
C2	Support B	665	) Mean = 492 lb.-in.
C3	Support A	390	)
C4	Support A	580	)

The mean of the values in Table 6.5, i.e., 492 lb.-in., agrees reasonably with the value of Tp (= 446 lb.-in.) from the control tests. The variation of the individual values, however, is out of all proportion to the consistency obtained in the main test results or the control test results.

The graphs of bending moment and torque against rotation show that in all cases the percentage difference between actual and predicted bending moments at full plasticity was small, whereas the percentage difference for the torque was large, although the order of the variations was about the same in both cases. A comparison of actual and predicted bending moments is shown in Table 6.6.

Table 6.6

Test	Location of Hinge	Predicted Bending Moment lb-in.	Experimental Bending Moment lb-in.	Percentage Differences
C1	Support A	3065	3070	+ .2
C1	Support B	3065	3180	+ 3.8
C2	Support A	3065	2900	- 5.4
C2	Support B	3065	2750	-10.3
C3	Support A	2890	2900	+ 0.3
C4	Support A	2850	2920	+ 2.5

The wide variation in the values of $(\alpha^2 M^2 + T^2)^{\frac{1}{2}}$ is clearly a reflection of the large deviations in torque, since the effect of torque on $(\alpha^2 M^2 + T^2)^{\frac{1}{2}}$ is considerable as the bending moment values are multiplied by α ($=$ .1265). Hence the effect of torsion on the yield criterion equation is large, for the small values of α in the "C" tests, whereas its effect on the collapse load is quite small. This can be seen in Fig. 6.22 where the values of torque against torsional rotation have been plotted on the same graph as the bending moment-bending rotation curve. The area under these curves represents the energy absorbed during collapse by the bending and twisting components, and it is evident that the twisting component has a comparatively small effect on the collapse load.

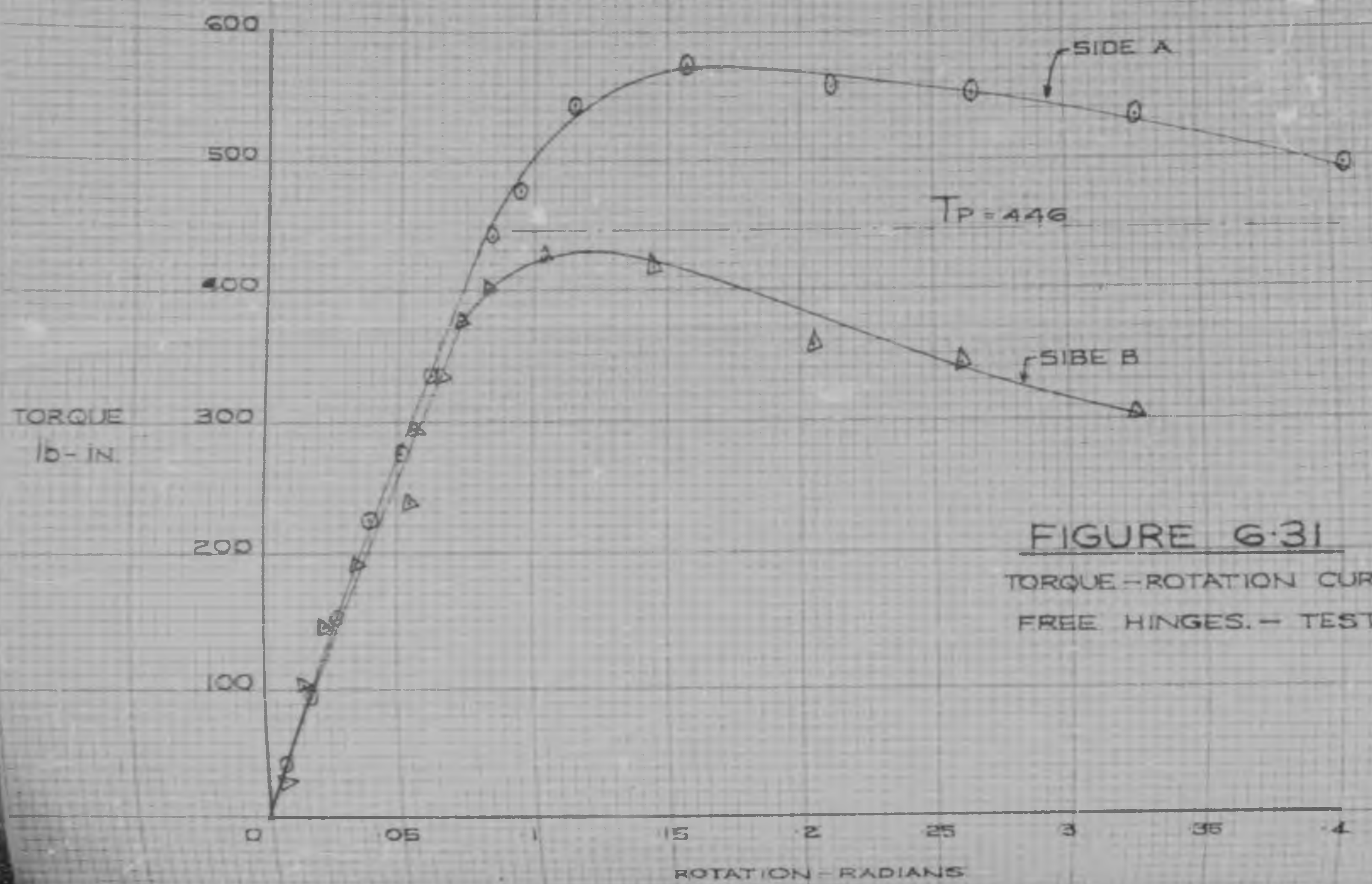

FIGURE 6·31

TORQUE - ROTATION CURVES

FREE HINGES. - TEST C1

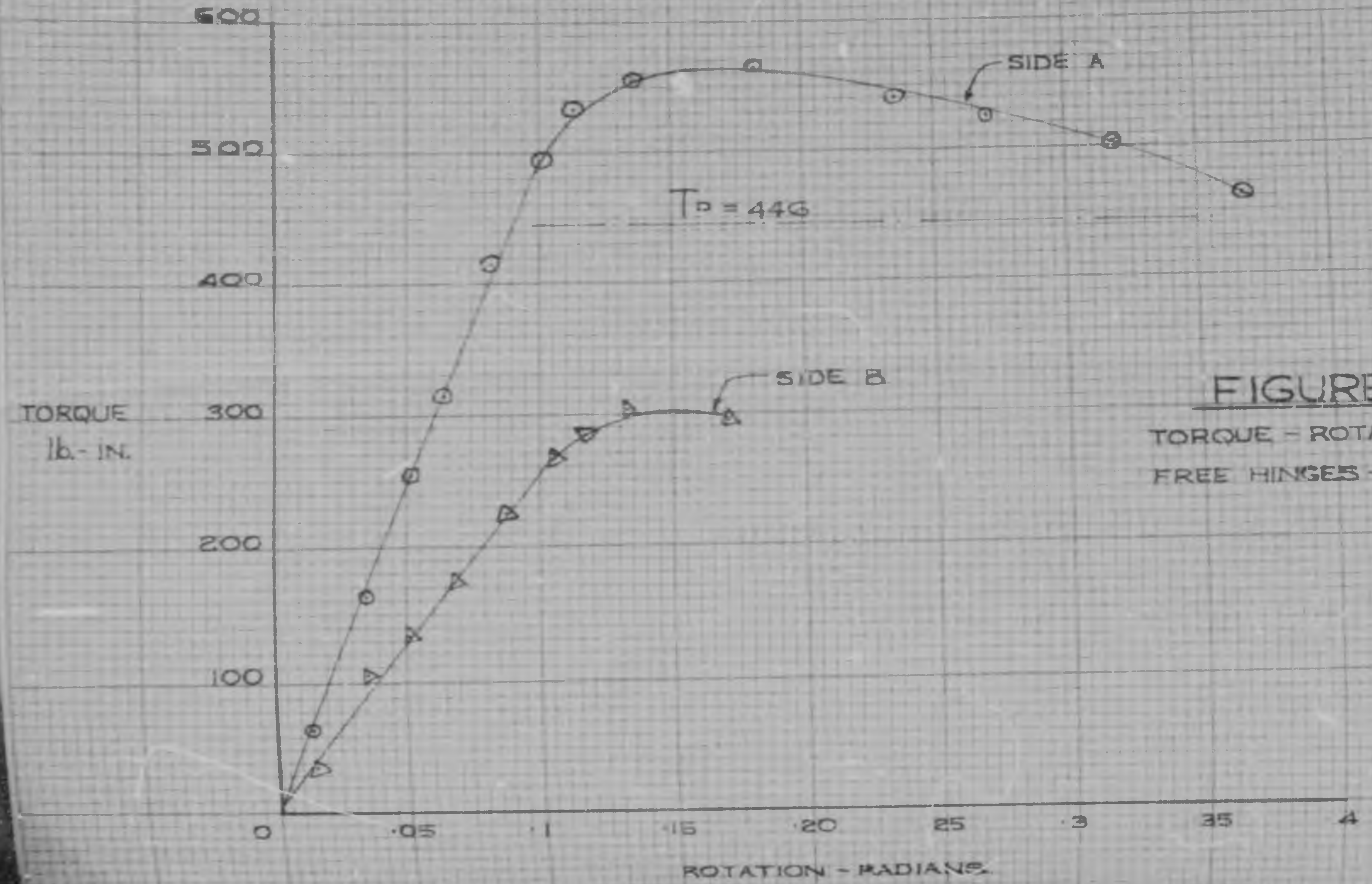

FIGURE C.32

TORQUE - ROTATION CURVES

FREE HINGES - TEST C2

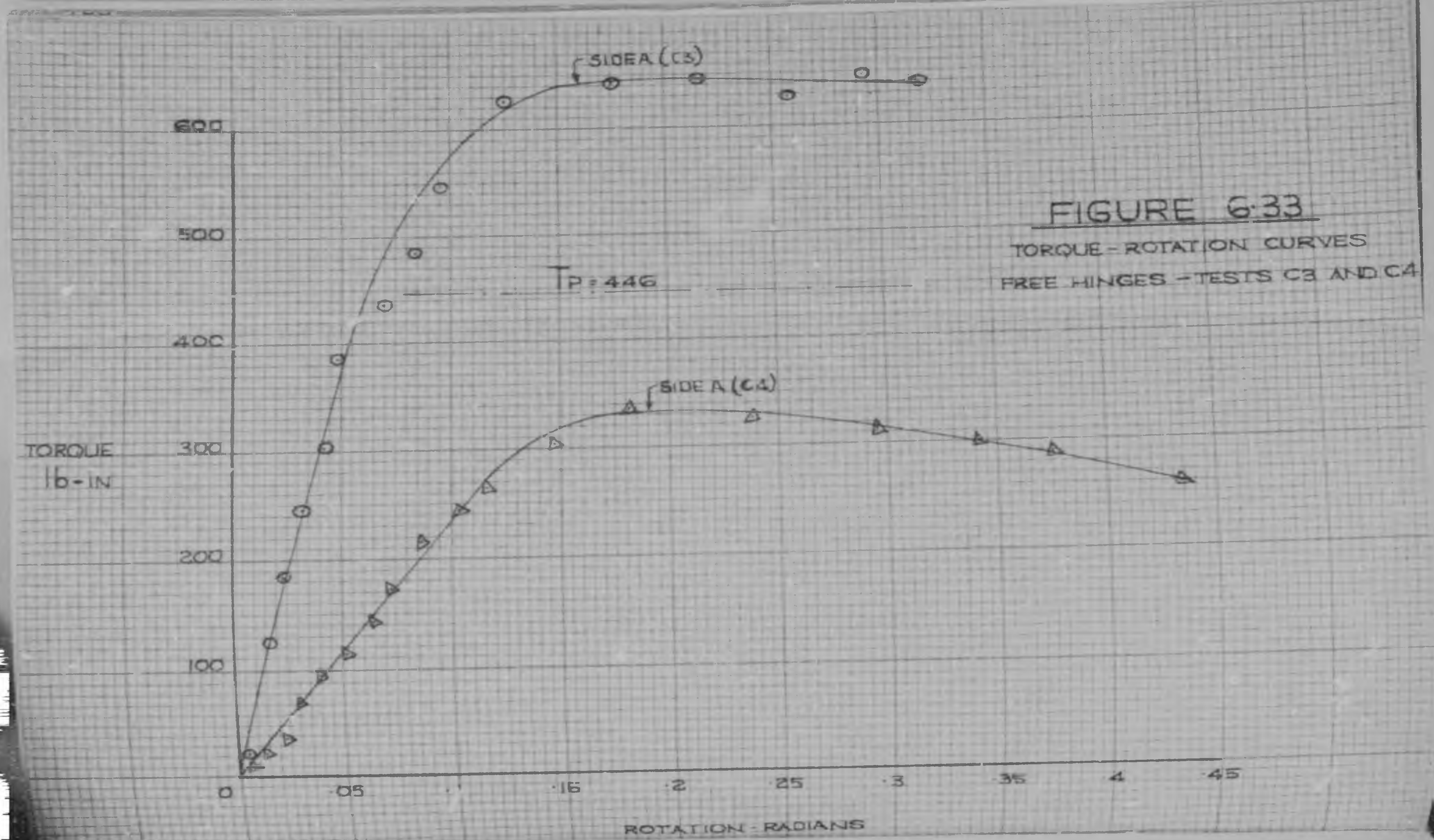

FIGURE 6·33
TORQUE - ROTATION CURVES
FREE HINGES - TESTS C3 AND C4
SIDE A (C3)
SIDE A (C4)
TP = 446
TORQUE
lb-IN
600
500
400
300
200
100
0
·05
·1
·15
·2
·25
·3
·35
·4
·45
ROTATION - RADIANS

A rough estimate shows the standard deviation of the bending moment and torque measurements is about 80 lb.-in. The end moments and torques were measured on lever arms at an angle of 45° to the tangent at the supports; the end bending moment and torque is proportional to the sum and difference of the two readings respectively. The possible error in bending moment and torque is the same, but the percentage influence on torque is much greater than on the bending moment. A large proportion of the variation in torque values may therefore be attributed to possible measuring errors; an estimate of how much the torque actually varies would require tests with more refined apparatus.

The values of torque in the free hinges at full plasticity abstracted from Figs. 6.31 to 6.33 are shown in Table 6.7.

Table 6.7

Test	Location of Hinge	Torque lb.-in.	
C1	Side A	580	)
C1	Side B	430	)
C2	Side A	565	) Mean = 477
C2	Side B	305	) lb.-in.
C3	Side A	650	)
C4	Side A	335	)

The mean value, i.e. 477 lb.-in., is in fair agreement with the full plastic moment in pure torsion found from the control tests (446 lb.-in.), but the deviations are much greater than in the control tests in which the standard deviation is 27 lb.-in. A large part of this deviation is possibly due to errors of measurement; but if the standard deviation of the individual values is about 80 lb.-in., the standard deviation of the mean would be about 80/6 = 13 lb.-in. The fairly close agreement of the mean plastic torque in the tests with the control value does provide some evidence which contradicts the suggestion in the discussion[4] on the paper by Boulton and Boonsukha that, since the free hinges in actual bow girders occur at isolated points, restriction of plastic warping would

cause values of torsion considerably higher than those obtained where plasticity occurs over the whole length of member, as in the control tests. The results of this investigation have also shown that the free hinges spread from two inches to four inches.

Another feature of the free hinge results is that the values of torsion decrease steadily at high values of rotation. It is probable that this effect is connected with the decline in collapse load at large deflections.

The consistency of the values of bending moment at the supports shows that the localised strain hardening (mentioned in section 6.2) had little effect on the results.

The values of collapse load for the "C" tests agree with the predicted values reasonably except for C2 (after the torsional rotation at the supports was stopped) and C4.

In test C2 it was expected that the load, on fixing the supports, would increase to the fully fixed value, but the load was already decreasing, probably owing to the effects of changes in geometry, and the attempt was unsuccessful.

The collapse load in test C4 was 8.9 per cent larger than predicted. The values of bending moment in the hinges at support A were very close to the expected value; the values of torsion in the free hinges, as calculated, were rather lower than the expected value from the control tests. The explanation for the high collapse load appears to be in the high values of moment in the hinge at the support B. Unfortunately, complete values of the rotations are not available but a fairly accurate calculation shows that the bending rotation at collapse in the hinge at supports is almost three times the bending rotation at hinge A. The value of the bending moment at collapse was about 4300 lb.-in., which is much greater than the value of bending moment in pure bending from the control tests (3526 lb.-in.). The energy absorbed in this hinge is therefore much greater than the energy absorbed in any other hinge in the test, and the large value of bending moment would

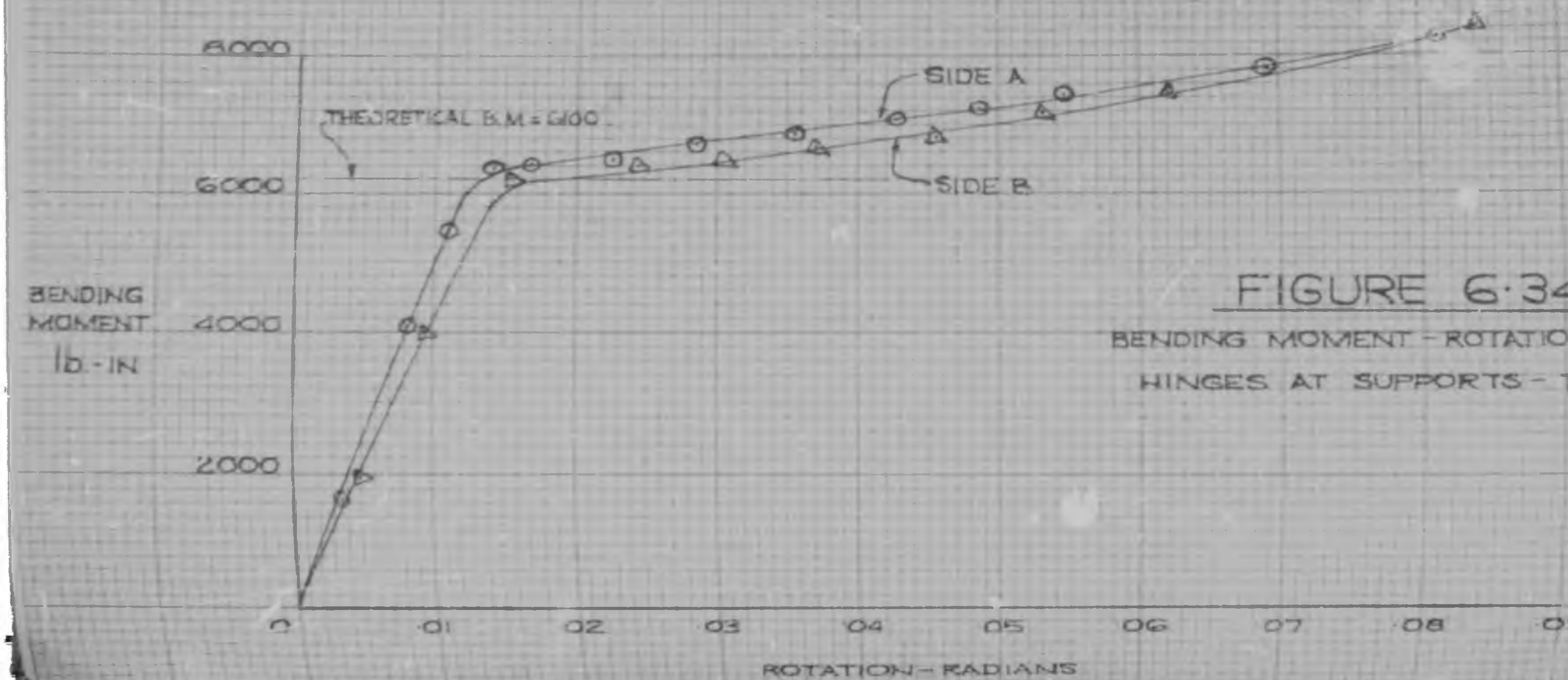

FIGURE 6·34.

BENDING MOMENT – ROTATION CURVES

HINGES AT SUPPORTS – TEST A1

FIGURE 6·35

TORQUE - ROTATION CURVES

HINGES AT SUPPORTS - TEST A1

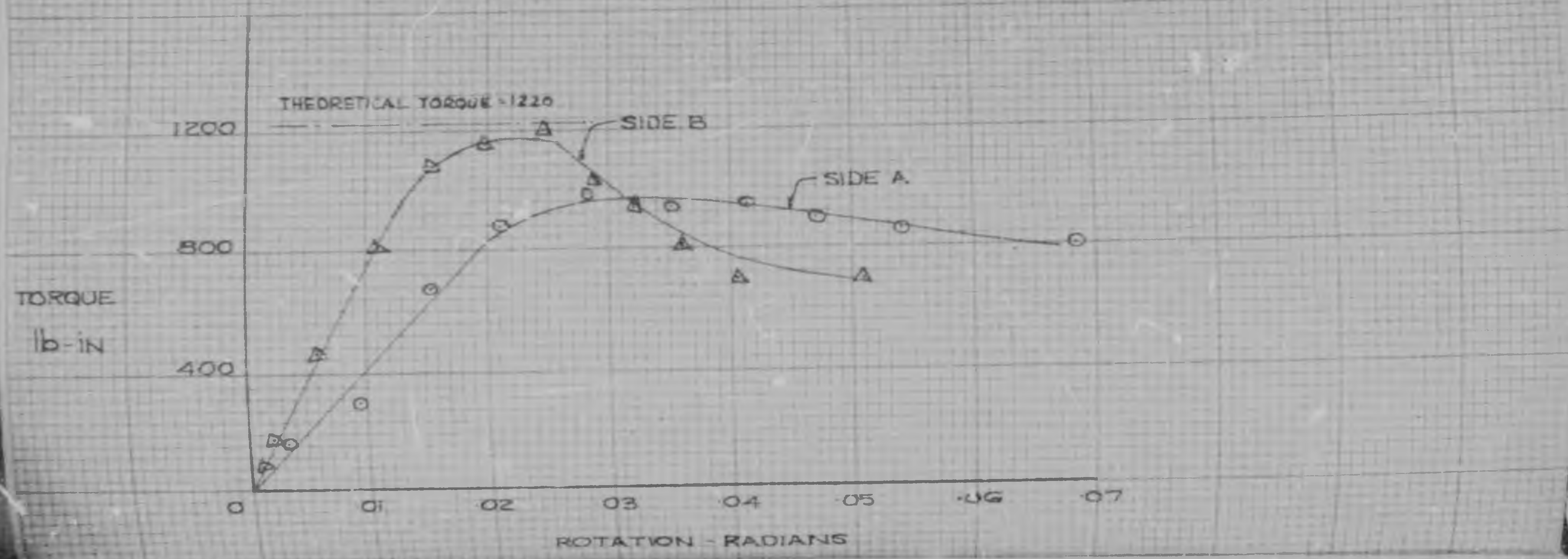

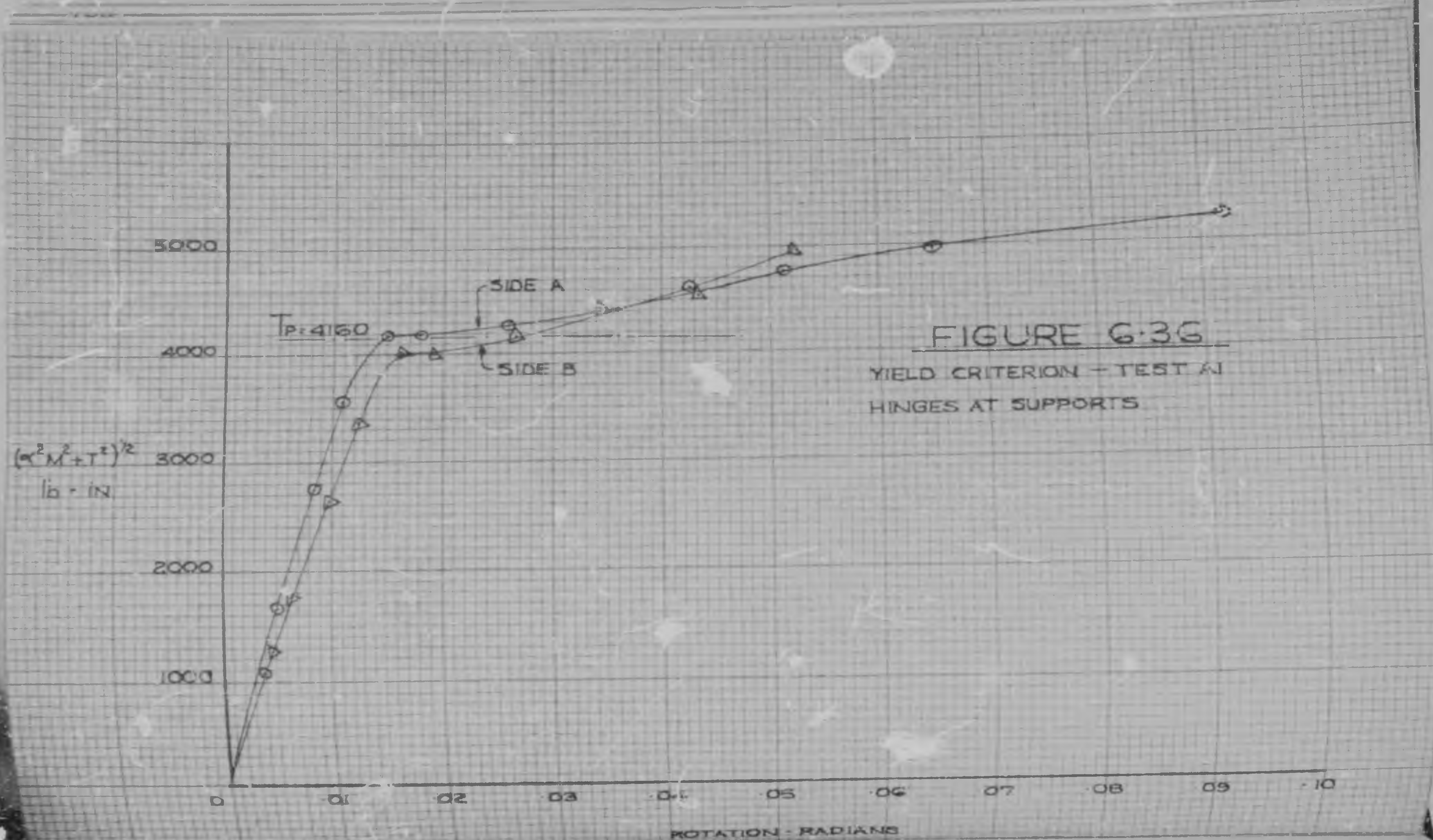

FIGURE 6.36
YIELD CRITERION - TEST A1
HINGES AT SUPPORTS
$T_P = 4160$
SIDE A
SIDE B
$(\alpha^2 M^2 + T^2)^{1/2}$
lb - IN
5000
4000
3000
2000
1000
0
.01
.02
.03
.04
.05
.06
.07
.08
.09
.10
ROTATION - RADIANS

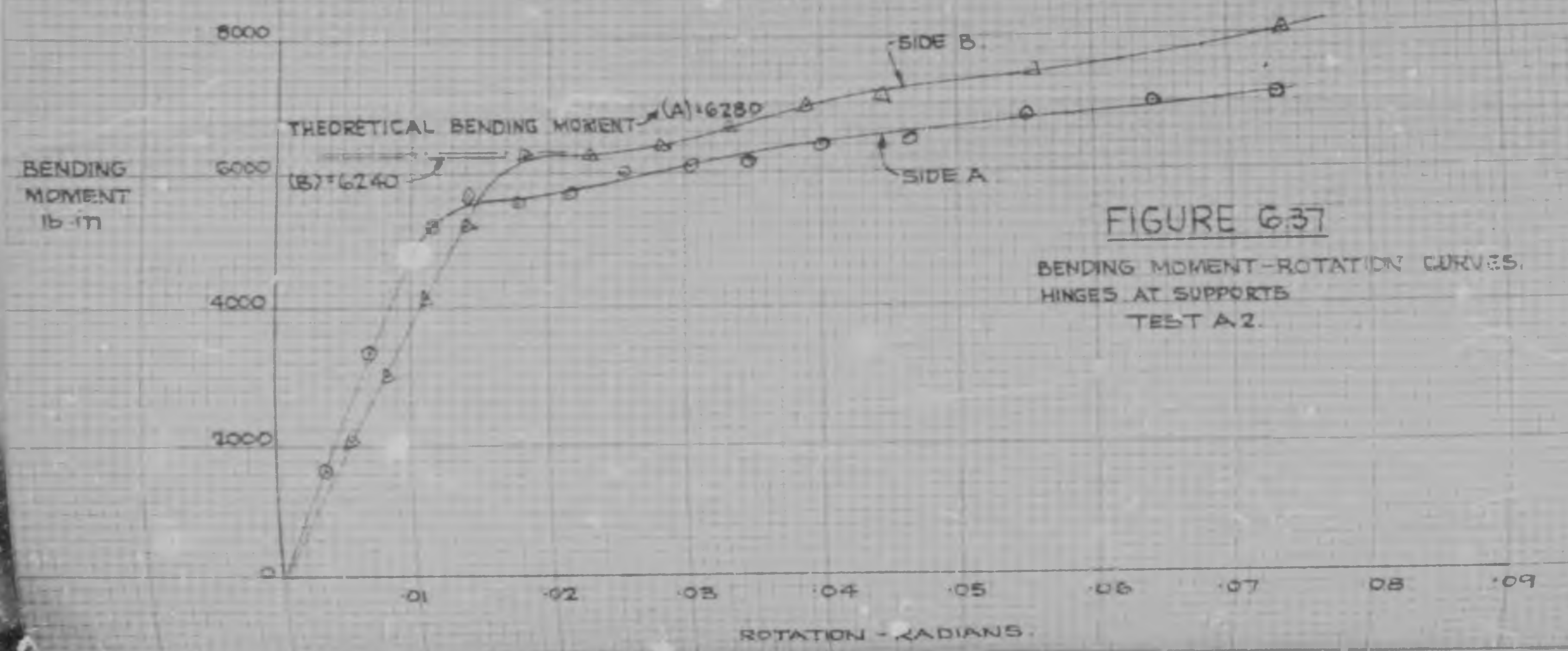

FIGURE G.37

BENDING MOMENT-ROTATION CURVES.
HINGES AT SUPPORTS
TEST A.2.

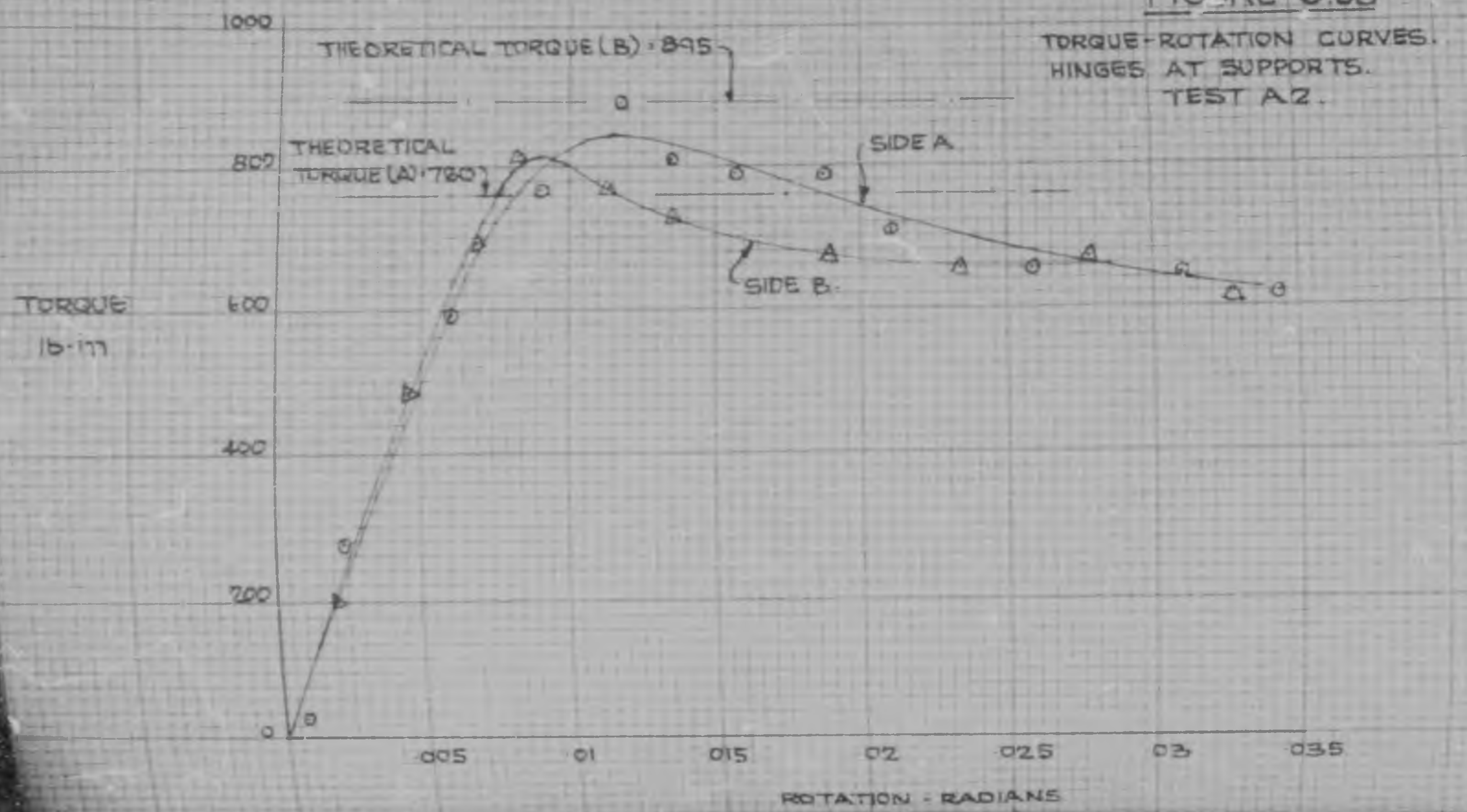

FIGURE 6.38

TORQUE-ROTATION CURVES.
HINGES AT SUPPORTS.
TEST A2.

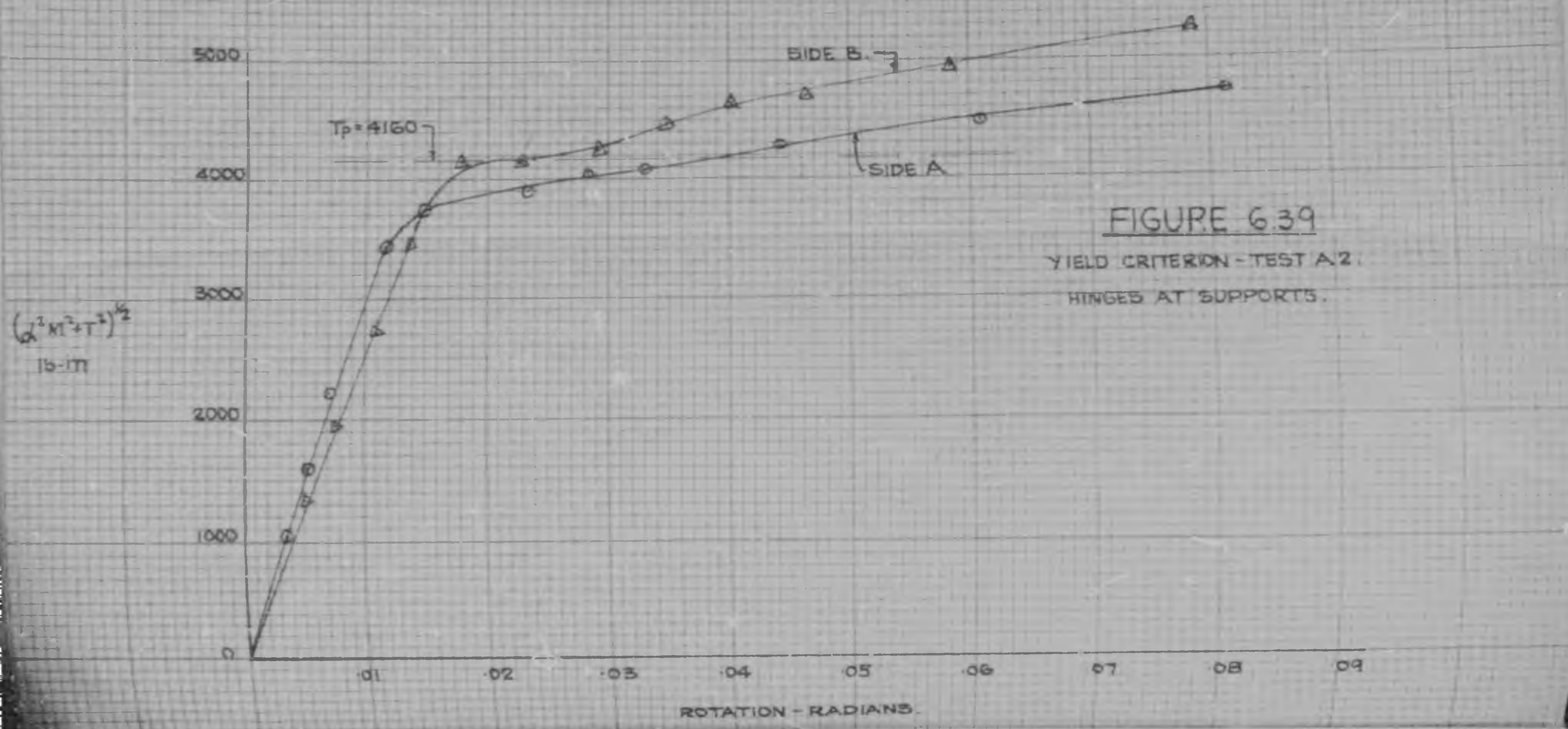

FIGURE 6.39

YIELD CRITERION - TEST A.2.

HINGES AT SUPPORTS.

cause a considerable increase in collapse load. The reason for the high value of bending moment is probably strain hardening either due to the large rotations, or the cold straightening which occurred in the preparation of the girders.

<u>"A" Tests</u>. The hinges investigated are those at the supports in A1 and A2, four hinges in all. In Figs. 6.34 to 6.39 the results are plotted in the same way as for the "C" tests.

The values of $(\alpha^2 M^2 + T^2)^{\frac{1}{2}}$, bending moment and torque at full plasticity of the section are compared with the predicted values in Table 6.8. It is seen that good agreement has been obtained; the agreement between the measured and predicted bending moments was, as in the "C" tests, better than between the measured and predicted torque. The agreement between actual values of $(\alpha^2 M^2 + T^2)^{\frac{1}{2}}$ and the predicted value ($= T_p$) appears to be slightly better than the agreement between individual values of moment and torque. The difference in the torque values might be largely experimental, but since the values of torque are much larger than in the "C" tests, the percentage deviations are much smaller.

As would be expected from the small standard deviations of the bending moment and torque in the control tests, and the results given above, the difference between measured and predicted collapse loads was very small.

<u>Variation of Direction of Axes of Rotation</u>. As the measurement of torque in the "C" tests yielded results which are not considered to be reliable, the directions of the axes of rotation has been calculated only for the four hinges at the supports in the "A" tests.

The results of this analysis are shown graphically in Figs. 6.40 and 6.41. The angle γ between the axis of rotation of the hinge and radius at the hinge is plotted against the value of load at values of load near collapse. The values at small loads were not plotted because the results at elastic deflections were not reliable as the rotational movements were extremely small. The angle γ is theoretically related to the torque and moment through equation (2.3), i.e.,

$$\tan \gamma = T/\alpha^2 M \quad \ldots\ldots\ldots\ldots\ldots\ldots \quad (2.3)$$

Table 6.8

Test	Location of Hinge	Predicted Values of M lb.-in.	Experimental Values of M lb.-in.	Predicted Values of T lb.-in.	Experimental Values of T lb.-in.	Predicted Values of $(\alpha^2M^2+T^2)^{\frac{1}{2}}$ lb.-in.	Experimental Values of $(\alpha^2M^2+T^2)^{\frac{1}{2}}$ lb.-in.
A1	Support A	6100	6580	1220	960	4160	4280
A1	Support B	6100	6400	1220	1200	4160	4150
A2	Support A	6280	5800	760	920	4160	4000
A2	Support B	6240	6400	895	820	4160	4220
						Mean	4163

In order to test the accuracy of this expression, the values of arc tan $(^T/_{a^2} M) = \gamma^1$, have also been plotted against the values of load.

The values of γ and γ^1 differ widely at the value of load assumed to be the collapse load except for hinge B in test A1. A feature of all the results was that the values of γ and γ^1 tended to agree progressively more closely at values of the load above the assumed collapse load.

CHAPTER 7

SUMMARY

The results of the analytical investigation described in this work may be summarised as follows:

(i) The use of the electronic computer provides a quick and useful solution to the many cases where ordinary solution would require a tedious trial-and-error method.

(ii) Methods have been proposed for the automatic computation (where this is advantageous) of collapse loads of girders loaded with a single concentrated load, both fully fixed and without torsional restraint; most of the possible modes of failure modes of circular beams under fully fixed support conditions with two concentrated loads have been investigated in detail.

(iii) A kinematic approach has been suggested, which leads to a more detailed visualization of the collapse modes involved.

(iv) The investigation of the effect of lack of torsional restraint at the supports shows that torsional movement of the supports can reduce the strength of a bow girder with low torsional strength, whereas for girders with torsional strength above a certain value the effect is negligible.

The results of the experimental investigation lead to the following conclusions:

(i) The application of the approximate interaction equation $\alpha^2 M^2 + T^2 = T_p^2$ for a plastic hinge yields satisfactory values of collapse loads, based on experimentally found values of the full plastic moments in pure torsion and pure bending: the positions of formation of the hinges was in close agreement with the predicted positions.

(ii) In the tests on girders with single concentrated loads it was found that at values of α slightly above the transition value to mode 3, the mode 3 failure occurred whether the beam was torsionally restrained or not. The failure load of girders for which α was below the transition value was greater when the ends were fully fixed than when the ends were torsionally unrestrained, and different failure modes occurred for the two support conditions. These results are in agreement with the theory.

(iii) The strength of the beams of low torsional strength decreased as failure progressed; no increase due to strain hardening was evident. This decrease is attributed to effects of changes in geometry and instability.

(iv) In the investigation of the behaviour of the hinges in the tests on beams with high and intermediate torsional strength ($\alpha = .652$ and $.224$ respectively), close agreement between the predicted and experimental values was obtained. In the tests on girders with low torsional resistance ($\alpha = .1265$) the values of torsion in the combined hinges showed a wide variation from the predicted values, while the bending moments agreed reasonably with expected values. In the free hinges in these tests a wide variation in the individual values of torque was obtained; these variations and those in torque in the combined hinges are partly attributable to imprecise instrumentation. The mean value of torque in free hinges was in reasonable agreement with the value of plastic moment in pure torsion obtained from the control tests, and did not show a marked increase due to warp restriction.

(v) The direction of the axes of rotation of the hinges in the "A" tests showed poor agreement with the expected directions.

Suggested subjects for further study are:

(i) The estimation of the strength of girders of other than circular shape, for instance, polygonal bow girders;

(ii) The prediction of the strength of girders under more diverse loading conditions, for instance, combinations of uniformly distributed and concentrated loads.

(iii) The extension of the virtual work method.

(iv) The testing of more realistic experimental bow girders; the tests described in the present work were on girders with ideal support conditions and were of very mild steel.

The same principles apply to any type of structure where bending moment and torque are the predominant structural actions.

APPENDIX

DETAILS OF COMPUTER PROGRAMMES

All the computer work was done on the University IBM 1620 digital computer. A flow diagram and the source programmes, as written in the FORTRAN language, are given in this Appendix.

The programmes which have been written and used are:

Programme 1: Mode 1 - fully fixed supports - single and double concentrated loads (sections 3.2 and 4.2).

Programme 2: Mode 2 - fully fixed supports - single and double concentrated loads (sections 3.2 and 4.2).

Programme 3: Mode 1 - no torsion at supports - single concentrated load (section 3.3).

Programme 4: Mode 2 - no torsion at supports - single concentrated load (section 3.3).

Programme 5: Mode 3A - fully fixed supports - two concentrated loads (section 4.2).

Programme 6: Mode 3B - fully fixed supports - two concentrated loads (section 4.2).

Before proceeding to a description of the individual programmes, some features common to all the programmes will be discussed.

All the equations used were in a dimensionless form. For the collapse load, the form was $\frac{Wr}{M_p}$, and the lengths were divided by r, the radius of the girder, for example, $\frac{r_{cg}}{r}$ or $\frac{\rho z}{r}$.

The programmes are all based on a trial-and-error procedure; in the programmes 1 to 4 above, a value of θ_1, known to be lower than the actual value, was loaded. The computer then incremented the value of θ_1, until a satisfactory solution was obtained. In the case of programmes 5 and 6, a value of ρ_1 was loaded, and incremented in the same way by the computer.

FIGURE A.1 - FLOW DIAGRAM.

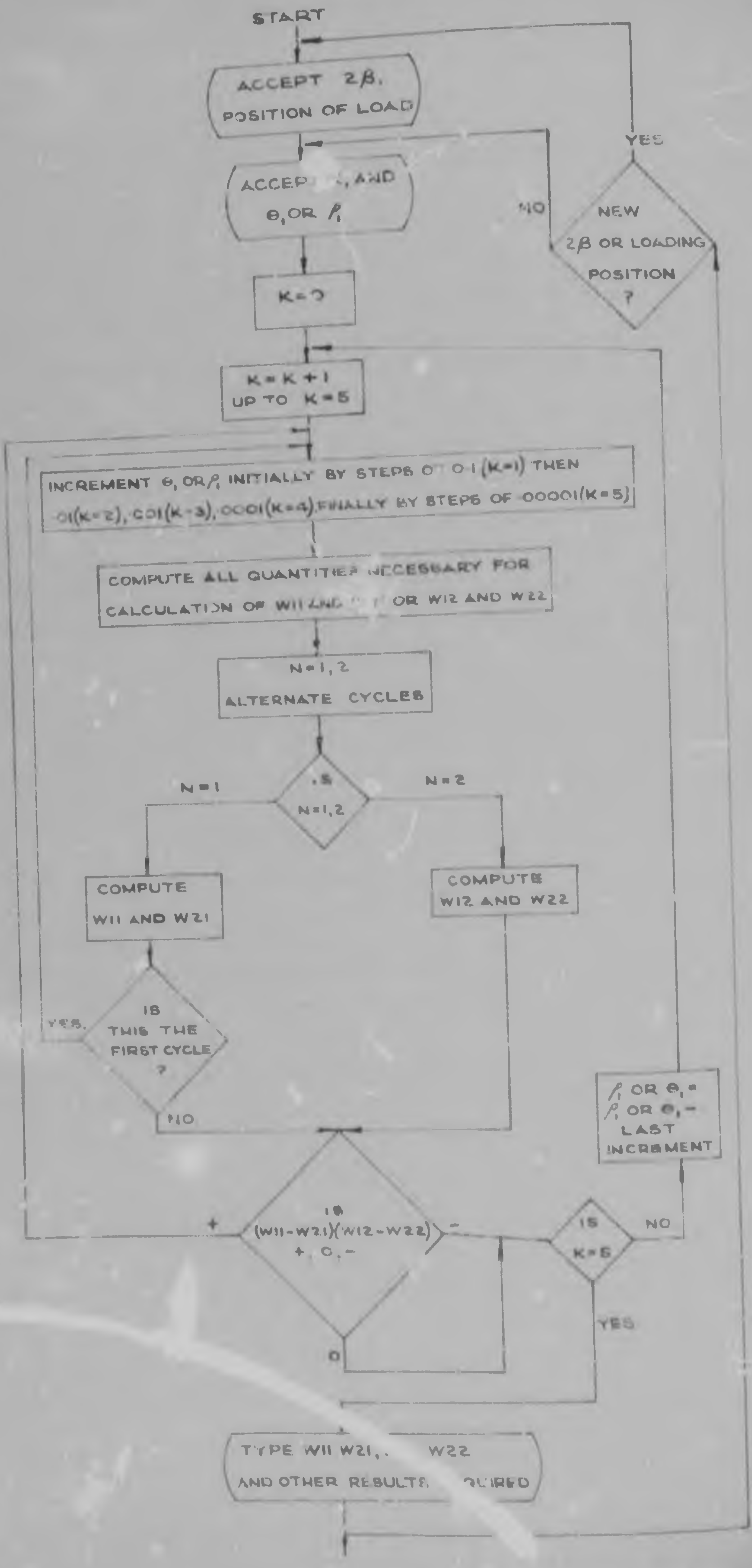

In all cases the final solution depended on the satisfaction of two simultaneous equations, the left hand side of which was in the form $\frac{W_r}{M_p}$. A number N was caused to alternate between the values 1 and 2, corresponding to successive cycles of calculation; each cycle corresponded to a value of θ_1 or ρ_1. At any value of θ_1 or ρ_1, the values of $\frac{W_r}{M_p}$ were calculated corresponding to the two simultaneous equations, and if N was equal to 1, these values were designated W11 and W21; if N was equal to 2, the values were designated W12 and W22. For a certain increment of θ_1 or ρ_1 (designated T1 and R1 respectively in the programmes), the sign of (W11 - W21) (W12 - W22) was ascertained. If the sign was positive, θ_1 or ρ_1 were incremented again, and if the sign was negative or zero the value of θ_1 or ρ_1 reverted to the previous value and smaller increments made (see below). If $\frac{W_r}{M_p}$ was close enough to the exact solution the final results were typed out. An IF (SENSE SWITCH 3) statement was inserted between the statements 50 and 51 in the programmes as in the first cycle the values of W12 and W22 were not obtained; the sense switch ON setting in the first cycle transferred the programme to the 6 PAUSE statement, at which stage it was switched to the OFF position.

The increments of T1 and R1 were initially equal to 0.1; the increments were continued until (W11 - W21) (W12 - W22) was negative or zero. The increments were then 0.01, and so on, until a solution was obtained corresponding to increments of 0.00001. The method of incrementing T1, for example, is as follows:

```
      DO 56 K = 1, 5
    7 T1 = T1 + 10. **(-K)
```

The flow diagram on which all the programmes were based is shown in Fig. A.1. Some details of the individual programmes follow.

<u>Programme 1</u>: The values to be loaded are 2β (=B), ϕ_{cg}(= FCG), r_{cg}(= RCG), α (= A) and θ_1 (= T1). The symbol for α^2 is AA. Through reference to equations (3.1), (3.5), (3.7) to (3.11) and (3.[illegible]) the development of the programme is clear. The simultaneous equations for final solution are (3.12a) and (3.12b). At some values of 2β, ϕ_{cg} and r_{cg}, as θ_1 is incremented the value of μ passes through $\frac{\pi}{2}$, and solutions are difficult to obtain as $\tan\mu$ becomes very large.

<u>Programme 2</u>: The values to be loaded are as for programme 1. Equations (3.1) and (3.15) to (3.19) are used directly. The co-ordinates of F, which are (x_F, y_F), are determined (see section 3.2) by the intersection of BF and EG.

If the equation of EG is written

$$y = m_1 x + c_1$$

and BF is written

$$y = m_2 x + c_2,$$

the point F is given by

$$x_F = (c_2 - c_1)/(m_1 - m_2)$$

and $$y_F = (m_1 c_2 - m_2 c_1)/(m_1 - m_2)$$

In the programme m_1 = AM, m_2 = BM, c_1 = C1 and c_2 = C2.

The equations (3.22a) and (3.22b) are to be simultaneously satisfied for the final solution; equations (3.23), (3.24) and (3.25) are also used in the solution.

<u>Programme 3</u>: The values of 2β (= B), ϕ(= F), α(= A) and θ_1(= T1) are loaded. Equations (3.28), (3.29) and (3.30) are used; (3.29a) and (3.29b) are the two simultaneous equations to be satisfied.

Programme 4: This is similar to programme 3 except that (3.31a) and 3.31b) are the equations to be satisfied by the trial-and-error procedure.

Programme 5: The values loaded are 2β(= B), ϕ_1(=F1), ϕ_2(= F2), ϕ_{cg}(= FCG), r_{cg}(= RCG), α (= A) and ρ_1(= R1). Equations (4.5) and (4.6) are used to find the co-ordinates of F by a method similar to that for programme 2 (see above). Equations (4.7) to (4.11) are used; (4.11a) and 4.11b) are the simultaneous equations to be satisfied.

Programme 6: The same values are loaded as for programme 5. The equations (4.13) to (4.16) are used, in addition to (3.17), (3.18) and (3.19); the simultaneous yield equations are the same as for programme 5.

PROGRAMME 1

```
1 FORMAT(F8.0,F8.0,F8.0)
2 FORMAT(F8.0,F8.0)
3 FORMAT(F8.5,F8.5,F8.4,F8.4,F8.4,F8.4)
4 ACCEPT 1,B,FCG,RCG
5 ACCEPT2,A,T1
  AA=1.-A*A
  N=2
6 PAUSE
  DO 56 K=1,5
7 T1=T1+10.**(-K)
  R1=2./(AA*(1.+COS(T1)))
  AMU=ATAN((COS(FCG)-R1*COS(T1)/RCG)/(R1*SIN(T1)/RCG-SIN(FCG)))
  P=RCG*COS(FCG-AMU)
  Z=P*AA
  AAA=-Z*Z*COS(B)*COS(B)-4.*Z*SIN(B)*SIN(AMU)+4.*SIN(AMU)*SIN(AMU)
  BB=(2.*Z*SIN(B)-4.*SIN(AMU))*(Z*COS(B)-2.*COS(AMU))
  C=-Z*Z*SIN(B)*SIN(B)-4.*Z*COS(B)*COS(AMU)+4.*COS(AMU)*COS(AMU)
  T3=ATAN((-BB-SQRT(BB*BB-4.*AAA*C))/(2.*AAA))
  IF(T3)31,30,30
30 T2=B-T3
  GO TO 32
31 T2=B-3.14159-T3
32 R2=2./(AA*(1.+COS(T2)))
  AL1=SQRT(R1*R1+RCG*RCG-2.*R1*RCG*COS(FCG-T1))
  AL2=SQRT(R2*R2+RCG*RCG-2.*R2*RCG*COS(B-FCG-T2))
  IF(N-1)40,41,40
40 N=0
41 N=N+1
  GO TO (50,51),N
50 W11=A*(AL1+AL2)/(AL2*(R1-1.))
  W21=A*(AL1+AL2)/(AL1*(R2-1.))
  IF(SENSE SWITCH 3 )6,55
51 W12=A*(AL1+AL2)/(AL2*(R1-1.))
  W22=A*(AL1+AL2)/(AL1*(R2-1.))
55 IF(SENSE SWITCH 1)53,54
54 IF((W11-W21)*(W12-W22))52,52,7
52 T1=T1-(10.**(-K))
56 N=N-1
53 TYPE 3,T1,T2,W11,W21,W12,W22
  IF(SENSE SWITCH 2) 4,5
  END
```

PROGRAMME 2

```
 1 FORMAT(F8.0,F8.0,F8.0)
 2 FORMAT(F8.0,F8.0)
 3 FORMAT(F8.5,F8.5,F8.4,F8.4,F8.4,F8.4)
 4 ACCEPT 1,B,FCG,RCG
 5 ACCEPT2,A,T1
   AA=1.-A*A
   N=2
 6 PAUSE
   DO 55 K=1,5
 7 T1=T1+10.**(-K)
   R1=2./(AA*(1.+COS(T1)))
   XE=R1*COS(T1)
   YE=R1*SIN(T1)
   AM=(YE-RCG*SIN(FCG))/(XE-RCG*COS(FCG))
   C1=RCG*SIN(FCG)-AM*RCG*COS(FCG)
   XS=(A*A*XE*COS(T1)+A*A*YE*SIN(T1)+1.-XE)/(1.-AA*XE)
   YS=(1.-XE)*(XS-1.)/(A*A*YE)
   TANG2=(XS*SIN(B)-YS*COS(B))/(1.-XS*COS(B)-YS*SIN(B))
   DFJ=ATAN(A*A*TANG2)
   D=B-1.57030+DFJ
   BM=SIN(D)/COS(D)
   C2=SIN(B)-BM*COS(B)
   XF=(C2-C1)/(AM-BM)
   YF=(AM*C2-BM*C1)/(AM-BM)
   S1=SQRT(A*A*COS(DFJ)*COS(DFJ)+SIN(DFJ)*SIN(DFJ))
   S2=SQRT((XF-COS(B))*(XF-COS(B))+(YF-SIN(B))*(YF-SIN(B)))
   T3=ATAN(YF/XF)
   IF(T3)31,30,30
30 T2=B-T3
   GO TO 32
31 T2=B-3.14159-T3
32 R2=SQRT(XF*XF+YF*YF)
   AL1=SQRT(R1*R1+RCG*RCG-2.*R1*RCG*COS(FCG-T1))
   AL2=SQRT(R2*R2+RCG*RCG-2.*R2*RCG*COS(B-FCG-T2))
   IF(N-1)40,41,40
40 N=0
41 N=N+1
   GO TO (50,51),N
50 W11=A*(AL1+AL2)/(AL2*(R1-1.))
   W21=A*(AL1+AL2)/(AL1*S1*S2)
   IF(SENSE SWITCH 3 )6,55
51 W12=A*(AL1+AL2)/(AL2*(R1-1.))
   W22=A*(AL1+AL2)/(AL1*S1*S2)
55 IF(SENSE SWITCH 1)53,54
54 IF((W11-W21)*(W12-W22))52,52,7
52 T1=T1-(10.**(-K))
56 N=N-1
53 TYPE 3,T1,T2,W11,W21,W12,W22
   IF(SENSE SWITCH 2) 4,5
   END
```

PROGRAMME 3

```
 1 FORMAT(F8.0,F8.0)
 2 FORMAT(F8.0,F8.0)
 3 FORMAT(F8.5,F8.5,F8.4,F8.4,F8.4,F8.4)
 4 ACCEPT1,B,F
 5 ACCEPT2,A,T1
   N=2
 6 PAUSE
   DO 56 K=1,5
 7 T1=T1+10.**(-K)
   AN1=(SIN(F)-SIN(T1)/COS(T1))/SIN(B)
   AN2=(COS(B)/SIN(B))*(SIN(T1)/COS(T1)*COS(F)-SIN(F))
   D=(COS(F)-1.)/SIN(B)-SIN(T1)/COS(T1)*COS(F)+SIN(F)
   T3=ATAN((AN1+AN2)/D)
   IF(T3)31,30,30
30 T2=B-T3
   GO TO 32
31 T2=B-3.14159-T3
32 AL1=SQRT(1./(COS(T1)*COS(T1))+1.-2.*COS(F-T1)/COS(T1))
   AL2=SQRT(1./(COS(T2)*COS(T2))+1.-2.*COS(B-F-T2)/COS(T2))
   IF(N-1)40,41,40
40 N=0
41 N=N+1
   GO TO (50,51),N
50 W11=A/(1./COS(T1)-1.)*(AL1+AL2)/AL2
   W21=A/(1./COS(T2)-1.)*(AL1+AL2)/AL1
   IF(SENSE SWITCH 3 )6,55
51 W12=A/(1./COS(T1)-1.)*(AL1+AL2)/AL2
   W22=A/(1./COS(T2)-1.)*(AL1+AL2)/AL1
55 IF(SENSE SWITCH 1)53,54
54 IF((W11-W21)*(W12-W22))52,52,7
52 T1=T1-(10.**(-K))
56 N=N-1
53 TYPE 3,T1,T2,W11,W21,W12,W22
   IF(SENSE SWITCH 2) 4,5
   END
```

Programme (4) is identical to this programme except for W21 and W22, e.g.

W21 = (cos (T2)/sin (T2)) * (AL1 + AL2)/AL1.

PROGRAMME 5

```
 1 FORMAT(F8.0,F8.0,F8.0,F8.0,F8.0)
 2 FORMAT(F8.0,F8.0)
 3 FORMAT(F8.5,F8.5,F8.4,F8.4,F8.4,F8.4)
 4 ACCEPT 1,B,F1,F2,FCG,RCG
 5 ACCEPT 2,A,R1
   N=2
 6 PAUSE
   XCG=RCG*COS(FCG)
   YCG=RCG*SIN(FCG)
   DO 56 K=1,5
 7 R1=R1+10.**(-K)
   XE=R1*COS(F1/2.)
   YE=R1*SIN(F1/2.)
   AM=(YE-YCG)/(XE-XCG)
   C=YCG-AM*XCG
   XF=C/(SIN(B/2.+F2/2.)/COS(B/2.+F2/2.)-AM)
   YF=AM*XF+C
   XI1=1.-XE
   ETA1=YE
   R2=SQRT(XF*XF+YF*YF)
   XI2=1.-R2*COS(B/2.-F2/2.)
   ETA2=R2*SIN(B/2.-F2/2.)
   AL1=SQRT((XE-XCG)**2+(YE-YCG)**2)
   AL2=SQRT((XF-XCG)**2+(YF-YCG)**2)
   IF(N-1) 40,41,40
40 N=0
41 N=N+1
   GO TO(50,51),N
50 W11=A*(AL1+AL2)/(AL2*SQRT(A*A*ETA1*ETA1+XI1*XI1))
   W21=A*(AL1+AL2)/(AL1*SQRT(A*A*ETA2*ETA2+XI2*XI2))
   IF (SENSE SWITCH 3)6,55
51 W12=A*(AL1+AL2)/(AL2*SQRT(A*A*ETA1*ETA1+XI1*XI1))
   W22=A*(AL1+AL2)/(AL1*SQRT(A*A*ETA2*ETA2+XI2*XI2))
55 IF((W11-W21)*(W12-W22))52,52,7
52 R1=R1-(10.**(-K))
56 N=N-1
   TYPE 3,R1,R2,W11,W21,W12,W22
   IF(SENSE SWITCH 2) 4,5
   END
```

PROGRAMME 5.

```
1 FORMAT(F8.0,F8.0,F8.0,F8.0,F8.0)
2 FORMAT(F8.0,F8.0)
3 FORMAT(F8.5,F8.5,F8.5,F8.4,F8.4,F8.4,F8.4)
4 ACCEPT 1,B,F1,F2,FCG,RCG
5 ACCEPT 2,A,R1
  N=2
6 PAUSE
  XCG=RCG*COS(FCG)
  YCG=RCG*SIN(FCG)
  DO 56 K=1,5
7 R1=R1+10.**(-K)
  XE=R1*COS(F1/2.)
  YE=R1*SIN(F1/2.)
  XI1=XE-1.
  ETA1=YE
  TANG1=XI1/(A*A*ETA1)
  XS=TANG1/(SIN(F1/2.)/COS(F1/2.)+TANG1)
  YS=XS*SIN(F1/2.)/COS(F1/2.)
  TANG2=(XS*SIN(B)-YS*COS(B))/(1.-XS*COS(B)-YS*SIN(B))
  D2=ATAN(A*A*TANG2)
  D1=B-1.57080+D2
  AM1=(YE-RCG*SIN(FCG))/(XE-RCG*COS(FCG))
  C1=RCG*SIN(FCG)-AM1*RCG*COS(FCG)
  AM2=SIN(D1)/COS(D1)
  C2=SIN(B)-AM2*COS(B)
  XF=(C2-C1)/(AM1-AM2)
  YF=(AM1*C2-C1*AM2)/(AM1-AM2)
  R2=SQRT(XF*XF+YF*YF)
  THET2=ATAN(YF/XF)
  XI2=R2*COS(B-THET2)-1.
  ETA2=R2*SIN(B-THET2)
  AL1=SQRT((XE-XCG)**2+(YE-YCG)**2)
  AL2=SQRT((XF-XCG)**2+(YF-YCG)**2)
  IF(N-1) 40,41,40
40 N=0
41 N=N+1
  GO TO(50,51),N
50 W11=A*(AL1+AL2)/(AL2*SQRT(A*A*ETA1*ETA1+XI1*XI1))
  W21=A*(AL1+AL2)/(AL1*SQRT(A*A*ETA2*ETA2+XI2*XI2))
  IF (SENSE SWITCH 3)6,55
51 W12=A*(AL1+AL2)/(AL2*SQRT(A*A*ETA1*ETA1+XI1*XI1))
  W22=A*(AL1+AL2)/(AL1*SQRT(A*A*ETA2*ETA2+XI2*XI2))
55 IF((W11-W21)*(W12-W22))52,52,7
52 R1=R1-(10.**(-K))
56 N=N-1
  TYPE 3,R1,R2,THET2,W11,W21,W12,W22
  IF(SENSE SWITCH 2) 4,5
  END
```

LIST OF REFERENCES

1. A.H. Gibson and E.G. Ritchie, "A Study of the Circular-Arc Bow-Girder". Constable, London, 1914.
2. A.J.S. Pippard, "Studies in Elastic Structures", p.202. Arnold, London, 1952.
3. K.W. Johansen and P. Lange Hansen, "Studies on the Load Carrying Capacity of Steel Structures", Technical University of Denmark, Copenhagen, 1954.
4. N.S. Boulton and B. Boonsukha, "Plastic Collapse Loads for Circular-Arc Bow Girders". Proc. I.C.E., London, Vol. 13, 1959, and discussion, Vol. 15, 1960.
5. R. Hill and M.P.L. Siebel, "On the Plastic Distortion of Solid Bars by Combined Bending and Twisting". J. Mech. Phys. Sol., Vol. 1, 1952 - 1953, p.207.
6. E.O. Imegwu, "Ultimate Strength of Plane Curved Girders". J.I. Struct. E., London, Vol. 42, No. 4, April 1964.
7. M.C. Steele, "The Plastic Bending and Twisting of Square Section Members". J. Mech. Phys. Sol., Vol. 3, 1954 - 1955, p.156.
8. J.F. Baker, M.R. Horne and J. Heyman, "The Steel Skeleton", Vol. 2, Cambridge Univ. Press, 1956.

--- ooOoo ---